NONLINEAR REDUCED ORDER MODELING OF BOLTED JOINTS

A THESIS SUBMITTED TO
THE GRADUATE SCHOOL OF NATURAL AND APPLIED SCIENCES
OF
MIDDLE EAST TECHNICAL UNIVERSITY

BY

GÖKHAN KARAPISTIK

IN PARTIAL FULFILLMENT OF THE REQUIREMENTS
FOR
THE DEGREE OF MASTER OF SCIENCE
IN
MECHANICAL ENGINEERING

SEPTEMBER 2019

Approval of the thesis:

NONLINEAR REDUCED ORDER MODELING OF BOLTED JOINTS

submitted by **GÖKHAN KARAPISTIK** in partial fulfillment of the requirements for the degree of **Master of Science in Mechanical Engineering Department, Middle East Technical University** by,

Prof. Dr. Halil Kalıpçılar
Dean, Graduate School of **Natural and Applied Sciences** _____

Prof. Dr. M. A. Sahir Arıkan
Head of Department, **Mechanical Engineering** _____

Prof. Dr. Ender Ciğeroğlu
Supervisor, **Mechanical Engineering, METU** _____

Examining Committee Members:

Assoc. Prof. Dr. M. Bülent Özer
Mechanical Engineering, METU _____

Prof. Dr. Ender Ciğeroğlu
Mechanical Engineering, METU _____

Assoc. Prof. Dr. Yiğit Yazıcıoğlu
Mechanical Engineering, METU _____

Assist. Prof. Dr. Orkun Özşahin
Mechanical Engineering, METU _____

Assoc. Prof. Dr. S. Çağlar Başlamışlı
Mechanical Engineering, Hacettepe University _____

Date: 09.09.2019

I hereby declare that all information in this document has been obtained and presented in accordance with academic rules and ethical conduct. I also declare that, as required by these rules and conduct, I have fully cited and referenced all material and results that are not original to this work.

Name, Surname: Gökhan Karapıstık

Signature:

ABSTRACT

NONLINEAR REDUCED ORDER MODELING OF BOLTED JOINTS

Karapıstık, Gökhan
Master of Science, Mechanical Engineering
Supervisor: Prof. Dr. Ender Ciğeroğlu

September 2019, 108 pages

Most of the structural systems assembled by using bolted joints. Therefore, bolted joint models have a critical importance to estimate the behavior of the overall assembled system. There are several linear bolted joint models, which consist of spring and dashpot elements in literature. While they can estimate the resonant frequency of the overall system with a sufficient accuracy, linear bolted joint models are inadequate for approximating the damping, which arises from the friction in the contact interface of assembled system. On the other hand, there are examples of nonlinear bolted joint models, which utilize 3D contact models to account for the frictional damping behavior in the literature. However, modeling the structures with many bolted joints by using high fidelity 3D contact models is very time consuming. Therefore, reduced order bolted joint models with sufficient accuracy are in need. In this thesis, a method for modeling bolted joints in frequency domain is introduced. The joint model consists of microslip friction elements each one of which is constructed by several dry friction elements in parallel and located at the contact interface.

Keywords: Joint Model, Reduced Joint Model, Microslip Friction, Multiple Macroslip Elements, Nonlinear Vibrations

ÖZ

CIVATALI BAĞLANTILARIN İNDİRGENMİŞ DOĞRUSAL OLMAYAN MODELİ

Karapıstık, Gökhan
Yüksek Lisans, Makina Mühendisliği
Tez Danışmanı: Prof. Dr. Ender Ciğeroğlu

Eylül 2019, 108 sayfa

Yapısal sistemlerin çoğu cıvatalı bağlantılar kullanılarak monte edilir. Bu nedenle, cıvatalı bağlantı içeren modeller montajlı sistemin davranışını tahmin etmek için kritik öneme sahiptir. Literatürde yaylı ve yaylı unsurlardan oluşan birkaç doğrusal cıvatalı bağlantı modeli vardır. Tüm sistemin rezonans frekansını yeterli bir doğrulukla tahmin edebilmelerine rağmen, doğrusal cıvatalı bağlantı modelleri, monte edilmiş sistemin temas ara yüzündeki sürtünmeden kaynaklanan sönümlendirmeye yaklaşmak için yetersizdir. Öte yandan, literatürde sürtünme kaynaklı sönümleme davranışını hesaba katan 3 boyutlu temas modellerini kullanan doğrusal olmayan cıvatalı eklem modellerine örnekler vardır. Fakat, yapıların yüksek kalitede 3 boyutlu temas modelleri kullanılarak birçok cıvatalı bağlantıyla modellenmesi çok zaman alır. Bu nedenle, yeterli hassasiyete sahip indirgenmiş cıvatalı bağlantı modellerine ihtiyaç vardır. Bu tez çalışmasında, cıvatalı bağlantıların frekans alanındaki modellenmesi için bir yöntem tanıtılmıştır. Bağlantı modeli, her biri paralel olarak birkaç kuru sürtünme elemanları tarafından oluşturulan ve temas yüzeyi üzerinde bulunan mikro kayma sürtünme elemanlarından oluşur.

Anahtar Kelimeler: Bağlantı Modeli, İndirgenmiş Bağlantı Modeli, Mikro-kayma sürtünmesi, Çok elemanlı makro-kayma, Doğrusal Olmayan Titreşimler

To my family

ACKNOWLEDGEMENTS

I would like to express my gratitude to my supervisor Prof. Dr. Ender CİĞEROĞLU for his guidance and support.

I am grateful to my family, who have provided me emotional support in my life.

I would like to express my appreciation to my friends; Sefa KIZILAY and Eren ÖNEY for their emotional and technical support.

I would like to thank Levent ÜNLÜSOY and Bilgehan ERDOĞAN for their technical support.

I would like to gratefully acknowledge the support provided by ROKETSAN A.Ş.

TABLE OF CONTENTS

LIST OF TABLES

TABLES

LIST OF FIGURES

FIGURES

CHAPTER 1

INTRODUCTION

1.1. Literature Survey

Nowadays, it is straightforward to model a single mechanical structure by utilizing analytic methods or finite element methods. However, many structural systems consist of mechanical parts, which are assembled together with structural joints. Bolts are one of the widely used structural joints, which are utilized to establish connection in many structural components. Fastening the structural components with bolts introduce complexity to the structural integrity in terms of both stiffness and damping characteristics. Because, the contact interface introduces nonlinearity, which effects the overall system. Instead of dealing with complex nonlinearities, several studies to estimate the behavior of the bolted joints with linear springs and dashpots are realized.

Tsai and Chou [1] suggested a method in order to calculate the dynamic properties of single bolted joint system. They obtained the stiffness and damping properties of the bolted joint system by utilizing only receptance functions, which are obtained through experimental methods. Their study was based on receptance coupling method. Since the mass of the bolt is too small compared to overall system, and the frequency range is not extremely high, it is modeled with only spring and damping elements. In order to obtain the parameters of spring and damping elements, least square method was utilized. As a result, they modeled the bolted joint as a single stiffness and damping matrices for a specified range of frequency.

Yang et al. [2] utilized the substructure synthesis method in order to obtain the linear joint model parameters. Obtained equations from the substructure synthesis method were solved with singular value decomposition method in order to decrease the noise present in the experimental data. In their joint model, only the stiffness properties were

investigated. They study two types of joint model. In the first joint model, they represent the joint as diagonal stiffness matrices, where the translation and rotational stiffness values are included. In the second joint model, they represent the joint as full stiffness matrices, where the translational, rotational and off-diagonal terms are included. In their study, instead of modeling the joint as a single stiffness matrix for whole frequency range, they divide the frequency range so that improved results are obtained for several frequency regions with several corresponding stiffness matrices. Besides, they also carry on a sensitivity analysis for the effect of translational and rotational stiffness values of joint model on response of overall system. They concluded that for a certain frequency range natural frequency of the overall system is sensitive to values of translational and rotational stiffness matrix, and it is insensitive for other frequency ranges.

Mehrpouya et al. [3] investigate two types of joint model. In both model they utilize receptance functions of assembled system and subsystems. In addition, they include the inertial effects into both joint models. In the first joint model, inertial effects in the compatibility equations of receptance coupling method and cross terms in the stiffness and damping matrices are ignored in order to have analytical solution. In the second joint model, both effects are included in order to observe the validity of the assumptions, which are made in the first joint model. Furthermore, instead of obtaining a single joint matrix or several joint matrices in certain frequency regions, they utilize joint model throughout the whole frequency region of interest. They concluded that the assumption in the first joint model is valid because the both joint model yield similar results.

In linear joint models, stiffness and damping matrices are replaced with the joint itself such that similar results can be obtained in assembled system. Some of them utilize a single joint matrix or several joint matrices, others utilize continuous joint matrix in the whole frequency region of interest. Although the linear joint models can estimate the resonance frequency of the overall system with a sufficient accuracy, inadequacy in capturing the energy loss of the structural system, especially with changing

excitation levels, is a shortcoming of the linear joint models. To deal with the shortage of damping estimation, high fidelity models have been studied in the past few decades.

Segalman [4] developed a new method, which is called whole joint model for modeling lap-type joints. The model based on a parallel-series Iwan system. By utilizing truncated power-law spectra, constitutive equations of the model expressed in terms of four parameter. In this model, both microslip and macroslip regime of the lap-type joint model is included.

Bograd et al [5] introduced three types of modeling methods of mechanical joints. The first one is node-to-node contact model utilizing the Jenkins friction elements. In this model, Jenkins friction elements (elastic spring in series with coulomb element) and nonlinear contact laws are utilized in tangential direction and normal direction respectively. Harmonic balance method with iterative solution is performed for the solution of node-to-node contact model. The second one is the thin layer elements. In this approach, they utilized damping, which do not depend on frequency and linear stiffness element in order to obtain the response of the structure. The third one is the zero thickness element. They modeled the joint contact surface by utilizing the zero thickness elements in FEM. The contact model based on Hertzian contact in normal direction and Mindlin's approach in tangential direction.

Liao et al. [6] proposed an analytical model of bolted joint beam in tangential direction for transient excitation. Bolted joint section is modelled by using cubic stiffness nonlinearity since results shows that cubic stiffness is more applicable for wide range frequency domain analysis. Iwan model with cubic stiffness is used to simulate nonlinear behavior of bolted joint beams. Results show that nonlinear stiffness and damping effect of bolted joints are dominant in specific frequency range. Analytical model and experimental results are compared and discussed and there is good agreement between the results.

Brake et al. [7] studied three different modeling techniques to determine the nonlinear dynamic response of structure under periodic force excitation of bolted lab joint. In

the first one, four-parameter Iwan model is utilized. In the second one, they realized the node-to-node contact model, which is developed by Bograd et al. [5]. In the third one, they used the FORSE, which is developed in Imperial College. They chose the Brake-Reuss beam [8] model for the benchmark study and compared the three different modeling techniques.

The disadvantage of the four-parameter Iwan model, which works in time domain, is because of the requirement of high computational costs. Brake et al [9] suggested an analytical solution for the four-parameter Iwan model. Besides, pinning behavior, which occurs in bolted joints is introduced into the model. Brake Reuss beam is utilized in order to study the developed method.

Petrov [10] proposed a new method to make sensitivity analysis of nonlinear structures under periodic force excitation for large finite element model. Multi harmonic force response is used for stability sensitivity analysis in frequency domain. In order to verify the proposed method, lumped parameter models and realistic finite element model with friction and gap nonlinearities are selected as test cases.

Lacayo et. al. [11] compared two different joint modelling approaches which are time domain whole joint approach and frequency domain node to node approach to simulate bolted joints. The whole joint approach is the Segalman's four parameter Iwan model. In node-to-node approach, 3D contact elements are utilized with multi-harmonic balance method. In comparison study, Brake-Reub beam and two beams jointed with bolt interface are utilized. First mode of models are tuned by using information obtained from experiment. Force response of nonlinear structures are performed by using multi harmonic balance method and modal superposition method in frequency domain.

Nonetheless, computational cost of high fidelity models is considerable if a structural system with many bolts is to be modeled. Main reason in this insufficiency of damping behavior in reduced order linear models is the absence of microslip friction model in the contact area. Structures with bolted joint have a complicated contact area

exhibiting a variable contact force distribution. The contact forces near the bolt hole are sufficiently high; whereas, they become very low at some distant. Due to variability in contact forces, microslip like behavior arises. Hence, it is crucial to model the microslip friction present in the contact area. In order to model the microslip behavior, either specific microslip models or distributed macroslip models are utilized. In macroslip models, entire surface associated with the friction model is either in slip state or in stick state. However, in microslip models, unlike macroslip models, partial slips in localized areas are allowed in the contact interface; hence, energy can be dissipated without the necessity of gross slip. Several studies are conducted about the friction models in literature.

Menq et al. [12] suggested a new method in order to analyze the dynamic response of frictionally damped structures where the contact interfaces are exposed to high normal loads. They introduced continuous microslip friction model by utilizing the two elastic bars combined with an elastoplastic shear layer. The important feature of this model is that the partial slip occurs at the interface such that even though the excitation levels are low, where the gross slip do not occur, energy is dissipated from the structural system. They conducted several numerical studies in order to show the effect of microslip friction. Afterwards, Menq et al. [13] performed experimental studies in order to validate the proposed microslip friction model. As a result of these experiments, when the contact pressure is high relative to the external excitation, they concluded that the effect of partial slip need to be taken into account.

Yang et al. [14] proposed a new friction contact model, which includes not only tangential motion but also normal motion. The stick-slip characteristics are studied in detail, and analytical expressions are obtained for the transitions between stick, slip and separation motions. Hysteresis loops for various cases are illustrated in order to understand the stick, slip and separation motions occurring during the cycle of motion. Nonlinear response of two degrees of freedom system by utilizing the proposed contact model is studied. Harmonic balance method is utilized for the solution of the nonlinear system. Besides by conducting a time domain analysis, Jump phenomenon,

which arises because of hardening or softening of spring effects, are studied. Hardening or softening of spring effects occurs mainly because of the separation motion.

Cigeroglu et al. [15] are studied one-dimensional microslip friction model by utilizing a one-dimensional beam model, which is similar to the model studied by Menq et al. [12]. They also included the inertia of the damper, and studied a non-uniform normal load distribution. They utilized uniform, convex and concave normal load distribution throughout the beam in order to achieve distinct stick-slip behavior. In order to show the effect of microslip, they constructed an equivalent point contact model. The parameters of the point contact model are determined such that the both models have the same total stiffness in full stick and full slipping states. Also both models starts gross slip at the same excitation levels. As a result, it is seen that in fully stick and full slip states results agree with each other. However, while the microslip model exhibits partial slip, point contact model was in full stick state. The importance of microslip until the gross slip occurs was demonstrated with numerical results.

Cigeroglu and Ozguven [16] proposed a new friction model, which is an approximation for microslip friction model, in order to analyze the turbine blades with dry friction dampers. The microslip approximation consist of a linear spring and a macroslip dry friction element. They utilized the proposed method on a dynamic model of bladed disk assembly.

Cigeroglu et al. [17] proposed a distributed parameter microslip friction model, where the stick-slip characteristics are studied in [14]. The transition criteria for the stick, slip and separation states are obtained for distributed parameter model. They utilized iterative multi-mode solution method with harmonic balance method. The proposed method is performed on one dimensional beam model and 3D blade model. They also examine the microslip friction effects, which arise from distributed macroslip elements.

Cigeroglu et al. [18] studied analysis of constraint and unconstraint structures coupled through the frictional contacts. They constructed a model of turbine blade with wedge damper. They utilized the contact model developed by Yang et al, [14]. Harmonic balance method with modal superposition method with six rigid body modes and several elastic modes is used for the forced response analysis of the proposed model.

1.2. Objective of Thesis

In this thesis, a new method for nonlinear reduced order modeling of bolted joints is presented. This method provides an accurate modeling of bolted joints while it is not computationally as expensive as the high fidelity methods [4-11] studied in the recent years. The method proposed mainly focuses on the reduction of the contact model, which is the most dominant nonlinearity reside in the bolted joint connections. Two types of reduction methodology are studied in this thesis. The first reduction methodology is based on conversion of the distributed macroslip friction elements into microslip friction elements, which are the combination of the macroslip elements. The second reduction methodology focused on the further reduction of the each microslip friction elements such that the hysteresis loops after the second reduction are similar with the first reduction while reducing the number of macroslip elements inside the reduced order microslip elements.

1.3. Outline of Thesis

In chapter 2, steady state analysis of nonlinear vibratory systems are explained. Firstly, equation of motion of a nonlinear oscillatory system is introduced. Afterwards, solution methods for nonlinear vibratory systems, which are utilized in this thesis, are mentioned briefly.

In chapter 3, Contact models for the nonlinear analysis of bolted joints are studied in detail. Two types of contact models, which are utilized in the reduced order models, are introduced. Detailed formulation for the contact kinematics are studied and transition angles for single harmonic motion are obtained.

In chapter 4, two-step reduced order modeling method by utilizing the 1D dry friction elements with constant normal load is introduced. Case study is conducted with a 3D FEM model in order to examine the effect of reduction methodologies.

In chapter 5, first step of the reduction methodology is studied in more detail by utilizing the 1D dry friction elements with normal load variation. Two different case studies are conducted with 3D FEM models.

In chapter 6, overview of the reduction method is realized. The new reduction method is also discussed. Besides, possible feature studies are mentioned.

CHAPTER 2

STEADY STATE DYNAMIC RESPONSE ANALYSIS OF NONLINEAR SYSTEMS

2.1. Equation of Motion of Nonlinear Systems

Equation of motion of a general nonlinear system is given in Equation (2.1),

$$\mathbf{M}\cdot\ddot{\mathbf{x}}+\mathbf{C}\cdot\dot{\mathbf{x}}+\mathbf{K}\cdot\mathbf{x}+i\cdot\mathbf{H}\cdot\mathbf{x}+\mathbf{f_N}=\mathbf{f} \tag{2.1}$$

Where M, C, K and H are the mass, viscous damping, stiffness and structural damping matrices respectively. f, f_N and x are the external forcing, nonlinear internal forcing and response vectors respectively. If harmonic excitation is assumed for the external forcing, than the response of the structure is also harmonic. As a result the external forcing and the response are defined in Equations (2.2) and (2.3),

$$\mathbf{f}=Im\left(\sum_{p=0}^{n}\mathbf{f_p}\,e^{ip\omega t}\right), \tag{2.2}$$

$$\mathbf{x}=Im\left(\sum_{p=0}^{n}\mathbf{x_p}\,e^{ip\omega t}\right), \tag{2.3}$$

Where n is number of harmonics. f_p and x_p are the complex valued amplitude vectors of external forcing and response of the structures for the p^{th} harmonic. If the response of the system is harmonic, nonlinear internal forcing can be expressed as in Equation (2.4)

$$\boldsymbol{f_N} = Im\left(\sum_{p=0}^{n} \boldsymbol{f_{N_p}}\, e^{ip\omega t}\right) \tag{2.4}$$

Where n is the number of harmonics, and f_{N_p} is the complex valued amplitude vector of nonlinear internal force vector for the p^{th} harmonic. It should be noted that f_{N_p} might be a function of x_p and ω. By substituting Equations (2.2), (2.3) and (2.4) into Equation (2.1) and assuming only structural damping, following nonlinear algebraic equation can be obtained.

$$(-(p\omega)^2\mathbf{M} + \mathbf{K} + i\mathbf{H}) \cdot \mathbf{x_p} + \mathbf{f_{N_p}} = \mathbf{f_p} \tag{2.5}$$

In the scope of this thesis, nonlinear algebraic equations are obtained by considering only the first harmonic terms. As a result equation (2.5) becomes,

$$(-\omega^2\mathbf{M} + \mathbf{K} + i\mathbf{H}) \cdot \mathbf{x} + \mathbf{f_N} = \mathbf{f} \tag{2.6}$$

2.2. Harmonic Balance Method

Harmonic balance method (HBM) is utilized in order to obtain the steady-state response of nonlinear differential equations. Considering the equation of motion defined by Equation (2.1), assumed response of the nonlinear system can be expressed as follows,

$$\mathbf{x} = \sum_{p=1}^{m} \left[\mathbf{x_{s_p}} \sin(p\theta) + \mathbf{x_{c_p}} \cos(p\theta)\right], \tag{2.7}$$

Where θ is expressed as,

$$\theta = \omega t, \tag{2.8}$$

In order to obtain the harmonic coefficients of internal nonlinear force, Fourier series expansion is utilized as follows,

$$\mathbf{f_N} = \sum_{p=1}^{m} \left[\mathbf{f_{N_s p}} \sin(p\theta) + \mathbf{f_{N_c p}} \cos(p\theta) \right], \tag{2.9}$$

Where $f_{N_s p}$ and $f_{N_c p}$ can be calculated as follows,

$$\mathbf{f_{N_s p}} = \frac{1}{\pi} \int_0^{2\pi} \mathbf{f_N} \sin(p\theta)\, d\theta, \tag{2.10}$$

$$\mathbf{f_{N_c p}} = \frac{1}{\pi} \int_0^{2\pi} \mathbf{f_N} \cos(p\theta)\, d\theta, \tag{2.11}$$

By substituting Equations (2.10) and (2.11) into Equation (2.6) and rewriting in terms of only real valued coefficients, equation of motion of nonlinear system can be expressed as follows,

$$\begin{bmatrix} \mathbf{K} - \omega^2 \mathbf{M} & -\mathbf{H} \\ \mathbf{H} & \mathbf{K} - \omega^2 \mathbf{M} \end{bmatrix} \begin{bmatrix} \mathbf{x_s} \\ \mathbf{x_c} \end{bmatrix} + \begin{bmatrix} \mathbf{f_{N_s}} \\ \mathbf{f_{N_c}} \end{bmatrix} = \begin{bmatrix} \mathbf{f_s} \\ \mathbf{f_c} \end{bmatrix}, \tag{2.12}$$

Where f_s and f_c are the sine and cosine coefficients of external forcing vector.

2.3. Modal Superposition Method

In the previous section, equation of motion of nonlinear system by using HBM is defined. If the HBM is utilized directly, the number of nonlinear equations to be solved can be very large for the structural systems with many degrees of freedom. Solving large number of equations might result in various numerical problems and increased computational times. In order to deal with these problems, Ferhatoğlu et al. [19] proposed modal superposition method to decrease the number of nonlinear equations.

In the modal superposition method, the response is written in terms of the linear system modes.

$$\mathbf{x(t)} = \sum_{r=1}^{N_m} a_r \, \boldsymbol{\phi}_\mathbf{r} \, e^{i\omega t}, \tag{2.13}$$

Where a_r is the complex coefficient of the r^{th} mode shape. ϕ_r is the r^{th} mode of the linear system. N_m is number of modes to be used in calculations. Matrix form of the equation is given as follows,

$$\mathbf{x} = \boldsymbol{\Phi a} e^{i\omega t}, \tag{2.14}$$

Substituting the Equation (2.14) into Equation (2.6) by assuming only structural damping and multiplying both sides with ϕ^T,

$$\left(-\omega^2 \boldsymbol{\Phi}^\mathbf{T}\mathbf{M}\boldsymbol{\Phi} + \boldsymbol{\Phi}^\mathbf{T}(\mathbf{K} + i\mathbf{H})\boldsymbol{\Phi}\right)\mathbf{a} + \boldsymbol{\Phi}^\mathbf{T}\mathbf{f_N} = \boldsymbol{\Phi}^\mathbf{T}\mathbf{f}, \tag{2.15}$$

If the modes shapes are mass normalized, the Equation (2.15) becomes,

$$\left(-\omega^2\mathbf{I} + \boldsymbol{\Omega}_\mathbf{n}(1 + i\gamma)\right)\mathbf{a} + \boldsymbol{\Phi}^\mathbf{T}\mathbf{f_N} = \boldsymbol{\Phi}^\mathbf{T}\mathbf{f}, \tag{2.16}$$

Where I is the identity matrix. Ω_n is diagonal matrix of natural frequencies of the system. γ is the proportional structural damping coefficient where,

$$\mathbf{H} = \gamma\mathbf{K}, \tag{2.17}$$

By only considering the real valued terms, Equation (2.16) can be rewritten as,

$$\begin{bmatrix} \boldsymbol{\Omega}_\mathbf{n} - \omega^2\mathbf{I} & -\gamma\boldsymbol{\Omega}_\mathbf{n} \\ \gamma\boldsymbol{\Omega}_\mathbf{n} & \boldsymbol{\Omega}_\mathbf{n} - \omega^2\mathbf{I} \end{bmatrix} \begin{bmatrix} \mathbf{a_s} \\ \mathbf{a_c} \end{bmatrix} + \begin{bmatrix} \boldsymbol{\Phi}^\mathbf{T}\,\mathbf{f_{N_s}} \\ \boldsymbol{\Phi}^\mathbf{T}\mathbf{f_{N_c}} \end{bmatrix} = \begin{bmatrix} \boldsymbol{\Phi}^\mathbf{T}\mathbf{f_s} \\ \boldsymbol{\Phi}^\mathbf{T}\mathbf{f_c} \end{bmatrix}, \tag{2.18}$$

Where a_s and a_c are the sine and cosine coefficients of mode shape matrix ϕ. In this method it is required to calculate complete nonlinear internal forcing vector. However, the number of nonlinear equations is determined by only the number of linear modes used to define the response of the system as shown in Equation (2.13). There are N_m number of complex equations and $2N_m$ number of real equations in total. Therefore, this method is especially important if the number of nonlinear elements is also large.

2.4. Solution of Nonlinear Algebraic Equations

In the steady state nonlinear vibration analysis, the equations governing the nonlinearities of the system converted into a set of nonlinear algebraic equations. Therefore, it is necessary to solve set of nonlinear algebraic equations in order to obtain the response of the nonlinear systems. For simple nonlinearities, analytic solution can be obtained for nonlinear algebraic equations. However, if the nonlinearities are complex, than iterative solution methods are necessary. In this thesis, Newton's method, which is one of the common and reliable iterative methods, is utilized for the iterative solution of nonlinear algebraic equations.

As shown in Equation (2.18) the nonlinear algebraic equations are depends on frequency, which means that there is a solution for each frequency. In most of the case, it is necessary to obtain the response for a certain frequency range, which is called frequency response functions (FRFs). In order to obtain FRFs path following methods are required. In path following methods, response of the function is obtained iteratively while the path following parameter changes in defined range. In nonlinear vibration analysis, path following parameter is the frequency. Therefore, the nonlinear response is obtained iteratively for each frequency point in order to generate the FRFs. In this thesis, Newton's method with Homotopy continuation and Newton's method with Arclength continuation is utilized in order to obtain the FRFs.

2.4.1. Newton's Method

Nonlinear algebraic equations defined in Equation (2.18) can be expressed as follows,

$$\mathbf{r}(\mathbf{a}, \omega) = 0, \tag{2.19}$$

Where,

$$\mathbf{r}(\mathbf{a}, \omega) = \begin{bmatrix} \boldsymbol{\Omega}_\mathbf{n} - \omega^2\mathbf{I} & -\gamma\boldsymbol{\Omega}_\mathbf{n} \\ \gamma\boldsymbol{\Omega}_\mathbf{n} & \boldsymbol{\Omega}_\mathbf{n} - \omega^2\mathbf{I} \end{bmatrix} \begin{bmatrix} \mathbf{a_s} \\ \mathbf{a_c} \end{bmatrix} + \begin{bmatrix} \boldsymbol{\Phi}^\mathbf{T}\,\mathbf{f}_{\mathbf{N_s}} \\ \boldsymbol{\Phi}^\mathbf{T}\mathbf{f}_{\mathbf{N_c}} \end{bmatrix} - \begin{bmatrix} \boldsymbol{\Phi}^\mathbf{T}\mathbf{f_s} \\ \boldsymbol{\Phi}^\mathbf{T}\mathbf{f_c} \end{bmatrix}, \tag{2.20}$$

Where,

$$\mathbf{a} = \begin{bmatrix} \mathbf{a_s} \\ \mathbf{a_c} \end{bmatrix}, \tag{2.21}$$

Expending the nonlinear equation set in Taylor series around a and neglecting higher order terms,

$$\mathbf{r}(\mathbf{a} + \boldsymbol{\delta}\mathbf{a}, \omega) = \mathbf{r}(\mathbf{a}, \omega) + \mathbf{J}(\mathbf{a}, \omega)\boldsymbol{\delta}\mathbf{a}, \tag{2.22}$$

Where $J(a, \omega)$ is,

$$\mathbf{J}(\mathbf{a}, \omega)_{i,j} = \frac{\partial \mathbf{r}_i}{\partial \mathbf{a}_j} = \frac{\mathbf{r}_i\left(\mathbf{a} + h_i e_j, \omega\right) - \mathbf{r}_i(\mathbf{a}, \omega)}{h_j}, \tag{2.23}$$

Where e_j is the unit vector in the j^{th} direction. h_j is a scaled step size. Considering $\mathbf{r}(\mathbf{a} + \boldsymbol{\delta}\mathbf{a}, \omega) = 0$ in Equation (2.22),

$$\boldsymbol{\delta}\mathbf{a} = -\mathbf{J}(\mathbf{a}, \omega)^{-1}\mathbf{r}(\mathbf{a}, \omega), \tag{2.24}$$

The iteration equation is,

$$\mathbf{a}^{\mathbf{new}} = \mathbf{a}^{\mathbf{old}} + \boldsymbol{\delta}\mathbf{a}, \tag{2.25}$$

Substituting Equation (2.24) into Equation (2.25),

$$\mathbf{a}^{i+1} = \mathbf{a}^i - \mathbf{J}(\mathbf{a}, \omega)^{-1}\mathbf{r}\left(\mathbf{a}^i, \omega\right). \tag{2.26}$$

2.4.2. Homotopy Continuation Method

Homotopy continuation method (HCM) is a path following solution method, which is utilized in order to solve the strongly nonlinear systems. In nonlinear vibration analysis, especially near the resonance region nonlinear internal forces becomes higher, and Newton's method fails to converge because of lack of initial guesses. In order to deal with this problem HCM can be enforced such that nonlinear system of equations are solved away from the resonance region where the nonlinear forces are very small by utilizing the solution of linear system as an initial guess. Afterwards by increasing or decreasing the frequency, system of nonlinear equations can be solved for a certain frequency range by using the previous solution as an initial guess to next solution.

In this method, nonlinear forces are assumed to be not changing too much as the frequency changes so that the solution of the nonlinear system is close to the solution of the previous case. If the nonlinear forces are changing too much for a certain frequency increment, then the increment size should be decreased in order to assure the convergence of the solution.

2.4.3. Arclength Continuation Method

HCM by utilizing the Newton's method may suffer convergence problem depending on the nonlinear system. This usually happens when the solution path turns back, where the Jacobian matrix becomes singular. Therefore, inverse of Jacobian matrix cannot be calculated. In order to solve this problem and follow the path Arclength continuation method (ACM) is proposed. In ACM, arclength parameter is added to the nonlinear system of equation in order to make the Jacobian matrix non-singular. The unknowns for the system becomes,

$$\mathbf{q} = \begin{bmatrix} \mathbf{a} \\ \omega \end{bmatrix}, \tag{2.27}$$

Equation for the new unknown, which is a sphere centered at previous solution is as follows,

$$(\mathbf{a}_k - \mathbf{a}_{k-1})^2 + (\omega_k - \omega_{k-1})^2 = s^2, \tag{2.28}$$

Where s is the path following parameter. k is the index of solution points. Equation (2.28) can be rewritten as follows,

$$h(\mathbf{a}_k, \omega_k) = \Delta\mathbf{q}_k^T \, \Delta\mathbf{q}_k - s^2 = 0, \tag{2.29}$$

Where,

$$\Delta\mathbf{q}_k = \begin{bmatrix} \Delta\mathbf{a}_k \\ \Delta\omega_k \end{bmatrix}, \tag{2.30}$$

Where,

$$\Delta\mathbf{a}_k = \mathbf{a}_k - \mathbf{a}_{k-1}, \tag{2.31}$$

$$\Delta\omega_k = \omega_\mathrm{k} - \omega_{k-1}, \tag{2.32}$$

Iteration step using the Newton's method can be rewritten for ACM as follows,

$$\mathbf{q}_{k+1} = \mathbf{q}_k - \begin{bmatrix} \dfrac{\partial \mathbf{r}(\mathbf{a}_k, \omega_k)}{\partial x} & \dfrac{\partial \mathbf{r}(\mathbf{a}_k, \omega_k)}{\partial \omega} \\ \dfrac{\partial h(\mathbf{a}_k, \omega_k)}{\partial x} & \dfrac{\partial h(\mathbf{a}_k, \omega_k)}{\partial \omega} \end{bmatrix}^{-1} \begin{bmatrix} \mathbf{r}(a_k, \omega_k) \\ h(a_k, \omega_k) \end{bmatrix} \tag{2.33}$$

Where,

$$\begin{bmatrix} \dfrac{\partial h(\mathbf{a}_k, \omega_k)}{\partial x} & \dfrac{\partial h(\mathbf{a}_k, \omega_k)}{\partial \omega} \end{bmatrix} = [2\Delta\mathbf{q}_k]^T, \tag{2.34}$$

CHAPTER 3

CONTACT MODELS

3.1. Overview

Contact is the utmost critical issue in the modeling of structural joints considering the fact that behaviors of the structures connected together are well-known. For decades variety of models are introduced in order to capture the nature of contact accurately. In chapter 2, several friction models, which are studied in literature, are briefly mentioned. In this chapter, two types of contact models utilized in the nonlinear analysis of bolted joints are introduced. The first one is the 1D dry friction element with constant normal load. This model is the extended version of Coloumb's friction model, where the linear spring is included in order to allow elastic deformation of the contact surface. The second one is the 1D dry friction element with normal load variation. This model is originally developed by Yang et al. [14].

3.2. 1D Dry Friction Element with Constant Normal Load

Representation of one dimensional dry friction element with constant normal load can be seen in Figure 3.1. Body 2 is considered to be grounded. u, w, k_d, μ and n_0 are tangential relative motion, tangential slip motion, tangential contact stiffness, coefficient of friction and constant normal load respectively.

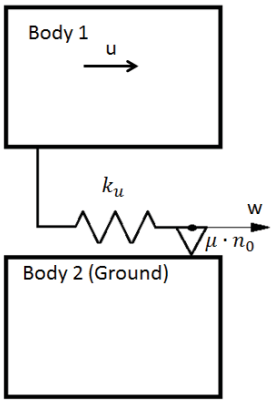

Figure 3.1. One dimensional dry friction element with constant normal load

Friction force (nonlinear internal force) can be expressed as,

$$f = k_t(u - w) \tag{3.1}$$

When the body 1 starts to slip, friction force can be expressed as follows,

$$f = \pm \mu n_0 \tag{3.2}$$

Equation (3.1) and (3.2) are equal to each other at the instant of slip to stick transition. By differentiating Equation (3.1) and (3.2),

$$\dot{f} = k_t(\dot{u} - \dot{w}) \tag{3.3}$$

$$\dot{f} = 0 \tag{3.4}$$

Therefore,

$$\dot{u} = \dot{w} \tag{3.5}$$

When the friction element sticks,

$$\dot{w} = 0 \tag{3.6}$$

Therefore from Equation *(3.5)*,

$$\dot{u} = 0 \tag{3.7}$$

It can be seen that slip to stick transition occurs when the relative motion reverses its direction. When the friction force increases and reaches its limiting value, stick to slip transition occurs. Friction force at the stick state can be given as

$$f = k_t(u - u_0) + f_0 \tag{3.8}$$

Where u_0 and f_0 are relative displacement and friction force at the begining of stick state respectively. Stick to slip transition can be determined utilizing Equations (3.2) and (3.8) as follows,

$$k_t(u - u_0) + f_0 = \pm\mu n_0 \tag{3.9}$$

By assuming a single harmonic motion, transition angles can be obtained analytically as follows,

$$u(t) = Asin(\theta) \tag{3.10}$$

Where A is amplitude of the motion. θ can be expressed as,

$$\theta = \omega t + \phi \tag{3.11}$$

Where ω and ϕ are frequency and phase angle respectively. By substituting Equation (3.10) into Equation (3.7), slip to stick angles can be obtained as follows,

$$\dot{u} = A\omega\, cos(\theta) = 0 \tag{3.12}$$

$$\theta_{stick} = \frac{\pi}{2}, \frac{3\pi}{2} \tag{3.13}$$

By utilizing Equation *(3.9)* stick to positive slip angles can be obtained as follows,

$$k_t(u - u_0) + f_0 = \mu n_0 \tag{3.14}$$

Previous state of contact before stick to positive slip transition is negative slip. Therefore,

$$u_0 = Asin\left(\frac{3\pi}{2}\right) = -A \tag{3.15}$$

$$f_0 = -\mu n_0 \tag{3.16}$$

By substituting Equations (3.15) and (3.16) into (3.14) stick to positive slip angle can be obtained as follows,

$$\theta_{sp} = asin\left(\frac{2\mu n_0}{Ak_t} - 1\right) \tag{3.17}$$

Stick to negative slip angle can also be calculated similarly as follows,

$$\theta_{sn} = asin\left(1 - \frac{2\mu n_0}{Ak_t}\right) \tag{3.18}$$

Therefore, when the stick-slip motion occurs, friction force for a single harmonic motion can be expressed as follows,

$$f(\theta) = \begin{cases} k_t(Asin(\theta) - A) + \mu n_0, & \frac{\pi}{2} \leq \theta \leq \theta_{sn} \\ -\mu n_0, & \theta_{sn} \leq \theta \leq \frac{3\pi}{2} \\ k_t(Asin(\theta) + A) - \mu n_0, & \frac{3\pi}{2} \leq \theta \leq \theta_{sp} \\ \mu n_0, & \theta_{sp} \leq \theta \leq \frac{5\pi}{2} \end{cases} \tag{3.19}$$

When the relative displacement (u(t)) is small such that the friction force never reaches its limiting value, the friction element is in complete stick state. The condition for complete stick case can be obtained by consedering stick to slip angles nonexistent as follows,

$$\left|\frac{\mu n_0}{A k_t}\right| \geq 1 \tag{3.20}$$

For a single harmonic motion friction force of complete stick case can be expressed as follows,

$$f(\theta) = k_t A sin(\theta) \tag{3.21}$$

In chapter 2, it is shown that nonlinear internal force can be expressed in terms of harmonic coefficients by using harmonic balance method. When there is a stick-slip motion, nonlinear force is expressed in Equation (3.19). By using Equation (2.9) nonlinear internal force can be expressed as follows,

$$f_n = f_s\, sin(\theta) + f_c cos(\theta) \tag{3.22}$$

Where,

$$f_s = \frac{1}{\pi}\left(\int_{\frac{\pi}{2}}^{\theta_{sn}} (k_t(Asin(\theta) - A) + \mu n_0)\, sin(\theta)\, d\theta + \int_{\theta_{sn}}^{\frac{3\pi}{2}} (-\mu n_0)\, sin(\theta)\, d\theta + \int_{\frac{3\pi}{2}}^{\theta_{sp}} (k_t(Asin(\theta) + A) - \mu n_0)\, sin(\theta)\, d\theta + \int_{\theta_{sp}}^{\frac{5\pi}{2}} \mu n_0\, sin(\theta)\, d\theta\right) \tag{3.23}$$

$$f_c = \frac{1}{\pi}\left(\int_{\frac{\pi}{2}}^{\theta_{sn}} (k_t(Asin(\theta) - A) + \mu n_0) cos(\theta) d\theta + \int_{\theta_{sn}}^{\frac{3\pi}{2}} (-\mu n_0)\, cos(\theta)\, d\theta + \int_{\frac{3\pi}{2}}^{\theta_{sp}} (k_t(Asin(\theta) + A) - \mu n_0)\, cos(\theta)\, d\theta + \int_{\theta_{sp}}^{\frac{5\pi}{2}} \mu n_0\, cos(\theta)\, d\theta\right) \tag{3.24}$$

It should be noted that nonlinear internal force in nonlinear algebraic equations does not depend on θ but it depends on ωt. Therefore, Equation (3.22) can be rewritten as follows,

$$F_n = F_s\, sin(\omega t) + F_c cos(\omega t) \tag{3.25}$$

Where,

$$F_s = f_s\, cos(\phi) - f_c sin(\phi) \tag{3.26}$$

$$F_c = f_s\, sin(\phi) + f_c cos(\phi) \tag{3.27}$$

By using Equations *(3.10)* and *(3.11)*, ϕ can be calculated as,

$$\begin{aligned} u(t) = Asin(\theta) &= Asin(\omega t + \phi) \\ &= A\,cos(\phi)\,sin(\omega t) + Asin(\phi)cos(\omega t) \\ &= a_s\,sin(\omega t) + b_s cos(\omega t) \end{aligned} \tag{3.28}$$

Hence,

$$A = \sqrt{a_s^2 + a_c^2} \tag{3.29}$$

$$\phi = atan\left(\frac{a_c}{a_s}\right) \tag{3.30}$$

When there is no stick-slip motion, friction element always sticks. In that case the equation for nonlinear internal force is given in Equation (3.21), which does not require Fourier series expansion.

3.3. 1D Dry Friction Element with Normal Load Variation

Schematic representation of dry friction element with normal load variation is shown in Figure 3.2.

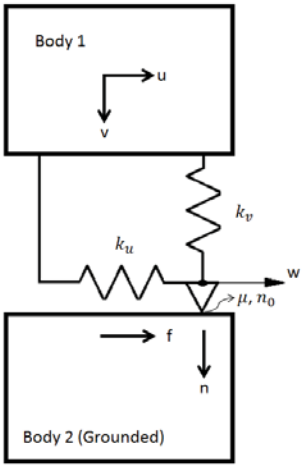

Figure 3.2. One dimensional dry friction element with normal load variation

Body 2 is considered to be grounded. u, v, w, k_u,k_v, μ, n_0,f and n are the tangential motion, normal motion, slip motion, tangential contact stiffness, normal contact stiffness, coefficient of friction, initial normal load, tangential friction force and variable normal load respectively. Tangential friction force and variable normal load can be expressed as follows,

$$f = k_u(u - w) \tag{3.31}$$

$$n = \begin{cases} n_0 + k_v v, & v \geq -\dfrac{n_0}{k_v} \\ 0, & v \geq -\dfrac{n_0}{k_v} \end{cases} \tag{3.32}$$

When tangential and normal motions are sufficiently small, the contact interface always sticks, where the friction element behaves as tangential and normal linear springs. As the vibratory motion grows larger, the contact surface might start to slip motion where the tangential friction force remains equal to variable slip load. At the instant the contact interface sticks again, tangential motion does not necessarily reverse its direction as in the case of dry friction model with constant normal load. This is because slip to stick transition depends on tangential motion (u) and variable

normal load (n), where it also depends on normal motion. The variable normal load might become smaller and smaller such that the contact surfaces separate during the course of vibration, where the tangential friction force becomes zero.

When the interface sticks, where the slip motion (w) becomes zeros, tangential friction force becomes,

$$f = k_u(u - u_0) + f_0 \tag{3.33}$$

Where u_0 and f_0 are the tangential motion and tangential friction force at the beginning of stick state. When the slip motion starts in positive direction, tangential friction force becomes,

$$f = \mu n \tag{3.34}$$

By substituting Equation *(3.32)* into Equation *(3.34)*,

$$f = \mu n_0 + \mu k_v v \tag{3.35}$$

Similarly tangential friction force for negative slip state can be expressed as follows,

$$f = -(\mu n_0 + \mu k_v v) \tag{3.36}$$

During the cycle of motion four distinct states, which are stick state, positive slip state, negative slip state and separation state might be possible. Therefore, transitions between the states need to be clarified.

Transition from stick state to positive slip state and negative slip state can be obtained by equating the tangential friction force at stick state to tangential friction force at positive slip state and tangential friction force at negative slip state respectively. Transition from stick state to positive slip state is expressed as follows,

$$k_u(u - u_0) + f_0 - (\mu n_0 + \mu k_v v) = 0 \tag{3.37}$$

$$k_u \dot{u} - \mu k_v \dot{v} > 0 \tag{3.38}$$

Equation (3.38) is used in order to assure the positive slip condition. Similarly transition from stick state to negative slip state can be obtained as follows,

$$k_u(u - u_0) + f_0 + (\mu n_0 + \mu k_v v) = 0 \tag{3.39}$$

$$k_u \dot{u} + \mu k_v \dot{v} < 0 \tag{3.40}$$

Again the Equation (3.40) is for the assurance of negative slip condition. From stick condition to separation condition occurs when the normal load becomes zero. Therefore,

$$n_0 + k_v v = 0 \tag{3.41}$$

$$\dot{v} < 0 \tag{3.42}$$

Where, the Equation (3.42) is to guarantee the separation condition. Slip motion for positive slip state can be obtained by differentiating Equations (3.31) and (3.35) as follows,

$$\dot{w} = \frac{k_u \dot{u} - \mu k_v \dot{v}}{k_u} \tag{3.43}$$

Transition from positive slip state to stick state is at the instant when the slip motion becomes zero. Therefore, by utilizing Equation (3.43),

$$\frac{k_u\dot{u} - \mu k_v\dot{v}}{k_u} = 0 \tag{3.44}$$

$$\frac{k_u\ddot{u} - \mu k_v\ddot{v}}{k_u} < 0 \tag{3.45}$$

Equation (3.45) is to assure positive slip condition. Similarly transition from negative slip state to stick state can be obtained as follows,

$$\frac{k_u\dot{u} + \mu k_v\dot{v}}{k_u} = 0 \tag{3.46}$$

$$\frac{k_u\ddot{u} + \mu k_v\ddot{v}}{k_u} > 0 \tag{3.47}$$

Transition from positive slip state and negative slip state to separation state is the same as transition from stick state to separation state given in equation (3.41) and (3.42). As the normal load starts to develop, end of separation occurs on the contact interface. Therefore, following equations must be satisfied,

$$n_0 + k_v v = 0 \tag{3.48}$$

$$\dot{v} > 0 \tag{3.49}$$

At the end of separation state, it is possible that positive slip state, negative slip state or stick state occur. Therefore, states after the end of separation should be clarified. If the state after the separation is stick state, slip motion should be zero. And also the following condition should be valid.

$$-\mu\dot{n} < \dot{f} < \mu\dot{n} \tag{3.50}$$

Where rate of change of tangential friction force and normal load are as follows,

$$\dot{f} = k_u \dot{u} \tag{3.51}$$

$$\dot{n} = k_v \dot{v} \tag{3.52}$$

Note that rate of change of friction force does not depend on slip motion since the slip motion is zero. By substituting the Equations (3.51) and (3.52) into equation (3.50) condition for stick state after the end of separation can be obtained as follows,

$$-\frac{\mu k_v \dot{v}}{k_u} < \dot{u} < \frac{\mu k_v \dot{v}}{k_u} \tag{3.53}$$

Similarly, conditions for positive slip state and negative slip state after the end of separation are as follows respectively,

$$\dot{u} > \frac{\mu k_v \dot{v}}{k_u} \tag{3.54}$$

$$\dot{u} < -\frac{\mu k_v \dot{v}}{k_u} \tag{3.55}$$

For a single harmonic motion transition angles can be obtained analytically by using the transition states mentioned above. Assuming a cyclic motion

$$u = a\ sin(\theta) \tag{3.56}$$

$$v = b\ sin(\theta + \phi) \tag{3.57}$$

Where

$$\theta = \omega t \tag{3.58}$$

ω and t are frequency of motion and time respectively. From the above transition states, eight transition angles need to be calculated. These transition angles are given in Table 3.1.

Table 3.1. *Representation of transition angles*

Transition angles	Representation
Transition angle from positive slip to stick	θ_E^P
Transition angle from negative slip to stick	θ_E^N
Transition angle from positive slip to stick to negative slip	${}_P\theta_N^E$
Transition angle from negative slip to stick to positive slip	${}_N\theta_P^E$
Transition angle for start of separation	θ_S^*
Transition angle for end of separation	θ_*^S
Transition angle from separation to stick to positive slip	${}_S\theta_P^E$
Transition angle from separation to stick to negative slip	${}_S\theta_N^E$

By substituting Equation *(3.56)* and *(3.57)* into Equation *(3.44)*, and solving for θ,

$$\theta_E^P = tan\left(\frac{-ak_u + b\mu k_v\, cos(\phi)}{b\mu k_v\, sin(\phi)}\right)^{-1} \tag{3.59}$$

Similarly negative slip to stick angle can be obtained as follows,

$$\theta_E^N = tan\left(\frac{ak_u + b\mu k_v\, cos(\phi)}{b\mu k_v\, sin(\phi)}\right)^{-1} \tag{3.60}$$

Since the stick to slip transition requires the condition from previous state, it is necessary to calculate the f_0 and u_0 in Equation *(3.39)* considering the positive slip state in order to calculate the transition angle from positive slip to stick to negative slip. Therefore, by using Equations (3.35), (3.56) and (3.57),

$$f_0 = \mu n_0 + \mu k_v b \sin(\theta_E^P + \phi) \tag{3.61}$$

$$u_0 = a \sin(\theta_E^P) \tag{3.62}$$

And by using Equations (3.39), (3.61) and (3.62) transition angle from positive slip to stick to negative slip can be expressed as follows,

$${}_P\theta_N^E = \cos\left(\frac{C_N}{\sqrt{A_N^2 + B_N^2}}\right)^{-1} + \tan\left(\frac{A_N}{B_N}\right)^{-1} \tag{3.63}$$

Where,

$$A_N = ak_u + b\mu k_v \cos(\phi) \tag{3.64}$$

$$B_N = b\mu k_v \sin(\phi) \tag{3.65}$$

$$C_N = -(2n_0\mu - ak_u \sin(\theta_E^P) + b\mu k_v \cos(\phi) \sin(\theta_E^P) + b\mu k_v \cos(\theta_E^P) \sin(\phi)) \tag{3.66}$$

Similarly transition angle from negative slip to stick to positive slip angles can be obtained as,

$${}_N\theta_P^E = \cos\left(\frac{C_P}{\sqrt{A_P^2 + B_P^2}}\right)^{-1} + \tan\left(\frac{A_P}{B_P}\right)^{-1} \tag{3.67}$$

Where,

$$A_P = ak_u - b\mu k_v \cos(\phi) \tag{3.68}$$

$$B_P = -b\mu k_v sin(\phi) \tag{3.69}$$

$$C_P = 2n_0\mu + ak_u\, sin(\theta_E^N) + b\mu k_v\, cos(\phi)\, sin(\theta_E^N) + b\mu k_v\, cos(\theta_E^N)\, sin(\phi) \tag{3.70}$$

Start and end of separation angles can be calculated by using Equation (3.41) as follows,

$$\theta_1^{Sep} = -\phi + sin\left(-\frac{n_0}{k_v b}\right)^{-1} \tag{3.71}$$

$$\theta_2^{Sep} = \pi - \phi - sin\left(-\frac{n_0}{k_v b}\right)^{-1} \tag{3.72}$$

$$\theta_S^* = \begin{cases} \theta_1^{Sep}, & b\, cos(\theta_1^{Sep} + \phi) < 0 \\ \theta_2^{Sep}, & b\, cos(\theta_2^{Sep} + \phi) < 0 \end{cases} \tag{3.73}$$

Similarly,

$$\theta_*^S = \begin{cases} \theta_1^{Sep}, & b\, cos(\theta_1^{Sep} + \phi) > 0 \\ \theta_2^{Sep}, & b\, cos(\theta_2^{Sep} + \phi) > 0 \end{cases} \tag{3.74}$$

Separation to stick to positive slip angle can be expressed by using the similar procedure as in the calculation of ${}_P\theta_N^E$ and ${}_N\theta_P^E$ as follows,

$${}_S\theta_P^E = cos\left(\frac{C_{SP}}{\sqrt{A_{SP}^2 + B_{SP}^2}}\right)^{-1} + tan\left(\frac{A_{SP}}{B_{SP}}\right)^{-1} \tag{3.75}$$

Where,

$$A_{SP} = ak_u - b\mu k_v cos(\,\phi\,) \tag{3.76}$$

$$B_{SP} = -b\mu k_v sin(\phi) \tag{3.77}$$

$$C_{SP} = \mu n_0 + a k_u sin(\theta_*^S) \tag{3.78}$$

Similarly,

$$_S\theta_N^E = cos\left(\frac{C_{SN}}{\sqrt{A_{SN}^2 + B_{SN}^2}}\right)^{-1} + tan\left(\frac{A_{SN}}{B_{SN}}\right)^{-1} \tag{3.79}$$

Where,

$$A_{SN} = a k_u + b\mu k_v cos(\ \phi\ ) \tag{3.80}$$

$$B_{SN} = b\mu k_v sin(\phi) \tag{3.81}$$

$$C_{SN} = -\mu n_0 + a k_u sin(\theta_*^S) \tag{3.82}$$

There are 13 distinct sequence of motion for a single harmonic motion, where it can be classified into 4 main cases, which are fully separated, separation, slip but no separation and fully stick. Fully separated condition occurs when normal load vanishes completely throughout the cycle of motion. When it is fully separated, both tangential friction force and normal load becomes zero. The condition for fully separation can be expressed as follows,

$$n_0 + k_v b < 0 \tag{3.83}$$

When the above condition is not satisfied and the normal motion grows to a point such that,

$$n_0 < k_v b \tag{3.84}$$

Then the separation case occurs. 10 different cycle of motion is possible in separation states, which are given in Table 3.2, where S, E, P and N denote separation state, stick state, positive slip state and negative slip state respectively. By using the Equations (3.53), (3.54) and (3.55), case P, case N and case E in *Table 3.2* should be decided first. Afterwards, according to occurrences of transition angles sub cases should be decided. For example, if the Equation (3.54) is satisfied, then it is necessary to decide on case N1, case N2 and case N3. If there is no negative slip to stick angle between the end of separation angle and start of separation angle, then case N3 for the cycle of motion should be chosen. Other cases can also be chosen similarly.

Table 3.2. *Stick slip motion when the separation occurs*

Case P			Case N			Case E			
Case P1	Case P2	Case P3	Case N1	Case N2	Case N3	Case E1	Case E2	Case E3	Case E4
θ_S^*	θ_S^*	θ_S^*	θ_S^*	θ_S^*	θ_S^*	θ_S^*	θ_S^*	θ_S^*	θ_S^*
S	S	S	S	S	S	S	S	S	S
θ_*^S	θ_*^S	θ_*^S	θ_*^S	θ_*^S	θ_*^S	θ_*^S	θ_*^S	θ_*^S	θ_*^S
P	P	P	N	N	N	E	E	E	E
θ_E^P	θ_E^P	θ_S^*	θ_E^N	θ_E^N	θ_S^*	${}_S\theta_P^E$	${}_S\theta_P^E$	${}_S\theta_N^E$	${}_S\theta_N^E$
E	E		E	E		P	P	N	N
${}_P\theta_N^E$	${}_P\theta_N^E$		${}_N\theta_P^E$	${}_N\theta_P^E$		θ_E^P	θ_S^*	θ_E^N	θ_S^*
N	N		P	P		E		E	
θ_E^N	θ_S^*		θ_E^P	θ_S^*		${}_P\theta_N^E$		${}_N\theta_P^E$	
E			E			N		P	
${}_N\theta_P^E$			${}_P\theta_N^E$			θ_S^*		θ_S^*	
P			N						
θ_S^*			θ_S^*						

When the conditions for fully separation and partial separation are not satisfied, then the occurrences of transition angle from positive slip to stick to negative slip and transition angle from negative slip to stick to positive slip decides the condition for slip but no separation or fully stick. If the slip to stick angles exist such that it can form the following cycle of motion,

$$\theta_{E}^{P} \rightarrow E \rightarrow {}_{P}\theta_{N}^{E} \rightarrow N \rightarrow \theta_{E}^{N} \rightarrow E \rightarrow {}_{N}\theta_{P}^{E} \rightarrow P \rightarrow \theta_{E}^{P} + 2\pi$$

Than the slip but no separation condition is realized. If none of the above conditions are satisfied, the contact state is said to be in fully stick state.

CHAPTER 4

REDUCED ORDER JOINT MODELING UTILIZING 1D DRY FRICTION ELEMENT WITH CONSTANT NORMAL LOAD

4.1. Overview

In chapter 3, dry friction element with constant normal load is explained in detail. In this chapter by utilizing the dry friction element with constant normal load, node-to-node contact model for Break-Reuß beam [8] is constructed. Then by utilizing a microslip approximation, a reduced order model is established. In order to create the node-to-node contact model and the reduced order model nonlinear static analysis is realized to obtain the normal load distribution. After obtaining the normal load distribution, node-to-node contact model is established. Frequency response functions (FRF) are obtained for node-to-node contact model at several excitation levels. Afterwards several type of reduced order models are created, and their FRF plots are obtained. Then the results are compared with the node-to-node contact model.

4.2. Nonlinear Static Analysis of Break-Reuß Beam

In Figure 4.1 3D model of Break-Reuß beam, which is widely used in the literature can be seen. Abaqus FEA software is used for the nonlinear static analysis of the Break-Reuß beam. The model consists of two beams, three bolts, six washers and six nuts. Steel material properties (Elastic modulus: 190GPa, Poisson's ratio: 0.3, Density: 7900 kg/m^3) are imposed for all the parts in the model. In this model; bolts, washers and nuts are connected to each other so that they behave as a single part (tie constraint). Surface to surface contact algorithm with the penalty method is imposed between the contacting surfaces of beam structures in order to obtain the contact pressure distribution. In order to discard singularity problem in static analysis, fix-free boundary condition is imposed. 11500 N preload is applied from the center of the bolt

shank to each bolt in the model. Finite element model (FEM) of Break-Reuß beam and the normal contact force distribution obtained through static analysis are shown in Figure 4.2

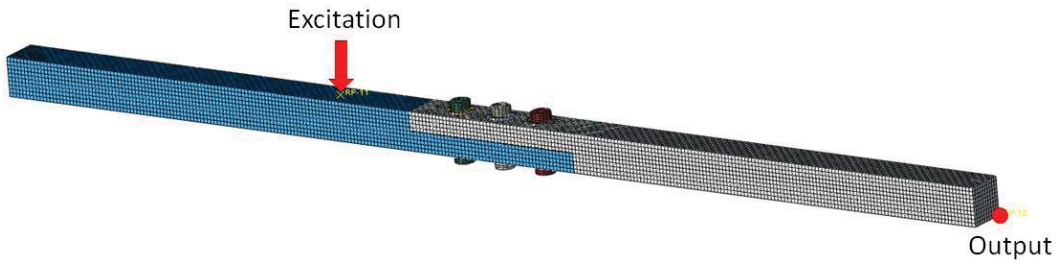

Figure 4.1. 3D model of Break Reuß beam

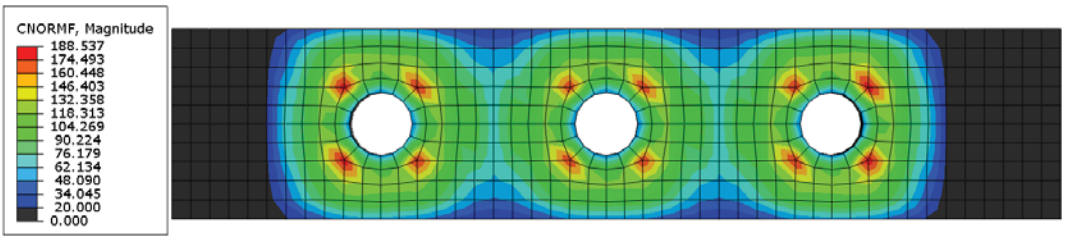

Figure 4.2. Normal force distribution of contact surface

4.3. Representative High Fidelity Model

In this model, all the nodes coincident to each other in the contact area are connected with one dimensional dry friction elements with constant normal loads. 1D-macroslip friction elements consist of three parameters: tangential stiffness, normal load and coefficient of friction. In this model, tangential stiffness and coefficient of friction for all the friction elements are assumed to be 1000 N/mm and 0.12, respectively. Normal contact forces obtained from nonlinear static analysis are used as the normal loads acting on the friction elements. Locations of the contact nodes used in the high fidelity model are shown in Figure 4.3 which are selected based on the normal contact force distribution given in Figure 4.2. Harmonic Balance Method with Modal Superposition

Method, which is explained in chapter 2 is implemented in order to obtain the nonlinear algebraic equation set. In order to apply Modal Superposition Method, resonance frequencies and mode shapes of the linear system are required. The linear system is the same model, which is used in nonlinear static analysis except that there is a nonlinear contact surface definition and fix-free boundary condition in nonlinear static analysis. In the linear system contact surface definition is removed and free-free boundary condition is imposed to the system. Afterwards modal analysis is realized by using the Abaqus FEA sofware in order to obtain the mode shapes and natural frequencies of linear system. It should be reminded that modal superposition method is utilized in order to decrease the nonlinear equation number to be solved. In order to do that response is assumed to be consists of linear mode shapes and their modal coefficients. In this analysis six rigid body modes and first three bending modes of the system are utilized in modal superposition method. Since the rigid body modes of the system are obvious, only the first three bending modes of the system are shown in Figure 4.4, Figure 4.5 and Figure 4.6.

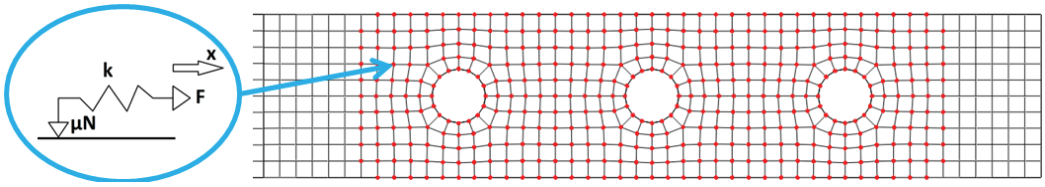

Figure 4.3. Location of nodes connected with dry friction elements

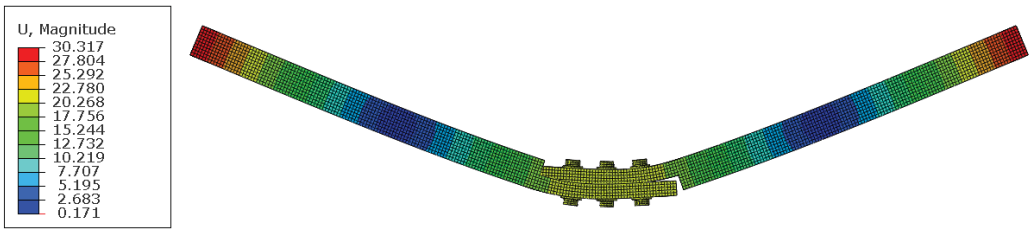

Figure 4.4. First bending mode: 126 Hz

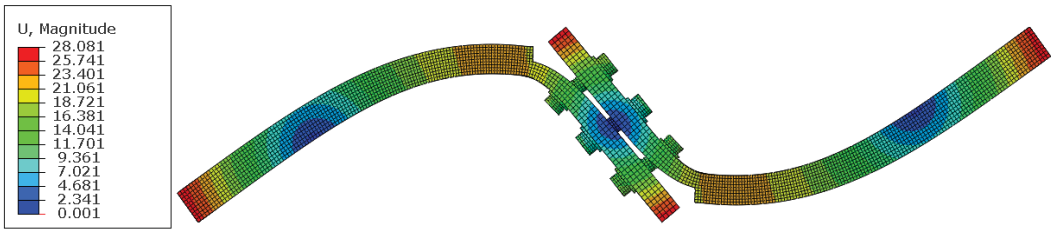

Figure 4.5. Second bending mode: 532 Hz

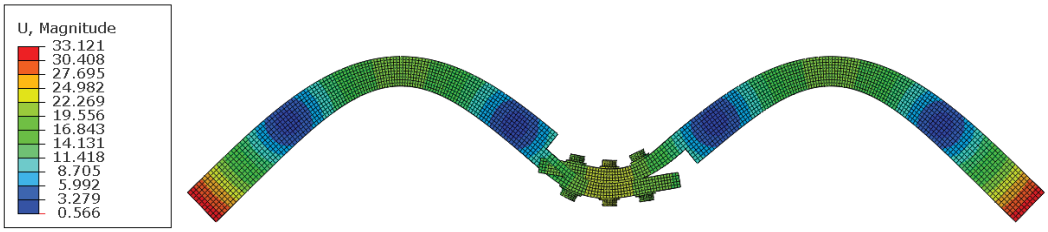

Figure 4.6. Third bending mode: 1068 Hz

After creating the node-to-node contact model FRFs for several excitation levels are obtained by utilizing the Homotopy continuation method, which is explained in chapter 2. The excitation location and output location are shown in Figure 4.1. FRF plots are shown in Figure 4.7 When the excitation levels are small (F = 1 N), Complete stick motion dominates the contact surface where there is no hysteretic behavior which means there is no energy loss in the system. As the excitation level increases, stick slip motion starts to dominate the contact surface. In that case hysteretic behavior causes the system to loose energy. Therefore, amplitude of FRF plots decreases. Besides, when the some of the macroslip elements on contact surface perform slip motions, overall system loses stiffness because there is a limiting value ($\pm\mu N$) for each macro slip element as stated in chapter 3. Hence, the resonance frequency of the system decreases also.

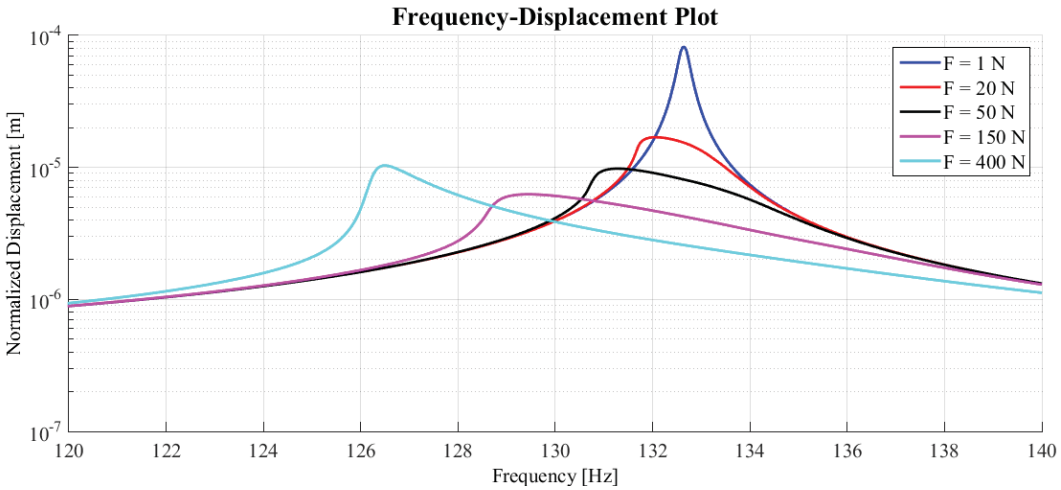

Figure 4.7. Receptance plots of node-to-node contact model

4.4. Reduced Order Bolted Joint Approximation

The main idea in the reduced order bolted joint approximation is that 1D dry friction elements with constant normal load are combined together such that they behave as a discrete microslip friction elements. Schematic representation of 1D dry friction element and its hysteresis loop is shown in Figure 4.8 and Figure 4.9

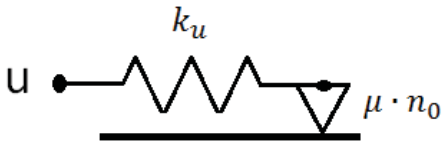

Figure 4.8. Schematic representation of 1D dry friction element

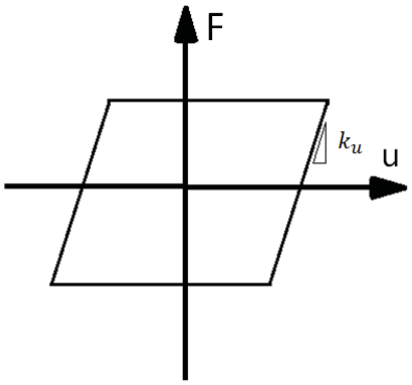

Figure 4.9. Hysteresis loop of 1D dry friction element

In 1D dry friction element with constant normal load when friction element reaches its limiting value ($\pm\mu N$), tangential friction force become constant. By using only one dry friction element only gross slip can be modeled, where the whole contact surface assumed to be sliding. However, the structures with bolted joint have a variable contact force distribution. The contact forces near the bolt hole are sufficiently high; whereas, they become very low at some distant. Microslip like behavior occurs due to variability in contact forces. Therefore, it is crucial to model the microslip friction. In this section, the microslip friction element developed by Cigeroglu et al. [17] is used in modeling of bolted connections. However, in this section, normal load variation is neglected. Effect of normal load variation is studied in next chapter. By combining the 1D dry friction element with constant normal load such as parallel connected linear spring elements, a microslip approximation can be obtained as can be seen in Figure 4.10. Representative hysteresis loop of approximated microslip model is given in Figure 4.11.

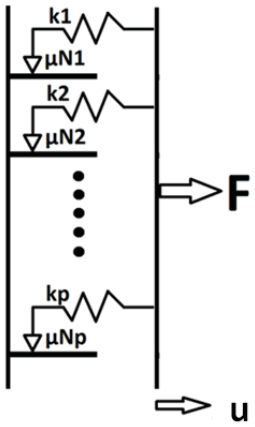

Figure 4.10. Schematic representation of approximated microslip element

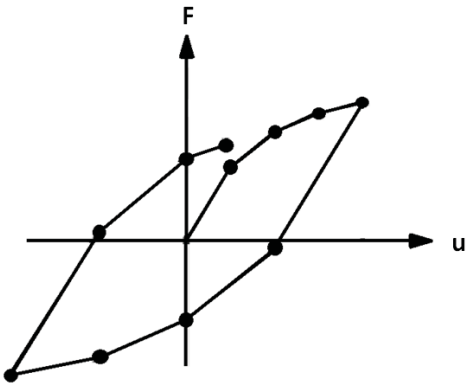

Figure 4.11. Hysteresis loop of approximated microslip element

Since the macroslip elements are connected in parallel, Fourier coefficient of approximated microslip element can be obtained by summation of individual macroslip elements as shown in Equation (4.1) and (4.2).

$$F_{s_{joint}} = \sum_{n=1}^{p} F_{s_n} \tag{4.1}$$

$$F_{c_{joint}} = \sum_{n=1}^{p} F_{c_n} \tag{4.2}$$

In this chapter, microslip approximation is realized with two reduction steps. In the first reduction step, contact surface is divided into several regions, and the individual macroslip elements inside the region became the sub element of approximated microslip element. Representation of the approximation is shown in Figure 4.12. In the second reduction step, approximated microslip element is further reduced into combination of several macroslip element such that hysteresis loop of microslip element with first reduction is very close to the hysteresis loop of microslip element with secondary reduction. The secondary reduction will be explained in detail after the first reduction.

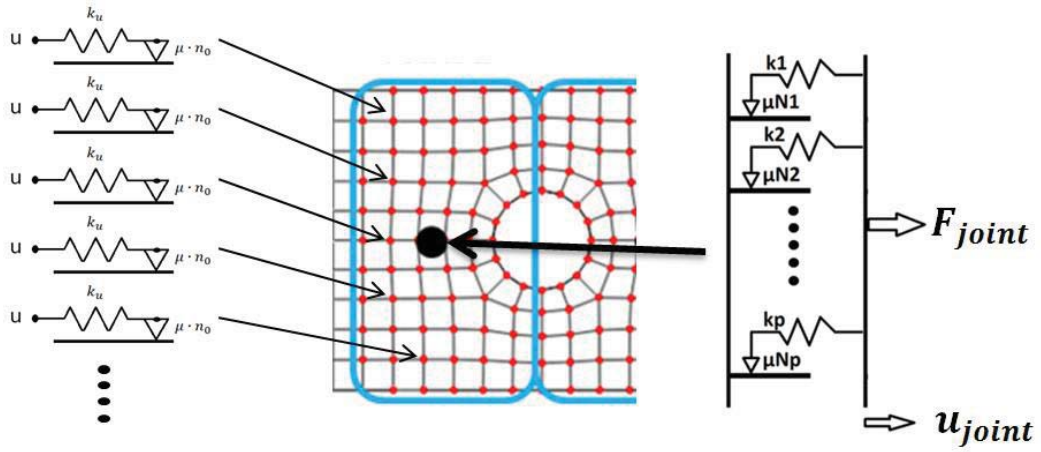

Figure 4.12. Schematic representation of reduced order joint model concept

The next important issue is how to impose the approximated microslip friction element. In the node-to-node contact model macroslip elements are connected to coincident nodes. Therefore, nonlinear tangential force can be calculated by utilizing the relative displacement of coincident nodes. By utilizing modal superposition method relative displacements for node-to-node contact model can be expressed as,

$$\mathbf{u}_A - \mathbf{u}_B = (\mathbf{\Phi}_A - \mathbf{\Phi}_B)\mathbf{a} \tag{4.3}$$

Where the ϕ_A and ϕ_B are mode shape matricies of coincident nodes at a region of contact surfaces. a, u_A and u_B are the coefficient vector and displacement vector of nodes in contact surface A and displacement vector nodes at contact surface B respectively. In the approximated microslip model, all the macroslip elements are combined into a single point. Therefore, the mode shapes in the region are averaged. Hence, Equation (4.3) becomes,

$$u_{joint} = \left(\frac{1}{p} \left(\sum_{n=1}^{p} \mathbf{\Phi}_{A_n} \right) - \frac{1}{p} \left(\sum_{n=1}^{p} \mathbf{\Phi}_{A_n} \right) \right) \mathbf{a} \tag{4.4}$$

Where, p is the number of macroslip element inside the region, and u_{joint} is the relative displacement of approximated microslip element. By utilizing the approximated microslip element with the first reduction three type of reduced order joint models are constructed. The first one is the three joint model. Joint regions for three joint model are shown in Figure 4.13, and obtained FRF plots are compared with the node-to-node contact model in Figure 4.14. The second one is the four joint model. Joint regions for four joint model can be seen in Figure 4.15, and calculated FRF plots are compared with the node-to-node contact model in Figure 4.16. The last one is the six joint model. Joint regions for six joint model are shown in Figure 4.17, and obtained FRF plots are compared with the node-to-node contact model in Figure 4.18.

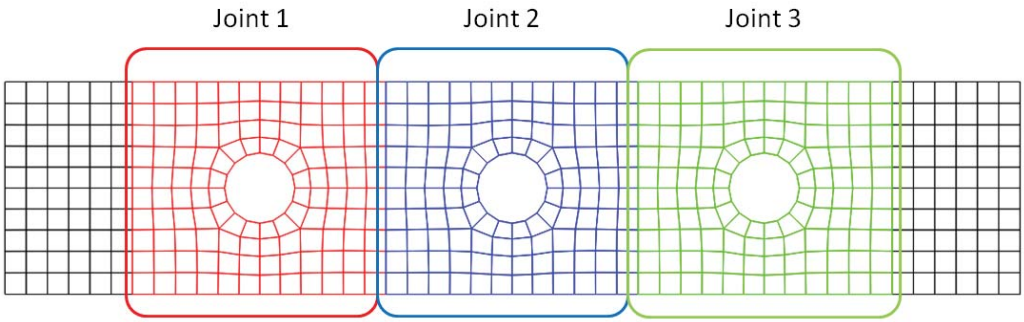

Figure 4.13. Selected locations of joints for three joint model

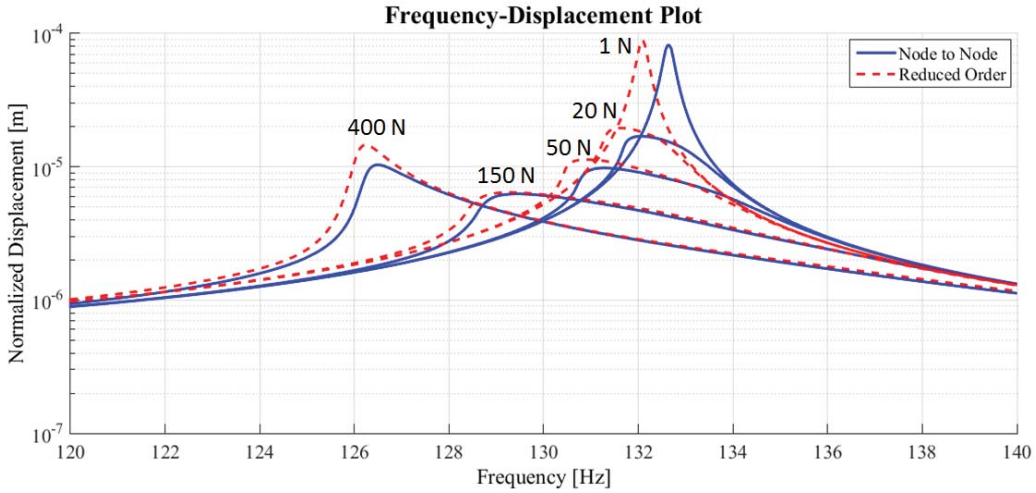

Figure 4.14. Comparison of receptance plots of three joint reduced order model and node-to-node contact model

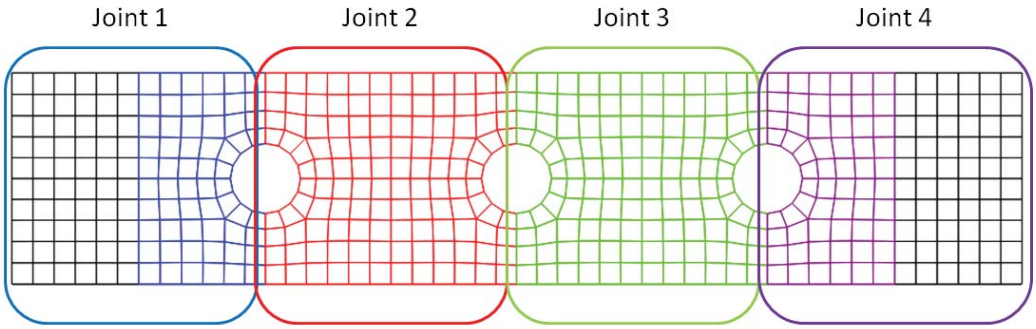

Figure 4.15. Selected locations of joints for four joint model

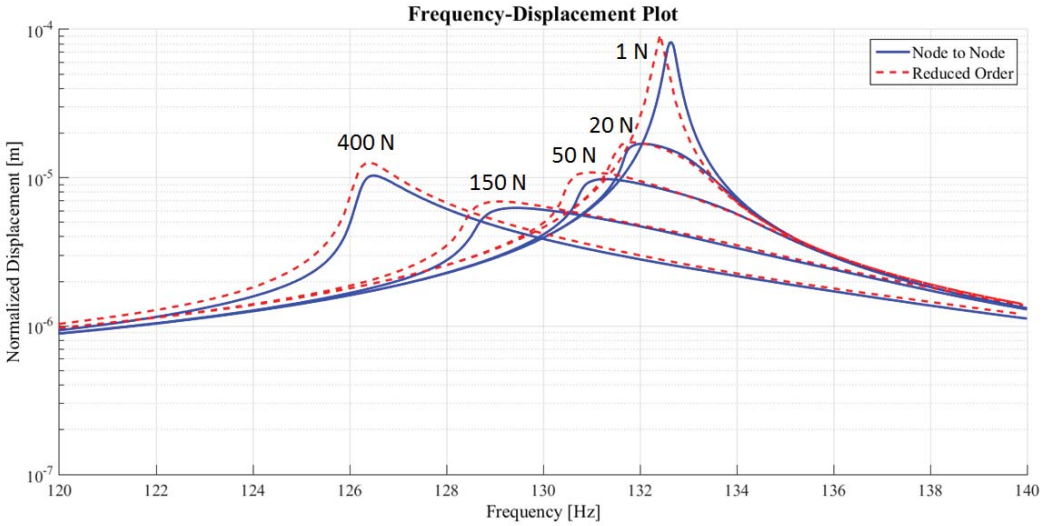

Figure 4.16. Comparison of receptance plots of four joint reduced order model and node-to-node contact model

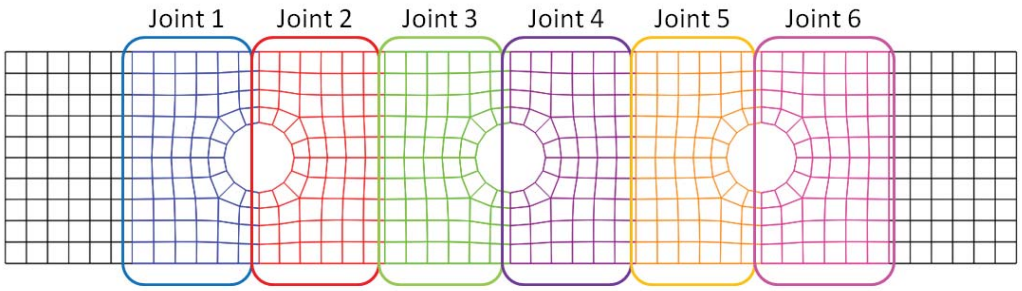

Figure 4.17. Selected locations of joints for six joint model

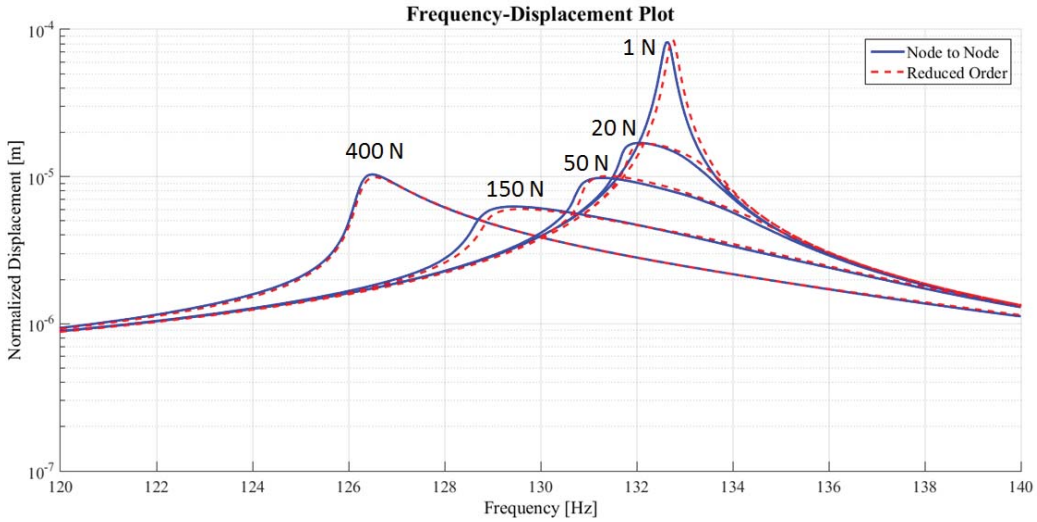

Figure 4.18. Comparison of receptance plots of six joint reduced order model and node-to-node contact model

The number of macroslip element inside each joint for three joint model, four joint model and six joint model are given in Table 4.1, Table 4.2 and Table 4.3 respectively.

Table 4.1. *Number of dry friction elements in three joint model*

Joint 1	128
Joint 2	137
Joint 3	135

Table 4.2. *Number of dry friction elements in four joint model*

Joint 1	59
Joint 2	137
Joint 3	137
Joint 4	67

Table 4.3. *Number of dry friction elements in six joint model*

Joint 1	59
Joint 2	69
Joint 3	68
Joint 4	69
Joint 5	68
Joint 6	67

As can be seen from Figure 4.14, Figure 4.16 and Figure 4.18 through the three types of joint models, six joint model gives the best results. Therefore, by only considering the six joint model secondary reduction is applied. As can be seen from Table 4.1, Table 4.2 and Table 4.3, each joint contains considerable number of macroslip elements. These numbers can be further reduced by utilizing several number of macroslip elements in approximated microslip element such that almost the same hysteresis loop can be obtained. Hysteresis loop of the first joint with 59 macroslip elements can be seen in Figure 4.19.

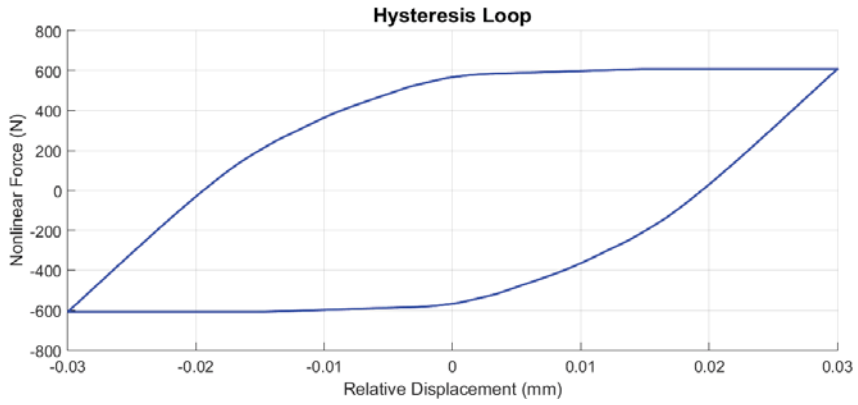

Figure 4.19. Hysteresis loop of first joint in six joint reduced order model

In order to obtain the similar hysteresis loop with less number of macroslip elements optimization problem is constructed. The cost function for the optimization problem is given in Equation (4.5).

$$Cost\ Function = \left(\begin{bmatrix} {F_{Hys}}_{59}^{A} \\ {F_{Hys}}_{59}^{B} \\ {F_{Hys}}_{59}^{C} \end{bmatrix} - \begin{bmatrix} {F_{Hys}}_{N}^{A} \\ {F_{Hys}}_{N}^{B} \\ {F_{Hys}}_{N}^{C} \end{bmatrix} \right)^{T} \left(\begin{bmatrix} {F_{Hys}}_{59}^{A} \\ {F_{Hys}}_{59}^{B} \\ {F_{Hys}}_{59}^{C} \end{bmatrix} - \begin{bmatrix} {F_{Hys}}_{N}^{A} \\ {F_{Hys}}_{N}^{B} \\ {F_{Hys}}_{N}^{C} \end{bmatrix} \right) \tag{4.5}$$

Where ${F_{Hys}}_{59}^{A}$ and ${F_{Hys}}_{N}^{A}$ are hysteresis loop function of 59 macroslip elements and N macroslip elements with maximum relative displacement of magnitude A respectively. B and C represents different magnitude of relative displacements. The reason for optimizing the hysteresis loops with different relative displacement magnitudes is the sensitivity of parameters constructing the hysteresis loop. Well-optimized parameters can be obtained only utilizing the hysteresis loop at very high magnitudes of relative displacement. However, small unfitted regions at high amplitudes change the total stiffness of the system such that resonance frequency of the system with optimized microslip elements might deviate a lot. One can impose a constraint in order to keep the total stiffness same. However in this study, optimizing with 3 different amplitudes of relative displacement is preferred. For the optimization,

built in function “fmincon” in MATLAB is utilized. Three type of secondary reduced joint models are constructed. 3, 4 and 7 macroslip elements are utilized for the first, second and third secondary reduced joint models respectively. Hysteresis loops of first, second and third secondary reduced joint models for joint 1 is shown in Figure 4.20, Figure 4.21 and Figure 4.22 respectively. Optimized parameters of the secondary reduced joints are shown in Table 4.4, Table 4.5 and Table 4.6. Also FRF plots of secondary reduced joint models are obtained and compared with node-to-node contact model as shown in Figure 4.23, Figure 4.24 and Figure 4.25. As can be seen from the figures, FRF results of all the secondary reduced joints are very close to the node-to-node approach.

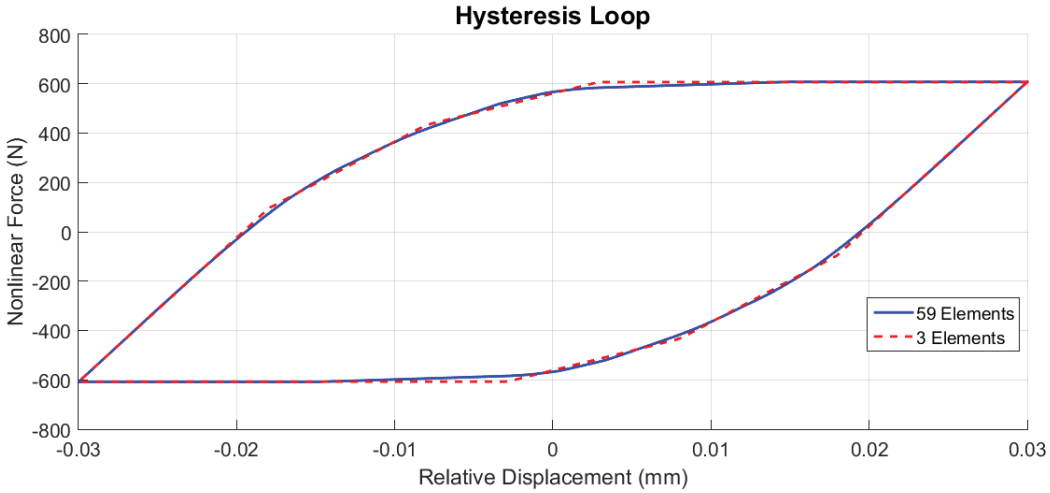

Figure 4.20. Comparison of hysteresis loops with 59 elements and 3 elements

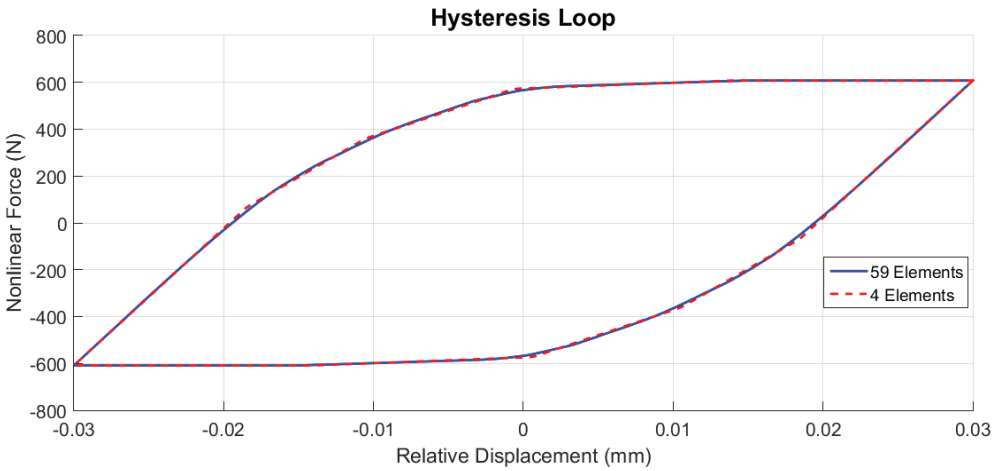

Figure 4.21. Comparison of hysteresis loops with 59 elements and 4 elements

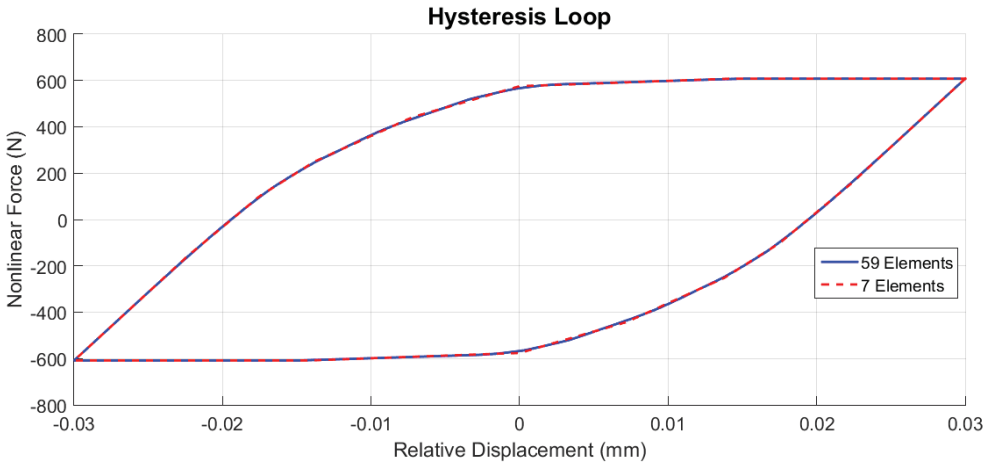

Figure 4.22. Comparison of hysteresis loops with 59 elements and 7 elements

Table 4.4. *Parameters of secondary reduced order model with three elements*

	k_1(N/mm)	k_2(N/mm)	k_3(N/mm)	μN_1(N)	μN_2(N)	μN_3(N)
Joint 1	15962.9	17953.9	24491.8	262.41	197.24	147.49
Joint 2	19022.8	23933.4	25437.8	302.88	139.32	287.41
Joint 3	14937.4	27442.7	24959.5	238.29	160.85	273.08
Joint 4	26674.6	24059.4	17691.8	299.45	136.53	277.89
Joint 5	16042.2	23668.2	27577.5	257.00	259.95	165.07
Joint 6	17329.4	27920.7	21156.9	285.47	170.66	248.62

Table 4.5. *Parameters of secondary reduced order model with four elements*

	k_1(N/mm)	k_2(N/mm)	k_3(N/mm)	k_4(N/mm)	μN_1(N)	μN_2(N)	μN_3(N)	μN_4(N)
Joint 1	18982.5	2436.5	21612.2	15544.4	278.83	53.62	124.83	151.06
Joint 2	25588.0	9732.0	18704.0	14828.5	308.79	40.94	135.81	244.12
Joint 3	13782.5	9501.1	22649.5	21924.6	221.64	38.41	160.76	251.22
Joint 4	13474.5	7093.6	20844.8	27497.6	219.34	25.92	140.79	327.82
Joint 5	14259.9	8147.5	23097.8	22362.2	232.33	32.21	160.80	256.60
Joint 6	4105.1	20870.1	15887.6	25770.6	84.23	116.65	142.48	362.48

Table 4.6. *Parameters of secondary reduced order model with seven elements*

	k_1(N/mm)	k_2(N/mm)	k_3(N/mm)	k_4(N/mm)	k_5(N/mm)	k_6(N/mm)	k_7(N/mm)
Joint 1	2281.8	3.0	5606.2	11215.3	10498.0	13108.3	16251.6
Joint 2	12761.5	2109.6	4818.8	14793.9	7821.0	13314.0	13365.7
Joint 3	10918.2	2098.3	8804.3	15801.3	11757.4	5221.3	13380.1
Joint 4	12792.0	2103.1	7491.7	5162.6	15112.6	13592.9	12726.5
Joint 5	11712.7	2088.2	4946.1	12623.0	15546.9	9989.2	11077.4
Joint 6	2182.0	14956.9	5728.5	8307.1	9807.2	12270.8	13709.6
	μN_1(N)	μN_2(N)	μN_3(N)	μN_4(N)	μN_5(N)	μN_6(N)	μN_7(N)
Joint 1	50.44	149.60	21.41	90.82	119.64	82.01	243.77
Joint 2	196.01	45.30	16.00	89.64	62.60	174.68	146.25
Joint 3	164.56	44.31	112.80	95.06	93.50	17.34	145.38
Joint 4	192.27	44.44	59.98	17.10	90.64	147.92	162.37
Joint 5	92.90	44.73	16.50	136.12	93.87	129.02	169.71
Joint 6	48.89	93.52	21.94	88.13	77.86	163.97	211.55

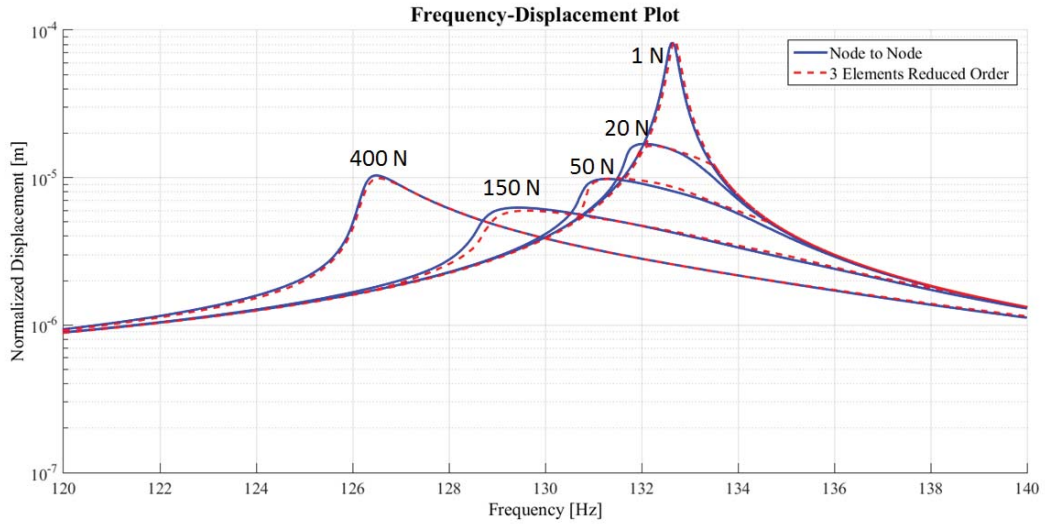

Figure 4.23. Comparison of receptance plots of six joint reduced order model with three elements and node-to-node contact model

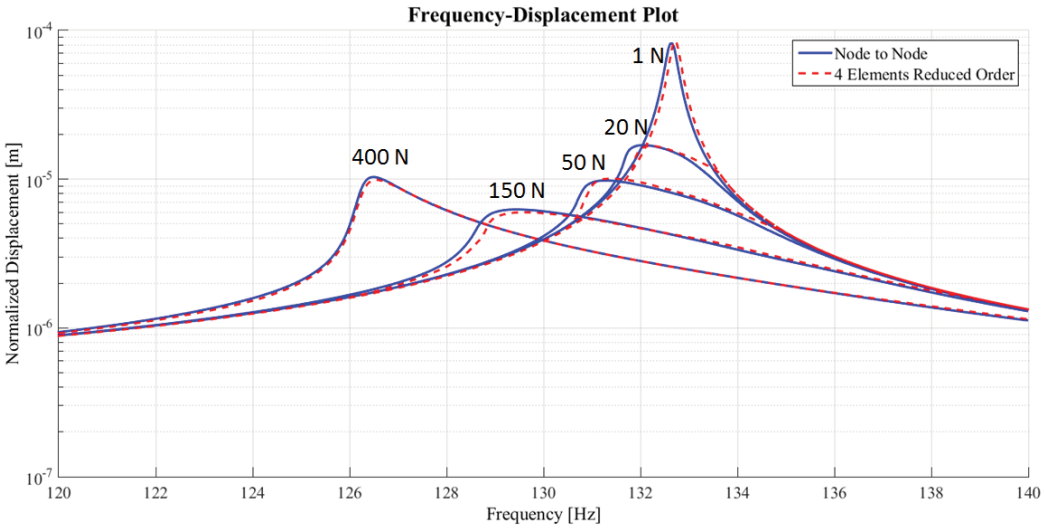

Figure 4.24. Comparison of receptance plots of six joint reduced order model with four elements and node-to-node contact model

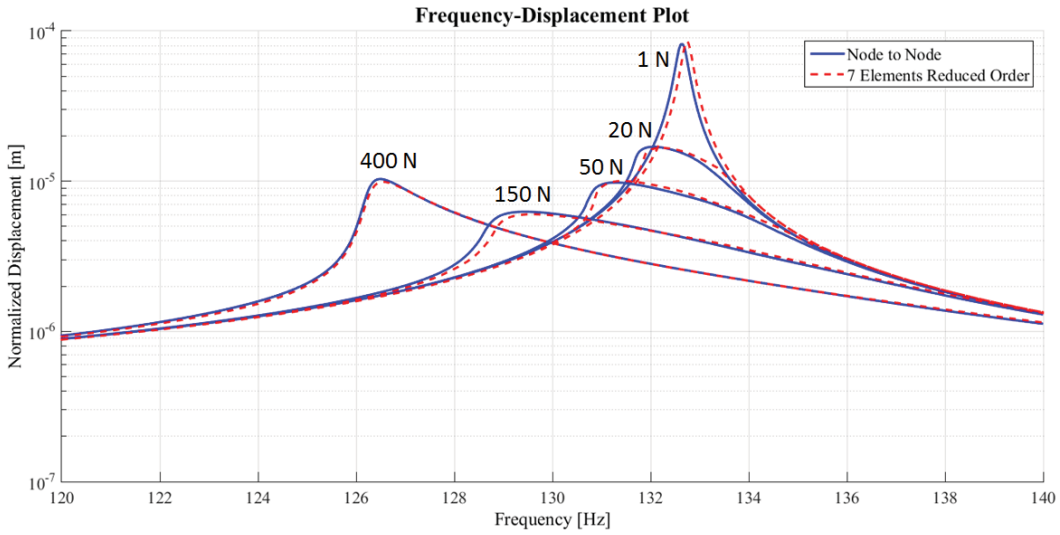

Figure 4.25. Comparison of receptance plots of six joint reduced order model with seven elements and node-to-node contact model

To sum up, node-to-node contact model is created by utilizing the 1D dry friction element with constant normal load. In this model 400 dry friction elements are used in total. Afterwards, three types of reduced order model is created. These are namely 3-joint, 4-joint and 6-joint models. In all of them, 400 dry friction elements are used in total. However, distributed macroslip elements are converted into lumped microslip elements, which is called first reduction in this study. Lastly, by utilizing an optimization for the six-joint model, reduced microslip elements are further reduced into combination of several macroslip elements, which is called secondary reduction in this study. As a result, instead of utilizing 400 dry friction elements with 400 different nodal location, very similar FRF plots are obtained by using 18, 24 and 42 elements as shown in Figure 4.23, Figure 4.24 and Figure 4.25 respectively.

CHAPTER 5

REDUCED ORDER BOLTED JOINT MODELING UTILIZING 1D DRY FRICTION ELEMENTS WITH NORMAL LOAD VARIATION

5.1. Overview

In chapter 4, a new reduced order modeling technique is introduced. Friction elements inside the certain area are combined into a single microslip friction element such that deviation of the overall behavior of the system is sufficiently small. In this chapter, same methodology will be utilized. Besides, effect of normal load variation will be included. Firstly, node-to-node contact model will be realized on an assembled system with single bolt. Then the first reduction technique mentioned in chapter 4 will be utilized in single bolted assembly. Afterwards, node-to-node contact model will be established on three-bolted assembly. Subsequently, the first reduction technique will be implemented again on three-bolted assembly. Thereafter, secondary reduction technique will be applied on three-bolted assembly. Lastly, obtained results will be discussed.

5.2. Single Bolted Assembly

3D model and dimensions of single bolted assembly can be seen in Figure 4.1 and Figure 5.2 respectively. The model consists of two beams connected to each other with a M8 bolt. Firstly, nonlinear static analysis is realized in order to obtain the normal load distribution in the contact area by utilizing the Abaqus FEA software. Steel material properties (Elastic modulus: 190GPa, Poisson's ratio: 0.32, Density: 7800 kg/m^3) are imposed for all the parts in the model. In this model, contacting surfaces of beams with each other are imposed with surface-to-surface penalty contact algorithm with 0.1 coefficient of friction. Since the contacting area of bolt heads with top surfaces of beams is small compared to the contacting surfaces of beams with each

other, the normal load distribution becomes higher. Hence, it is assumed that these surfaces stays in stick condition for low and medium excitation levels. Therefore, contacting surfaces of bolt heads with top surface of beams are enforced with tie constraints, which ties the surfaces together so that there is no relative motion between them. In order to eliminate singularity problem in static analysis, fix-free boundary condition is applied to the assembly. 10 kN preload is applied from the center of the bolt shank. Normal load distribution obtained from the static analysis can be seen in Figure 5.3. Since the effect of normal load variation is included in this model, gap distribution is also necessary. By imposing the multiplication of gap and corresponding stiffness values on the macroslip elements as negative normal loads, clearance can also be modeled. Gap distribution can be seen in Figure 5.4. In order to capture the gap distribution better, exaggerated view after the nonlinear static analysis can be seen in Figure 5.5.

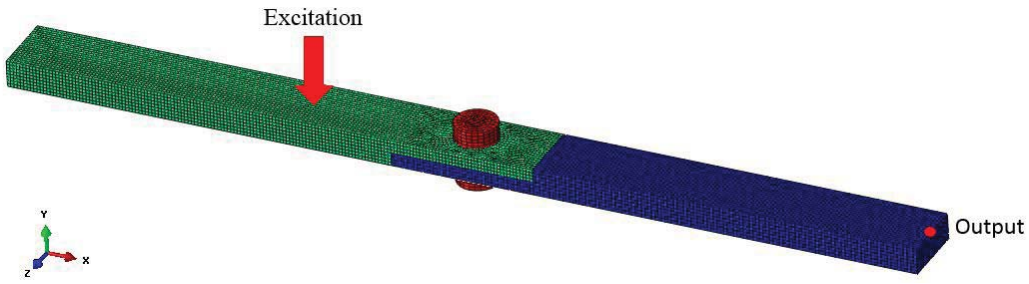

Figure 5.1. 3D model of single bolted assembly

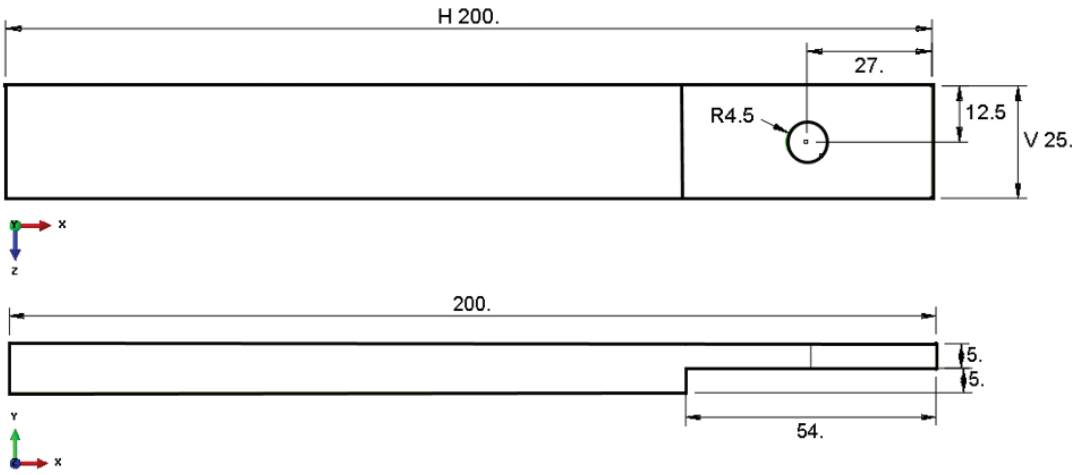

Figure 5.2. Dimensions of single bolted assembly [mm]

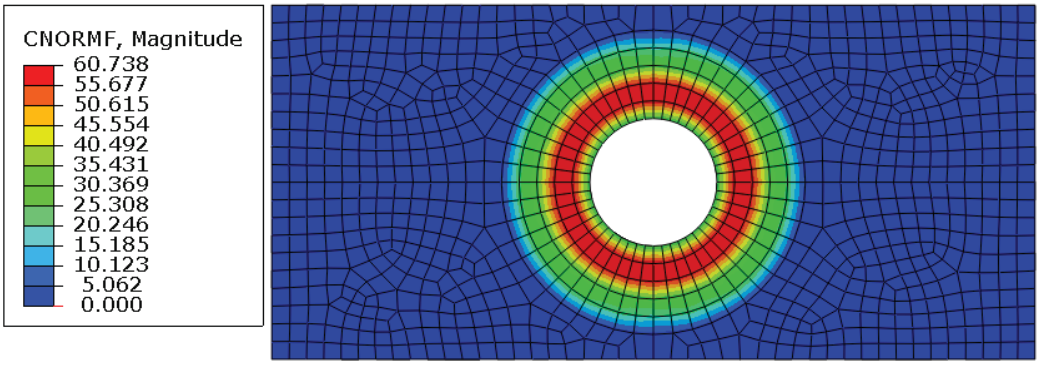

Figure 5.3. Normal load distribution of single bolted assembly [N]

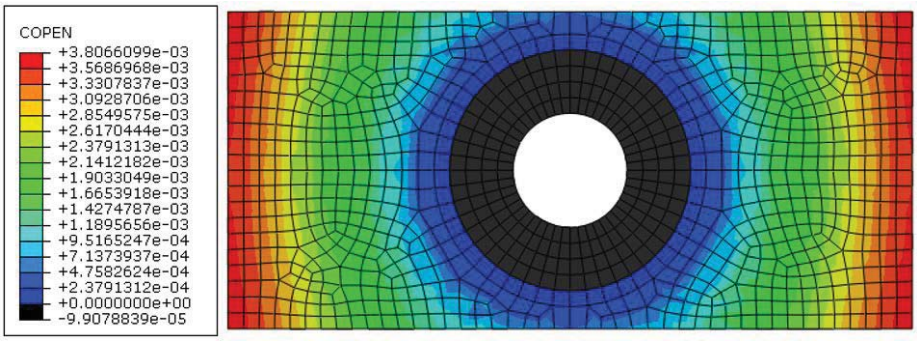

Figure 5.4. Gap distribution of single bolted assembly after the preload [mm]

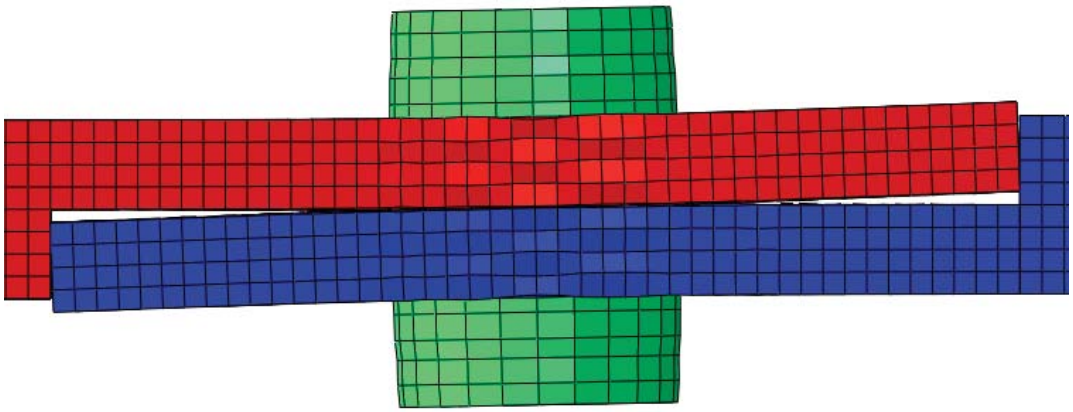

Figure 5.5. Exaggerated front view after nonlinear static analysis of single bolted assembly

5.2.1. Node to Node Contact Model

In this model, all the nodes coincident to each other are connected with 1D dry friction element with normal load variation, which is introduced in chapter 3. 1D dry friction element with normal load variation consists of 4 parameters: tangential stiffness (k_u), normal stiffness (k_v), coefficient of friction (μ) and initial normal load (n_0). Tangential stiffness, normal stiffness and coefficient of friction are given in Table 5.1. Normal load distribution and gap distribution, which are obtained from the nonlinear

static analysis, are utilized in order to calculate the initial normal load as shown in Equation (5.1).

Table 5.1 *Parameters of 1D dry friction element with normal load variation*

k_u	100 kN/mm
k_v	100 kN/mm
μ	0.1

$$n_0 = N_{static} - k_v v_{gap} \tag{5.1}$$

Where, N_{static} and v_{gap} are normal load and initial gap obtained from the nonlinear static analysis. Location of the nodes utilized in the node-to-node contact model is shown in Figure 5.6.

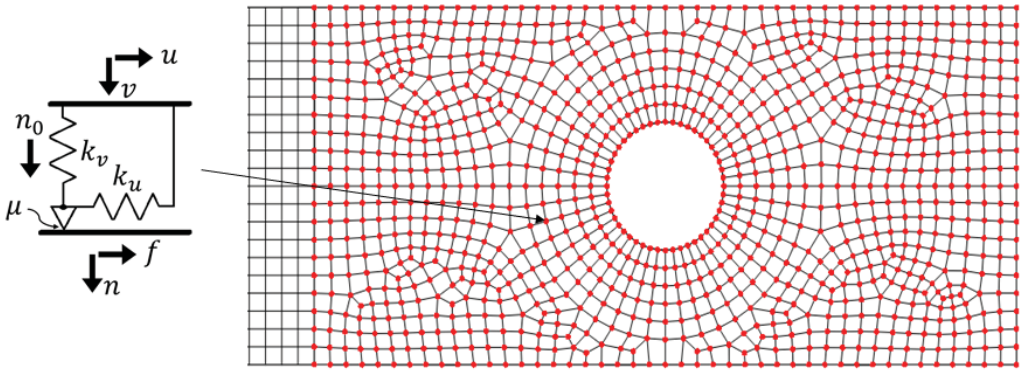

Figure 5.6. Location of the nodes connected with 1D dry friction elements with normal load variation

Harmonic Balance Method with Modal Superposition Method, which is explained in chapter 2, is utilized in order to obtain the nonlinear algebraic equation set. In order to impose Modal Superposition Method, resonance frequencies and mode shapes of the linear system need to be calculated. The linear system is the same with nonlinear static analysis model except the nonlinear contact surface definition and fix-free boundary

condition. Contact surface definition is removed and free-free boundary condition is imposed to the linear system. Subsequently, natural frequencies and mode shapes are calculated by utilizing the Abaqus FEA software. Mode shapes utilized in modal superposition method are shown in Figure 5.7, Figure 5.8, Figure 5.9 and Figure 5.10.

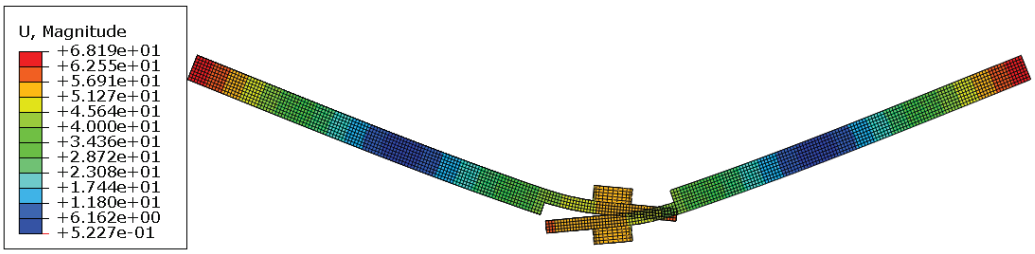

Figure 5.7. Bending mode 191 Hz

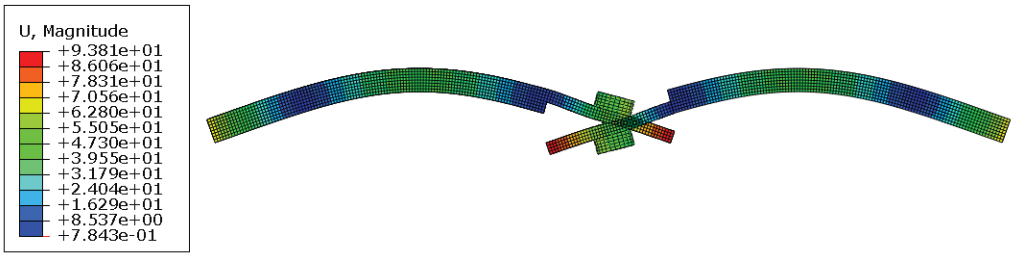

Figure 5.8. Bending mode 1632.5 Hz

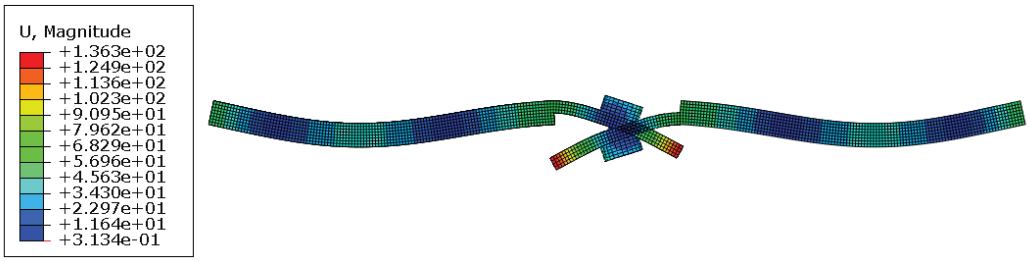

Figure 5.9. Bending mode 3347.3 Hz

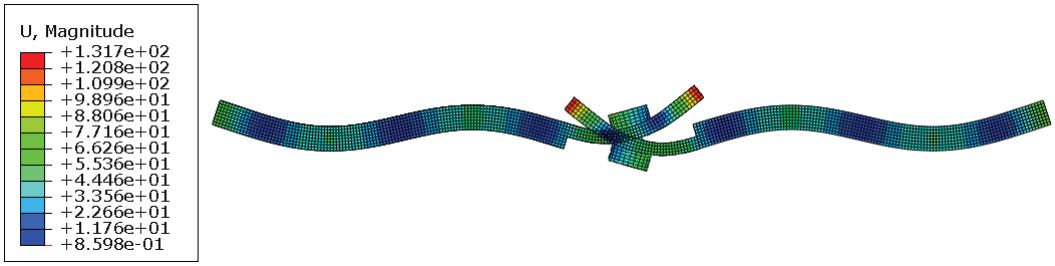

Figure 5.10. Bending mode 5924.4 Hz

After establishing the node-to-node contact model, normalized FRFs for several excitation levels are calculated by utilizing the Arclength continuation method, which is explained in chapter 2. The obtained FRFs are shown in Figure 5.11. Excitation and output locations of the normalized FRFs are shown in Figure 4.1. Contact states of the each friction elements for each FRF plots at their maximum amplitude are also extracted, which are shown in Figure 5.12 to Figure 5.19.

As can be seen from the figures, at low excitation levels most of the friction elements are either in full stick state or in full separation state. As the excitation force increases, the friction elements in full stick state switch to stick slip motion without separation. It should be noted that the order of friction elements switching to stick slip motion is consistent with both the first bending mode shape and normal load distribution. As the excitation levels increase further (greater and equal to 2 N) separation with stick slip

motion appears at the regions where there are low normal loads and high relative displacements of first bending mode.

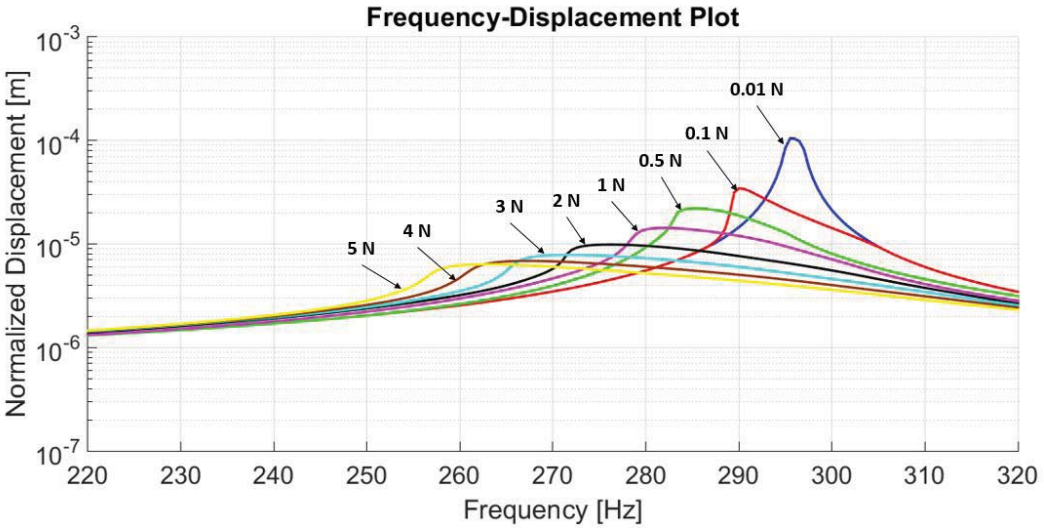

Figure 5.11. Frequency displacement plots of node-to-node contact single bolted assembly model

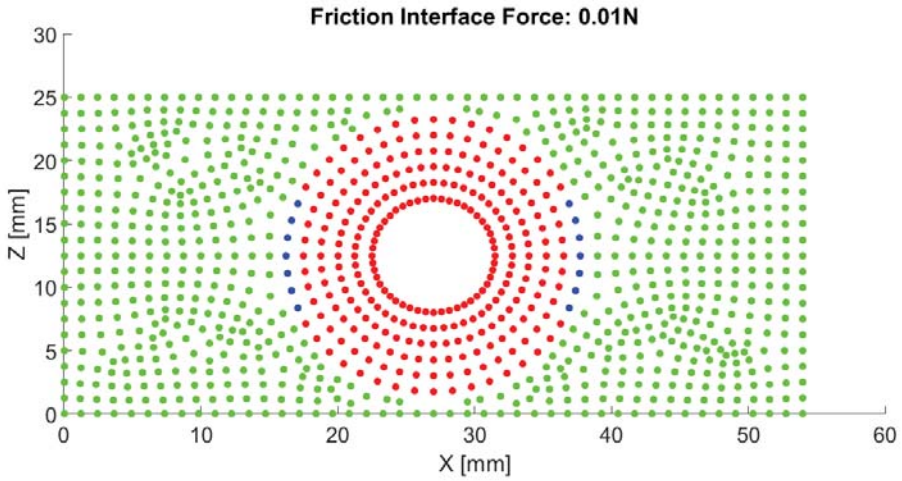

Figure 5.12. Contact states of peak point of FRF at 0.01 N excitation level (green: full separation, black: separation with stick-slip motion, blue: stick-slip motion without separation and red: full stick motion)

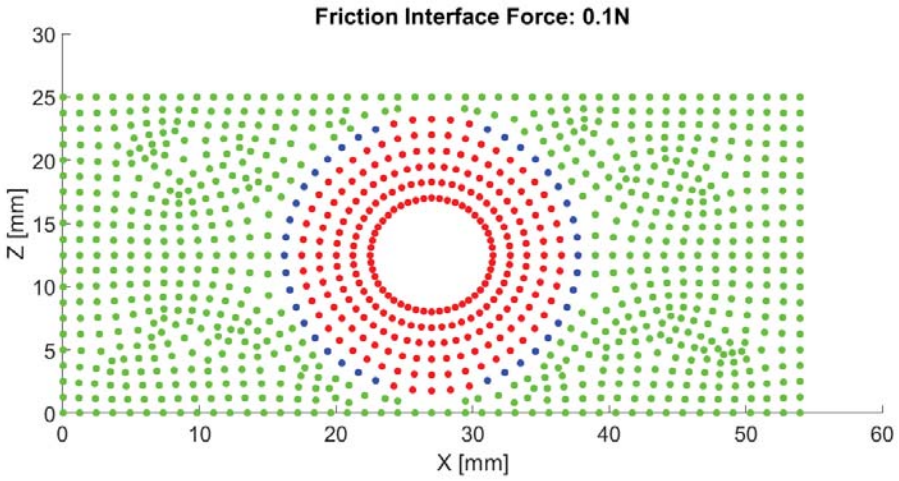

Figure 5.13. Contact states of peak point of FRF at 0.1 N excitation level (green: full separation, black: separation with stick-slip motion, blue: stick-slip motion without separation and red: full stick motion)

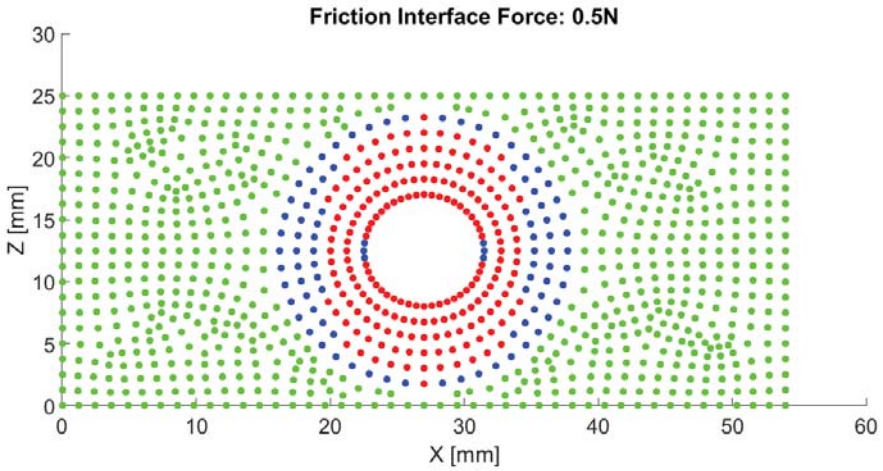

Figure 5.14. Contact states of peak point of FRF at 0.5 N excitation level (green: full separation, black: separation with stick-slip motion, blue: stick-slip motion without separation and red: full stick motion)

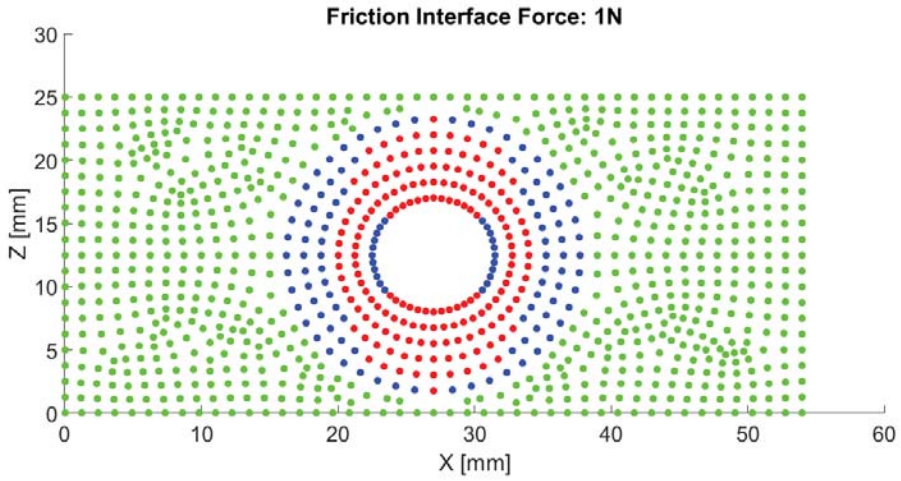

Figure 5.15. Contact states of peak point of FRF at 1 N excitation level (green: full separation, black: separation with stick-slip motion, blue: stick-slip motion without separation and red: full stick motion)

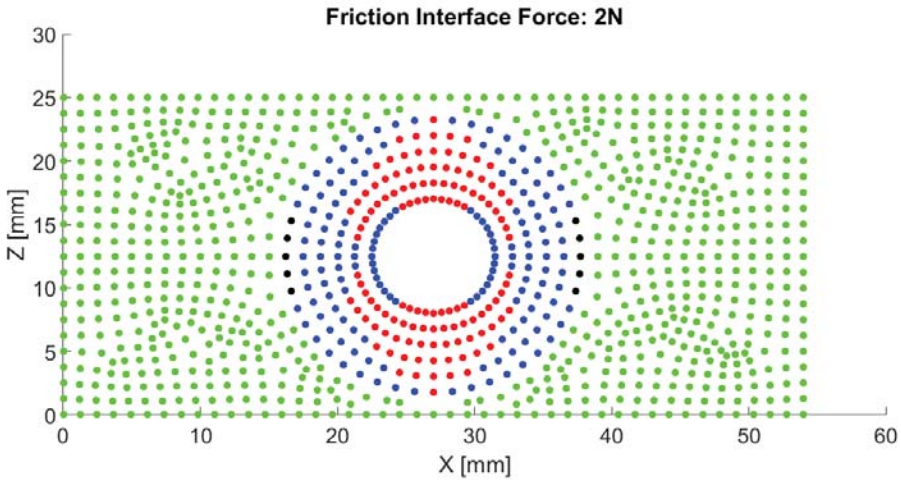

Figure 5.16. Contact states of peak point of FRF at 2 N excitation level (green: full separation, black: separation with stick-slip motion, blue: stick-slip motion without separation and red: full stick motion)

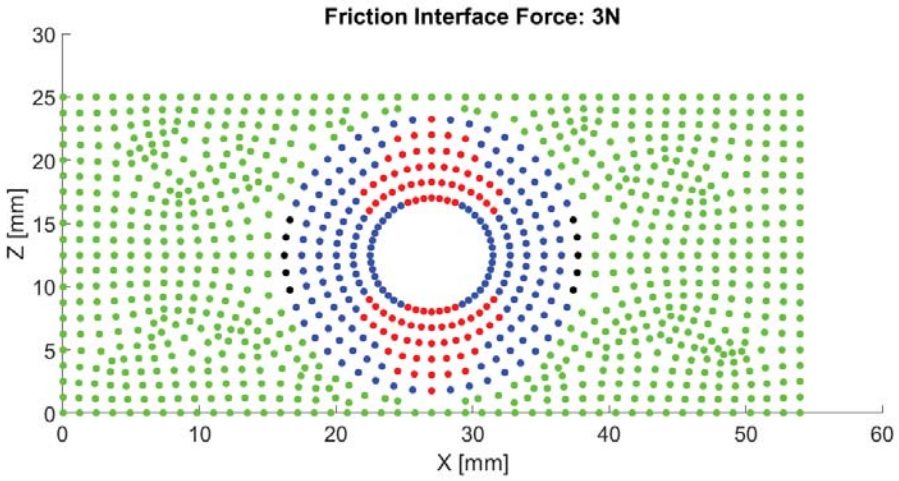

Figure 5.17. Contact states of peak point of FRF at 3 N excitation level (green: full separation, black: separation with stick slip motion, blue: stick slip motion without separation and red: full stick motion)

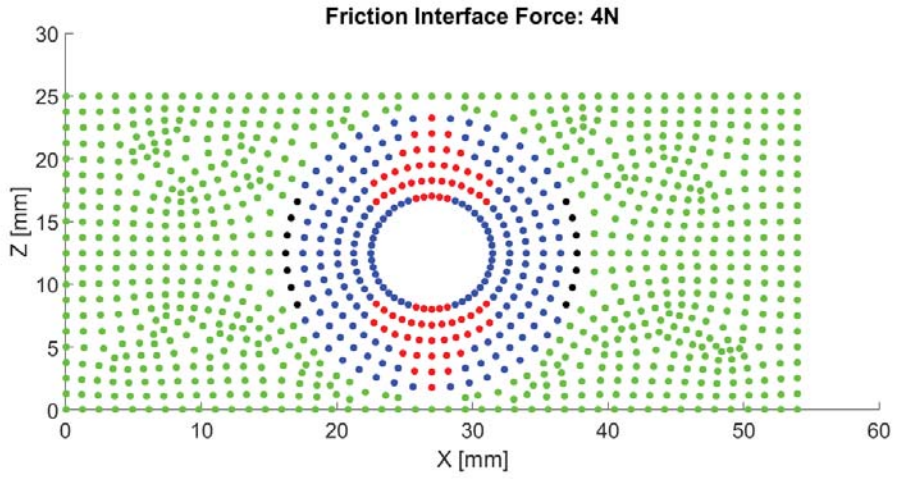

Figure 5.18. Contact states of peak point of FRF at 4 N excitation level (green: full separation, black: separation with stick slip motion, blue: stick slip motion without separation and red: full stick motion)

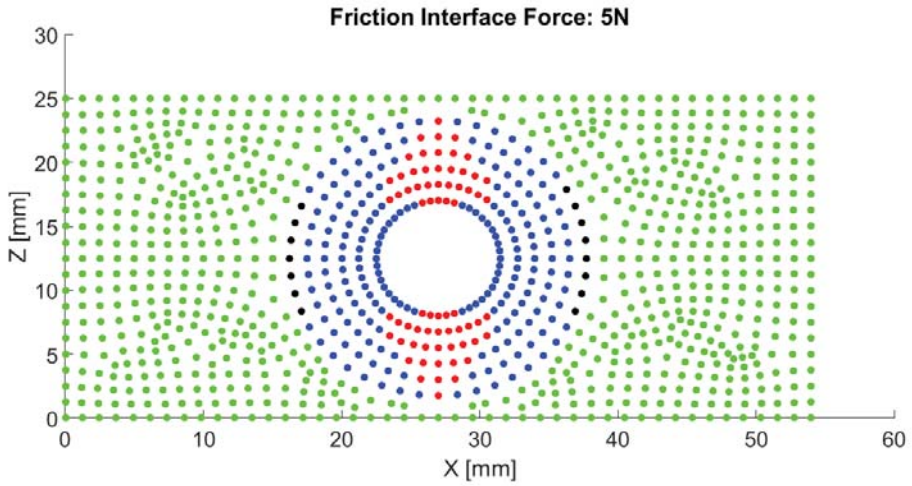

Figure 5.19. Contact states of peak point of FRF at 5 N excitation level (green: full separation, black: separation with stick slip motion, blue: stick slip motion without separation and red: full stick motion)

5.2.2. Reduced Order Bolted Joint Model of Single Bolted Assembly

In chapter 4, two-step reduction methodology is introduced in order to construct a reduced order bolted joint model utilizing dry friction elements with constant normal load. In this section, same methodology will be performed on the dry friction elements with normal load variation. However, only the first reduction step will be realized. Schematic representation of dry friction element with normal load variation and microslip approximation of the dry friction element are shown in Figure 5.22 and Figure 5.23. In Figure 5.24 representation of reduced order joint model is given. Calculation of the Fourier coefficients of the microslip element can be obtained with the summation of Fourier coefficients of individual macroslip elements as can be seen in Equation (4.1), (5.3), (5.4) and (5.5). In order to apply the reduced order microslip element, relative displacement should be clarified also. In Equation (4.3) and (4.4),

calculation of relative displacement by utilizing an averaging method is given. Same equation is also applicable here.

Two types of joint model is studied. In the first one, reduced order model consists of two joints. In the second one, it consists of four joints. The regions, in which the dry friction elements are to be lumped, are decided according to the normal load distribution plotted from the mid-section of the beam. The path for the mid-section of the beam can be seen in Figure 5.20. The normal load distribution obtained from the path is given in Figure 5.21. It can be seen that there is a symmetric distribution along the x-axis. In the first joint type, the joint regions are adjusted such that contact surface are divided into two regions from the symmetry axis which is shown in Figure 5.21. Location of the reduced order joints on 3D mesh can be seen in Figure 5.25. After constructing the reduced order model, FRFs for several excitation levels are obtained, and comparison with the node-to-node contact model results are shown in Figure 5.26.

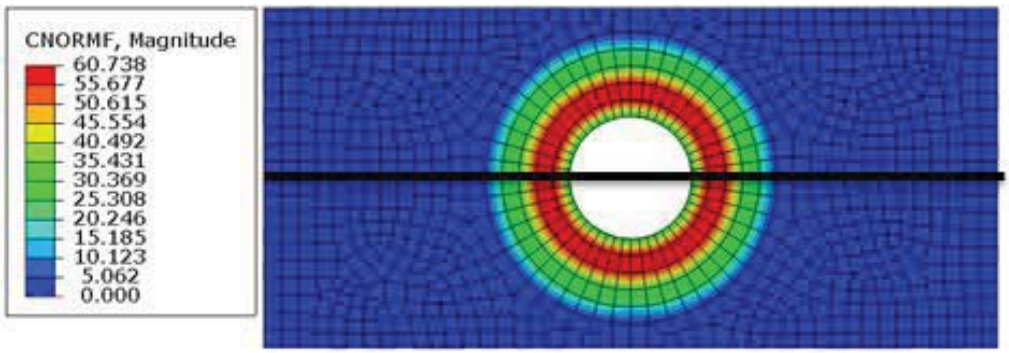

Figure 5.20. Mid-section path for the normal load distribution plot

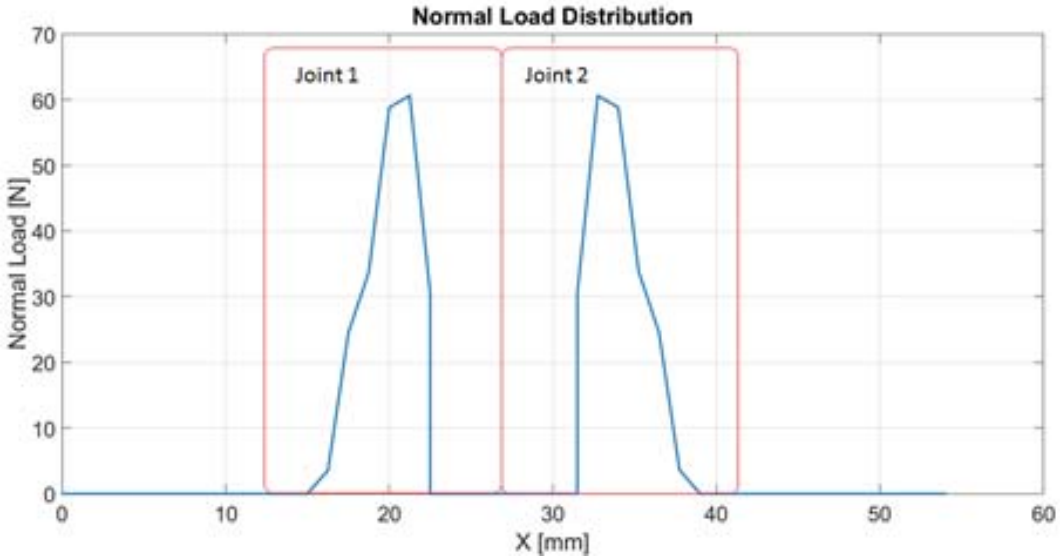

Figure 5.21. Normal load distribution plot from the mid-section of the beam for two-joint reduced order model

$$F_{s_{joint}} = \sum_{q=1}^{p} f_{s\,q} \tag{5.2}$$

$$F_{c_{joint}} = \sum_{q=1}^{p} f_{c\,q} \tag{5.3}$$

$$N_{s_{joint}} = \sum_{q=1}^{p} n_{s\,q} \tag{5.4}$$

$$N_{c_{joint}} = \sum_{q=1}^{p} n_{c\,q} \tag{5.5}$$

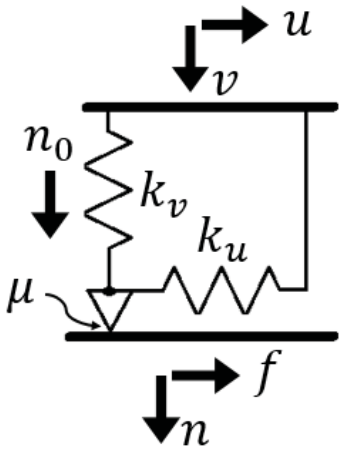

Figure 5.22. Schematic representation of dry friction element with normal load variation

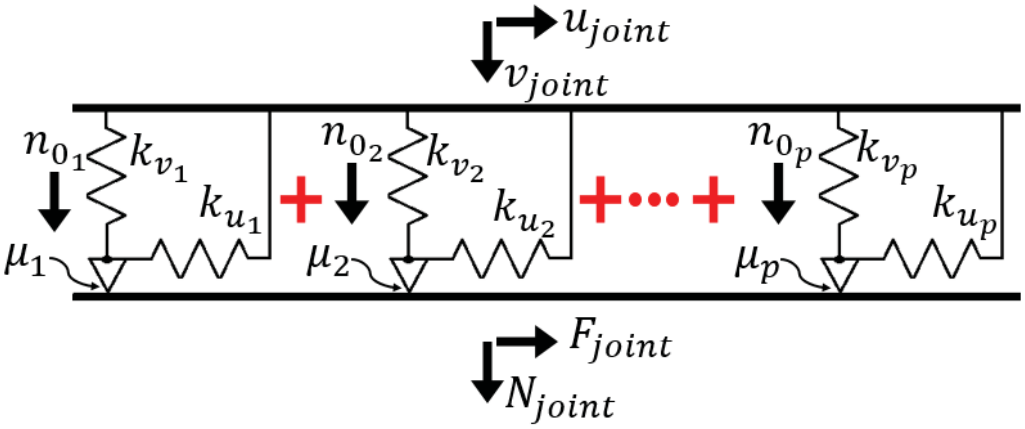

Figure 5.23. Schematic representation of microslip element with normal load variation

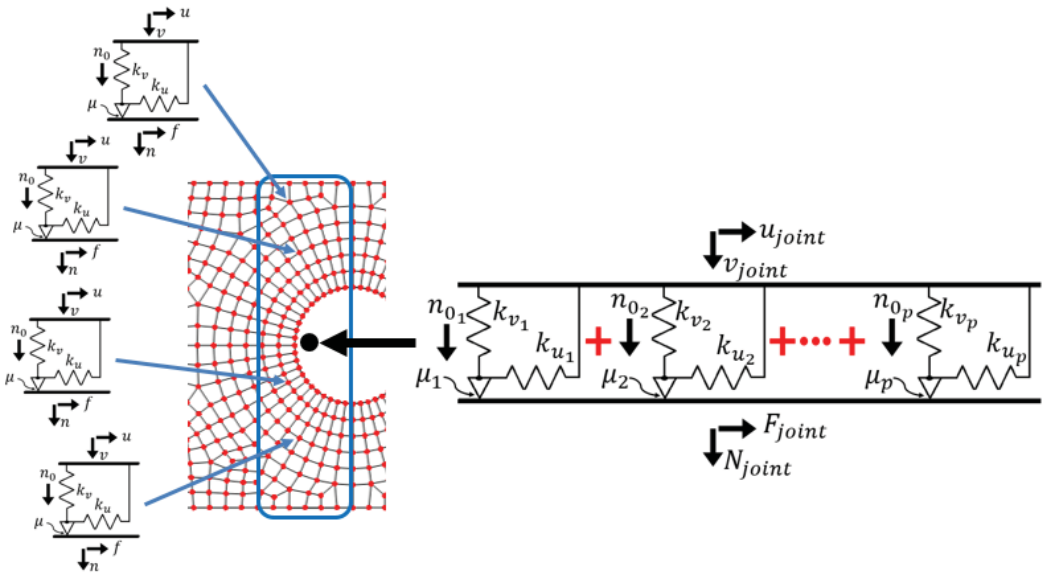

Figure 5.24. Schematic representation of reduced order joint model with normal load variation

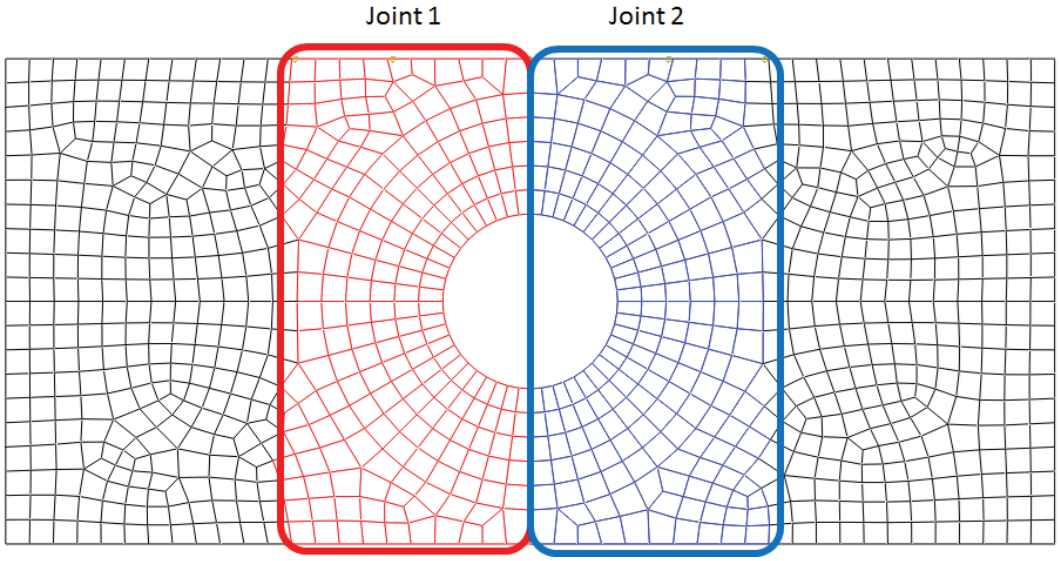

Figure 5.25. Location of joints in reduced order model with two joints

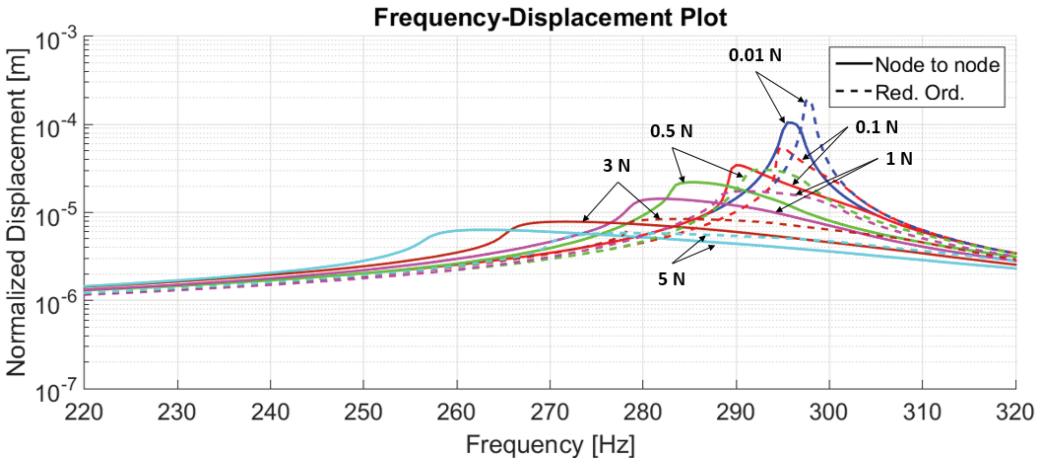

Figure 5.26. Comparison of normalized FRF plots of node to node contact model and reduced order model with two joints

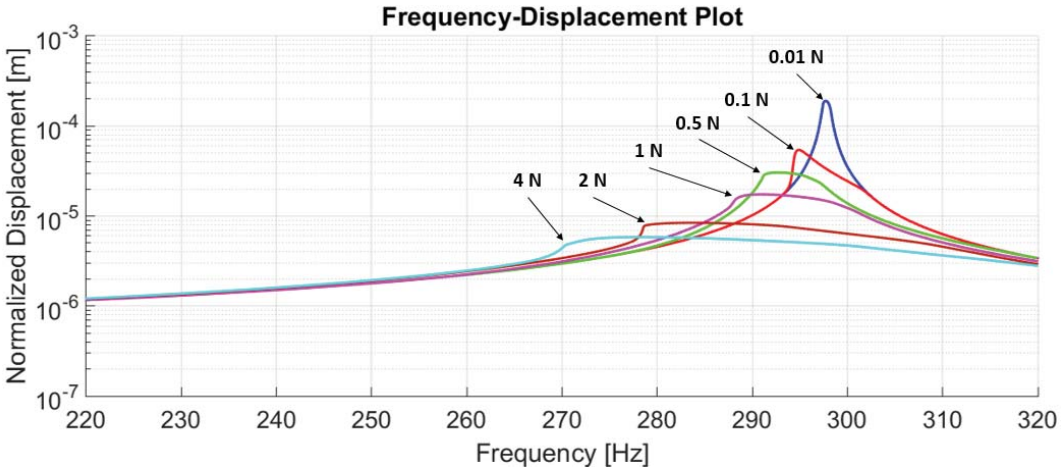

Figure 5.27. Normalized FRF plots of reduced order model with two joints

As can be seen from Figure 5.26, normalized FRF plots of reduced order model seem to be close to the node-to-node contact model at low excitation levels. However as the excitation level increases, the FRF plots deviates a lot. It can be seen from the Figure

5.11 and Figure 5.27 that although overall trends for the reduced order model with two joints is similar with the node-to-node contact model, it is not accurate enough since the resonance frequencies are not close to each other. In order to increase the accuracy of the reduced order model, number of the joints are increased to four joints, which is the second type of joint model studied in this thesis.

In the four-joint reduced order model, each joint of the two-joint reduced order model further divided into two regions. Second division locations are selected such that while the joint 1 and joint 4 approximate the low normal loads, joint 2 and joint 3 approximate the high normal loads as shown in Figure 5.28. The locations for the lumped dry friction elements for the four-joint model on 3D mesh are shown in Figure 5.29.

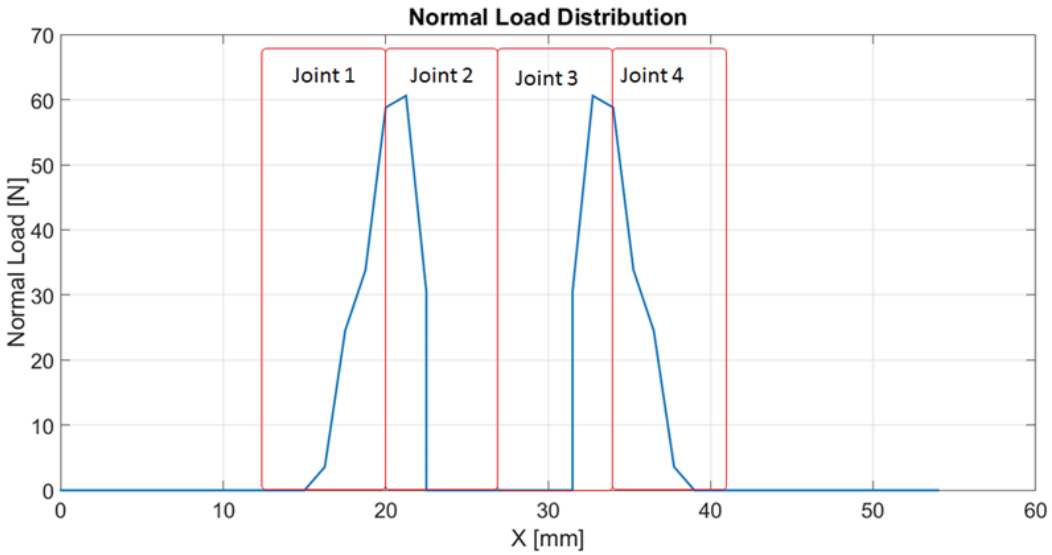

Figure 5.28. Normal load distribution plot from the mid-section of the beam for four-joint reduced order model

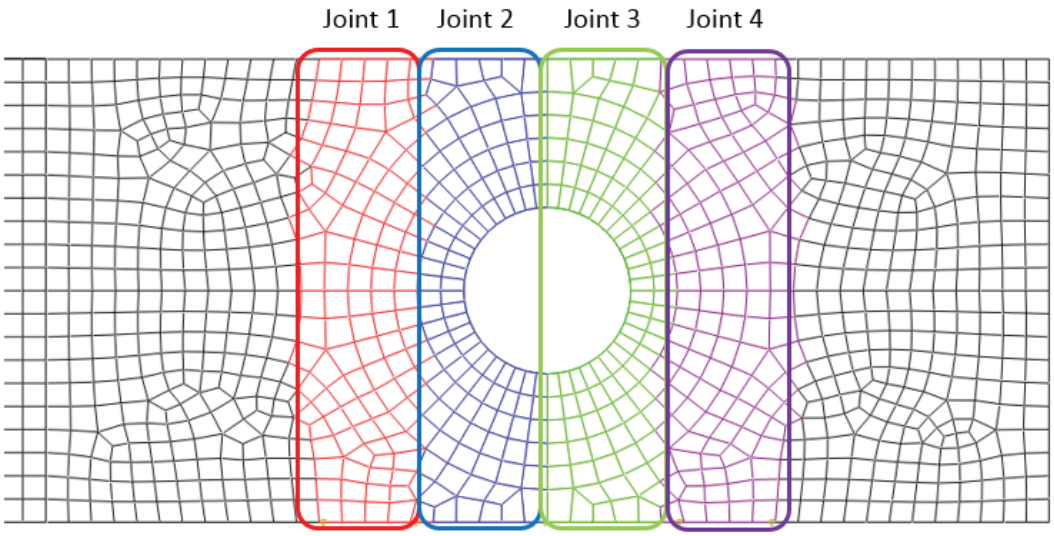

Figure 5.29. Location of joints in reduced order model with four joints

By following the same procedure with the two joint model, FRF plots are calculated, and the comparison with the node-to-node contact model is given in Figure 5.30. As can be seen from the figure, the FRF plots are close to each other. Since there is normal load variation effect, it is seen that the contact area should be divided into smaller regions in order to have better accuracy with the reduced order model.

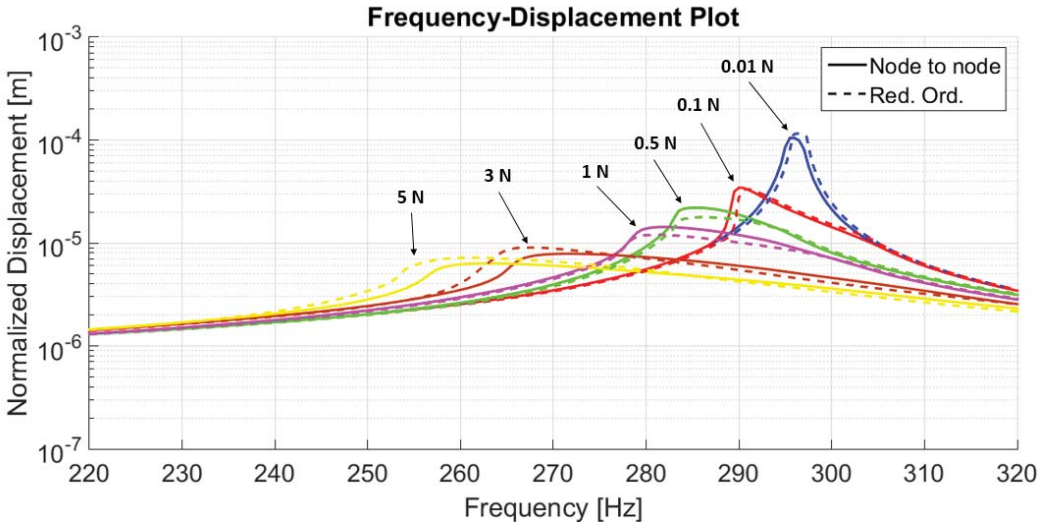

Figure 5.30. Comparison of normalized FRF plots of node to node contact model and reduced order model with four joints

The analysis by utilizing the dry friction element with normal load variation is performed by taking the normal and tangential stiffness values as 100 kN/mm. The analysis are repeated by decreasing the stiffness values in order to see the effect of the stiffness values on reduction methodology. Parameters of the dry friction element with low stiffness values are given in Table 5.2. Firstly, node-to-node contact model is constructed by utilizing the same normal load distribution and gap distribution utilized previously. Subsequently, reduced order model with four joint is created. The contact states for the node-to-node contact model with low contact stiffness are given in Figure 5.31 to Figure 5.36. Similar behavior with the high contact stiffness model can be seen from the figures. Comparison of the FRF plots of node-to-node contact model with reduced order model is given in Figure 5.37. It is clearly seen from the FRF plots that the reduced order model methodology with four joints approximate the node-to-node contact model with a good accuracy with low contact stiffness values also.

Table 5.2 *Parameters of 1D dry friction element with normal load variation for low stiffness values*

k_u	47 kN/mm
k_v	47 kN/mm
μ	0.1

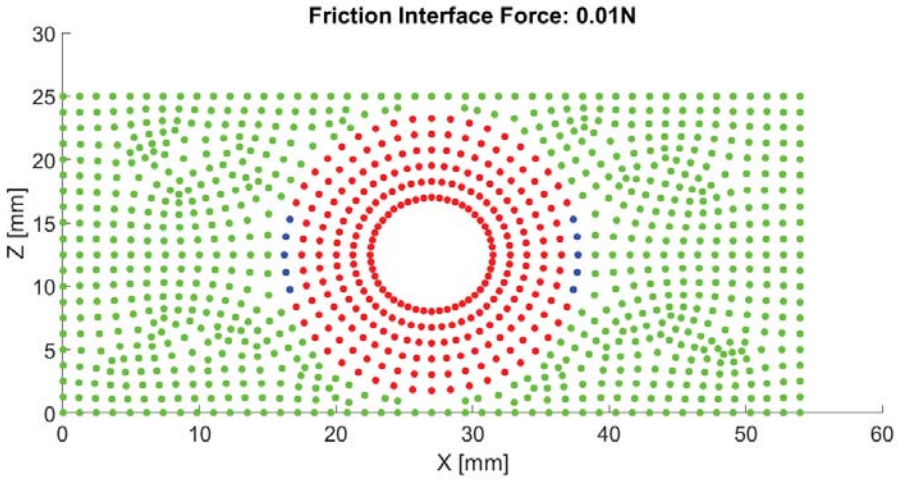

Figure 5.31. Contact states of peak point of FRF at 0.01 N excitation level for the single bolted assembly with low contact stiffness (green: full separation, black: separation with stick slip motion, blue: stick slip motion without separation and red: full stick motion)

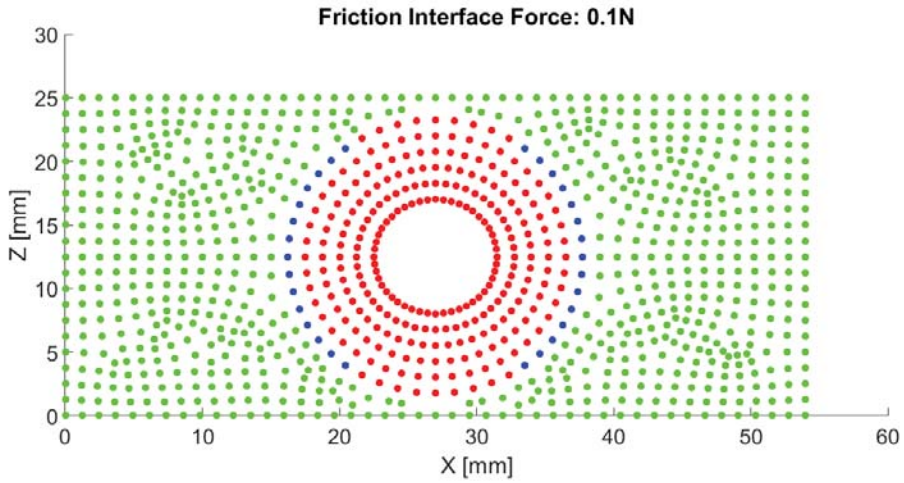

Figure 5.32. Contact states of peak point of FRF at 0.1 N excitation level for the single bolted assembly with low contact stiffness (green: full separation, black: separation with stick slip motion, blue: stick slip motion without separation and red: full stick motion)

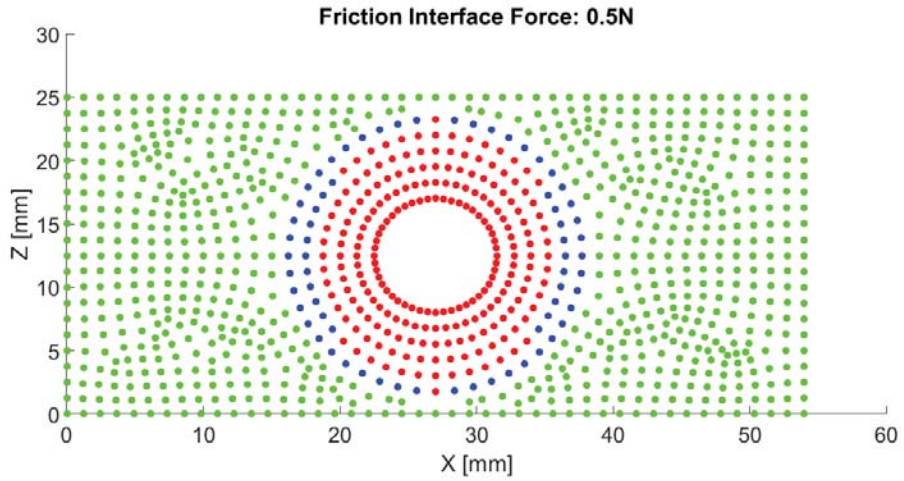

Figure 5.33. Contact states of peak point of FRF at 0.5 N excitation level for the single bolted assembly with low contact stiffness (green: full separation, black: separation with stick slip motion, blue: stick slip motion without separation and red: full stick motion)

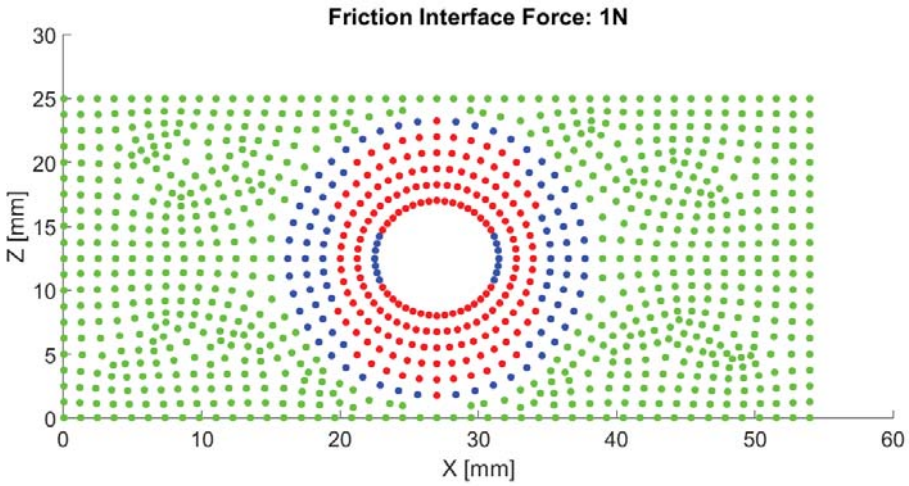

Figure 5.34. Contact states of peak point of FRF at 1 N excitation level for the single bolted assembly with low contact stiffness (green: full separation, black: separation with stick slip motion, blue: stick slip motion without separation and red: full stick motion)

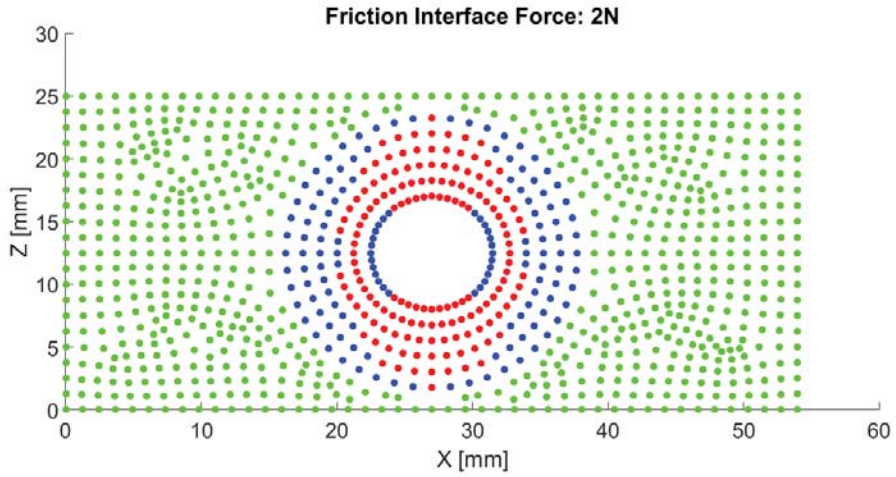

Figure 5.35. Contact states of peak point of FRF at 2 N excitation level for the single bolted assembly with low contact stiffness (green: full separation, black: separation with stick slip motion, blue: stick slip motion without separation and red: full stick motion)

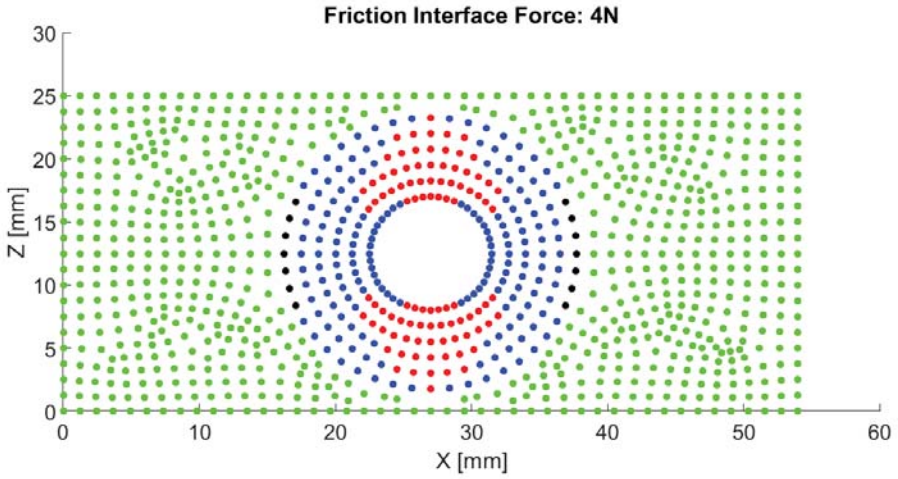

Figure 5.36. Contact states of peak point of FRF at 4 N excitation level for the single bolted assembly with low contact stiffness (green: full separation, black: separation with stick slip motion, blue: stick slip motion without separation and red: full stick motion)

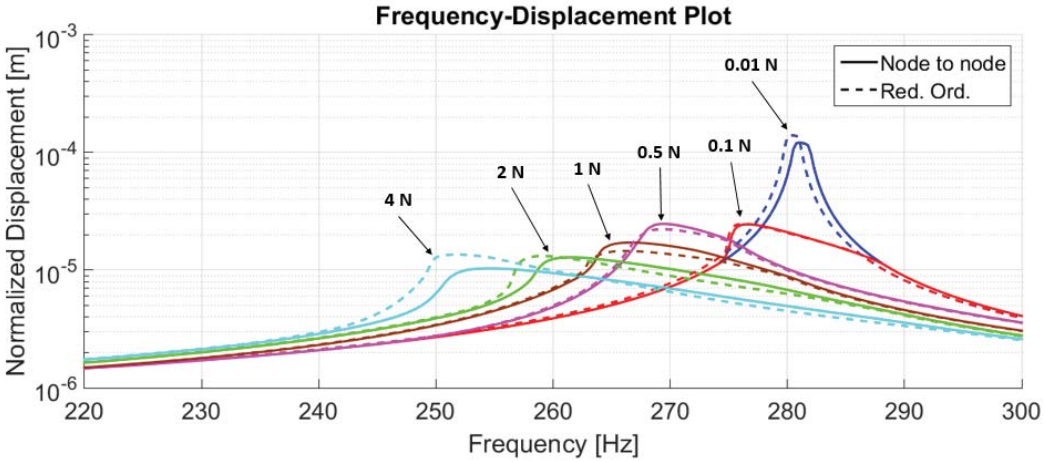

Figure 5.37. Comparison of Frequency displacement plots of node to node contact single bolted assembly model with low contact stiffness values

Although the same number of dry friction elements are used in both the node-to-node contact model and the reduced order model, nonlinear forces for the reduced order model are calculated from only 8 degrees of freedom (4 dofs for tangential motion and 4 dofs for normal motion). By further decreasing the number of friction elements in each reduced order microslip friction element, secondary reduction might be realized by utilizing an optimization problem with hysteresis loops as performed in chapter 4. However, it should be noted that the hysteresis loops depends on both tangential and normal motion since the effect of normal load variation is included. Therefore, the hysteresis loops for the optimization problem should be obtained for not only tangential motion but also for normal motion. However, in the scope of this thesis, secondary reduction for the dry friction element with normal load variation is not studied.

5.3. Three-Bolted Assembly

In the previous section, two types of reduced order model is constructed by utilizing two joints and four joints for the single bolted assembly. It is seen that four joint system approximated the node-to-node contact model better. Therefore, in this section, reduced order model of three-bolted assembly will be constructed by utilizing the four joint model. 3D model and dimensions of three-bolted assembly is given in Figure 5.38 and Figure 5.39 respectively. Same methodology with the analysis of single bolted assembly is performed. Firstly, static analysis is realized in order to obtain normal load and gap distribution of the contact surface. Same material properties, contact surface definitions, kinematic surface enforcements (tie constraint) and boundary conditions with the static analysis of single bolted assembly are utilized. 10 kN preload from the center of bolt shank for each bolt is applied. Normal load distribution and gap distribution of contact surface after the nonlinear static analysis are given in Figure 5.40 and Figure 5.41 respectively. Exaggerated view after the nonlinear static analysis is given in Figure 5.42 in order to capture the gap distribution better.

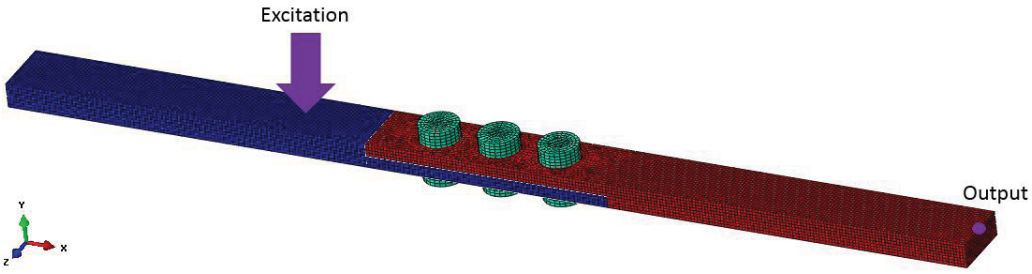

Figure 5.38. 3D model of three bolted assembly

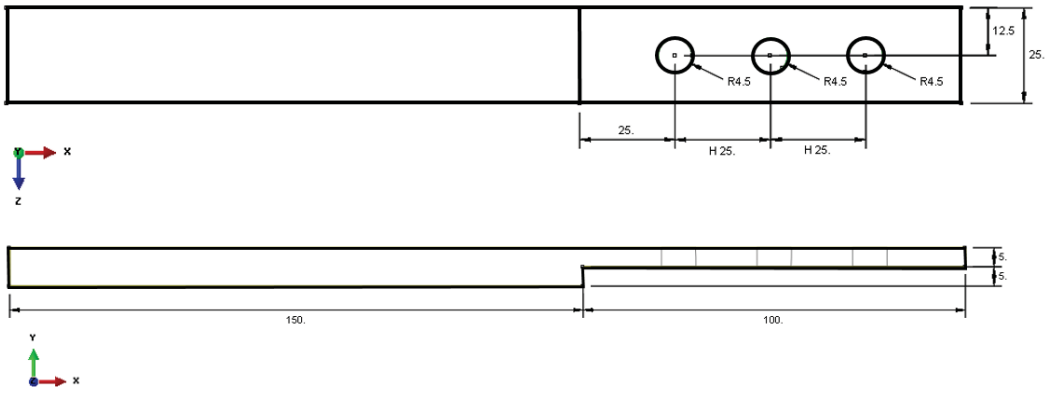

Figure 5.39. Dimensions of the beam utilized in three bolted assembly [mm]

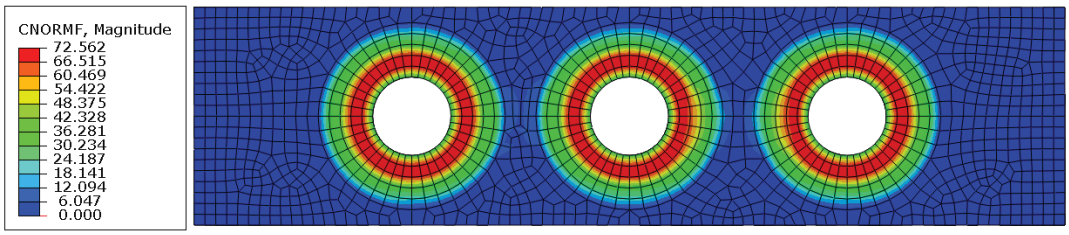

Figure 5.40. Normal load distribution of three bolted assembly [N]

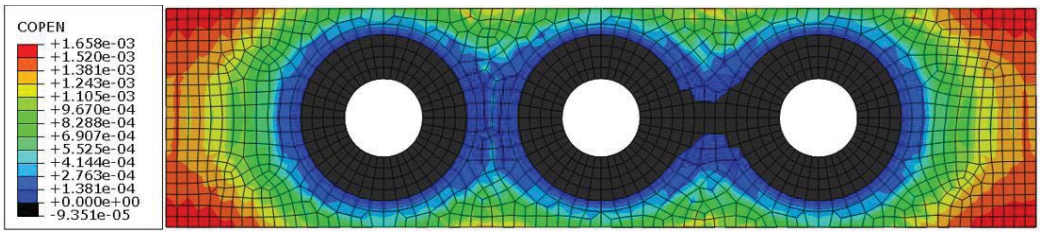

Figure 5.41. Gap distribution of three bolted assembly [mm]

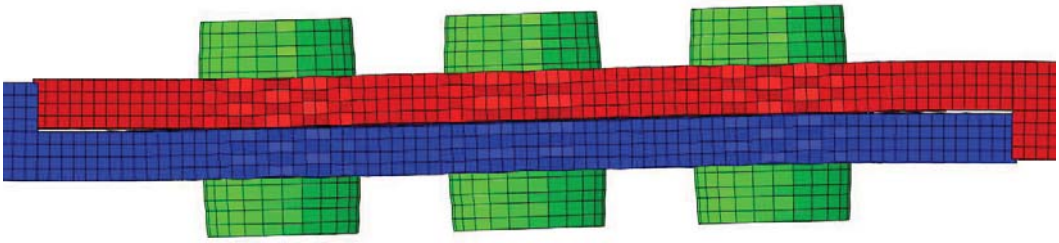

Figure 5.42. Exaggerated front view after nonlinear static analysis of three bolted assembly

5.3.1. Node to Node Contact Model

After obtaining the normal load distribution and gap distribution, linear FEM model of three-bolted assembly is constructed by discarding the nonlinear contact surface definition and enforcing free-free boundary condition. Subsequently, modal analysis is performed in order to obtain the natural frequencies and mode shapes. The mode shapes utilized in modal superposition method is given in Figure 5.43 to Figure 5.46.

After obtaining the mode shapes and natural frequencies of the system, node-to-node contact model is constructed by utilizing the dry friction elements with normal load variation as shown in Figure 5.47. Tangential stiffness (k_u), normal stiffness (k_v), coefficient of friction (μ) of the dry friction element are given in *Table 5.3*. Normal load values (n_0) are recalculated according to Equation (4.3) by utilizing the normal load and gap distributions shown in Figure 5.40 and Figure 5.41. By utilizing the

harmonic balance method with modal superposition method, FRF plots are obtained as shown in Figure 5.48. Besides contact states of the dry friction elements for each FRF plots at their peak amplitude are given in Figure 5.49 to Figure 5.58. Linear system behavior can be seen at 0.001 N, where the stick condition dominates the system. As the excitation level increases (up to 2N), stick-slip without separation can be seen at left side and right side of the bolt holes while the most of the friction elements around the bolt hole in the center still stays in stick condition. When the excitation levels increase more (higher than 2 N), separation with stick slip condition arise in the dry friction elements at the right and left bolt holes.

Table 5.3 *Parameters of 1D dry friction element with normal load variation for three-bolted assembly*

k_u	300 kN/mm
k_v	300 kN/mm
μ	0.1

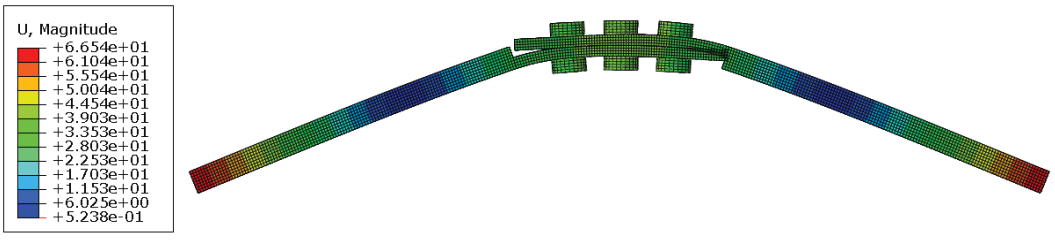

Figure 5.43. Bending mode 170 Hz

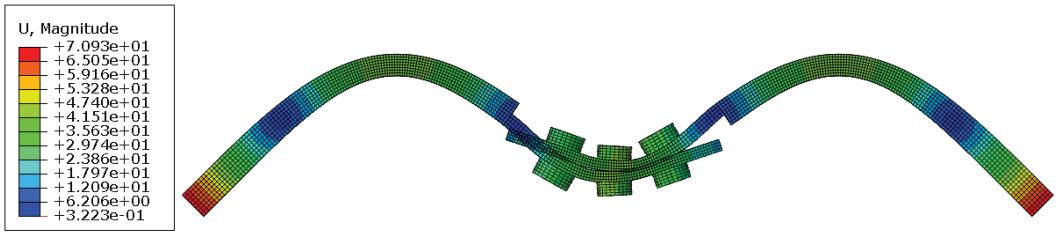

Figure 5.44. Bending mode 1488.7 Hz

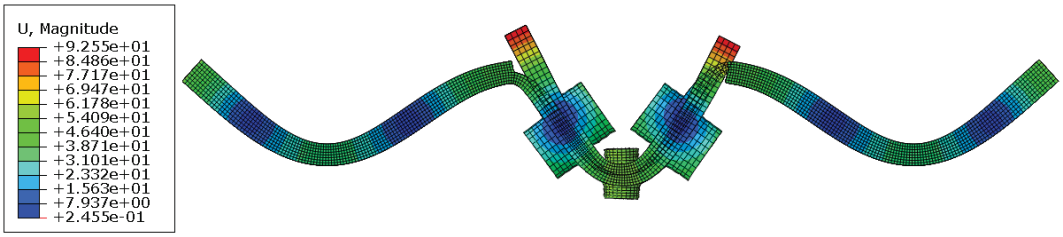

Figure 5.45. Bending mode 3387.2 Hz

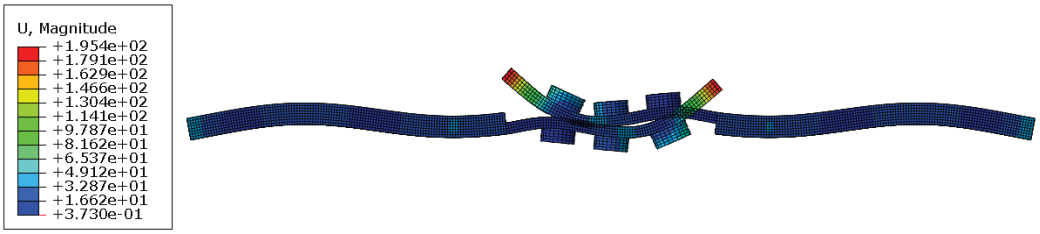

Figure 5.46. Bending mode 4506.2 Hz

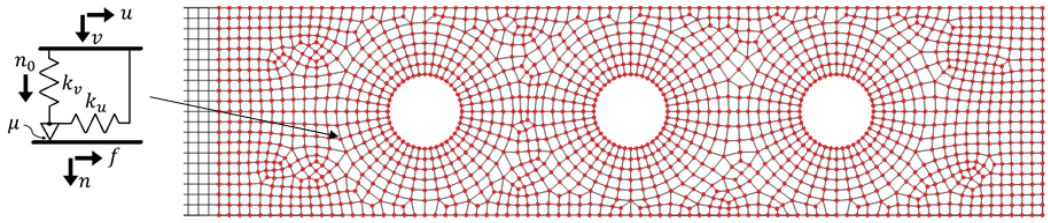

Figure 5.47. Location of the nodes connected with 1D dry friction elements with normal load variation in three bolted assembly

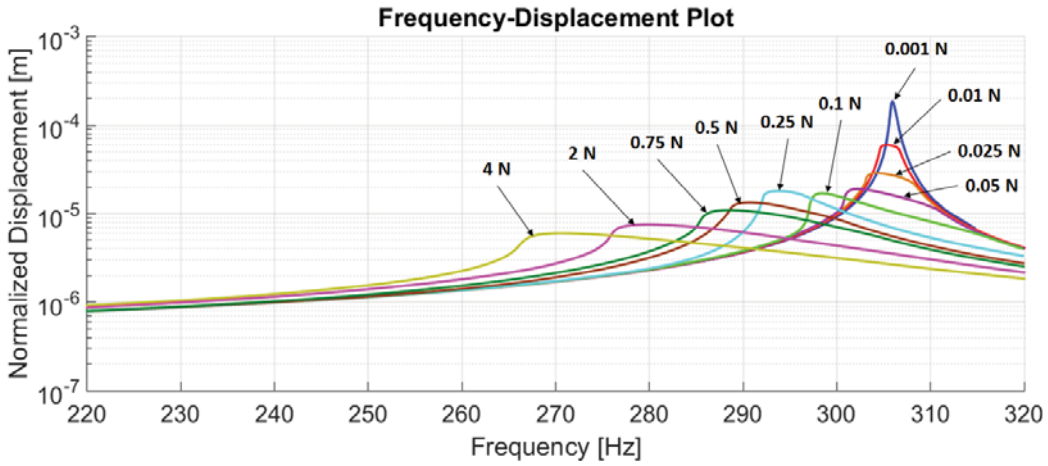

Figure 5.48. FRF plot of node to node contact model of three bolted assembly for several excitation levels

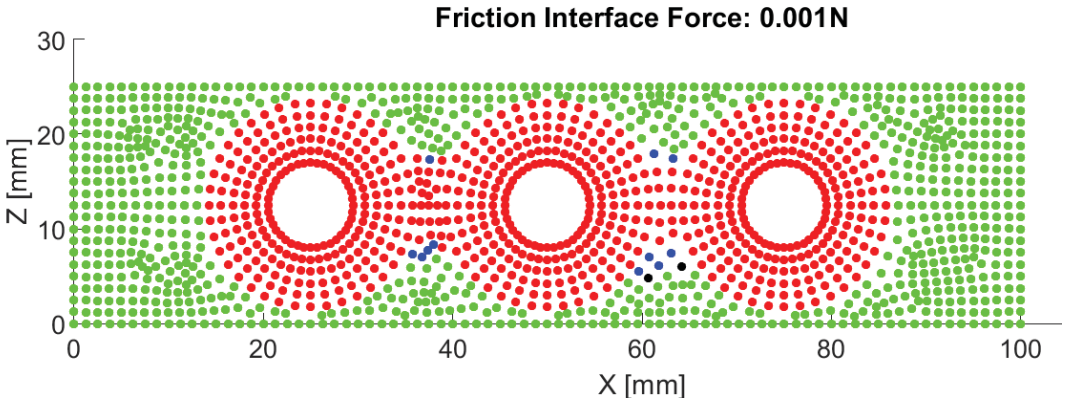

Figure 5.49. Contact states of peak point of FRF at 0.001 N excitation level for the three bolted assembly (green: full separation, black: separation with stick slip motion, blue: stick slip motion without separation and red: full stick motion)

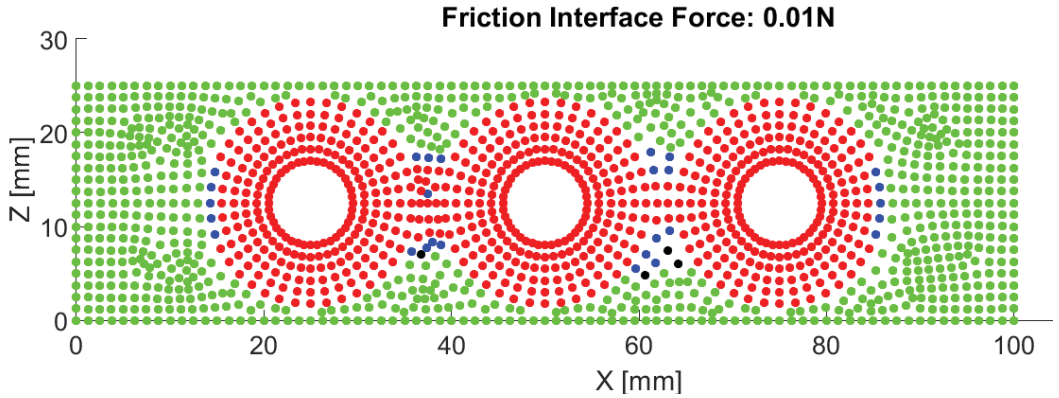

Figure 5.50. Contact states of peak point of FRF at 0.01 N excitation level for the three bolted assembly (green: full separation, black: separation with stick slip motion, blue: stick slip motion without separation and red: full stick motion)

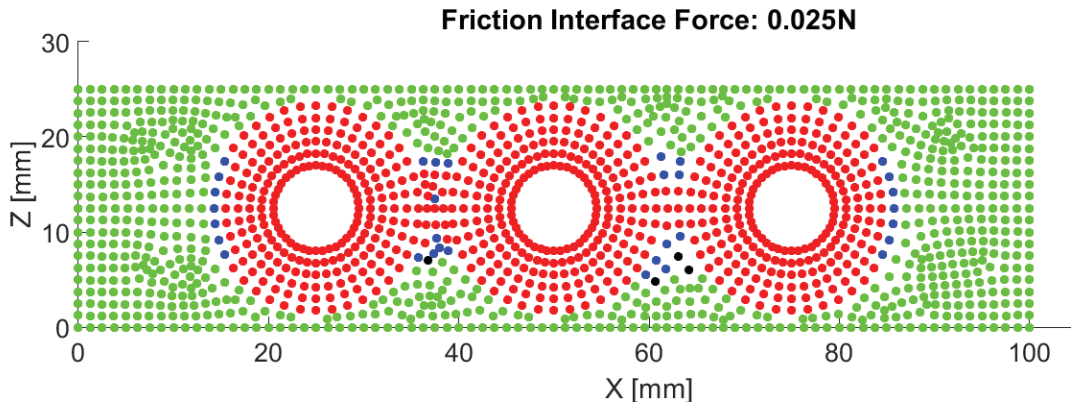

Figure 5.51. Contact states of peak point of FRF at 0.025 N excitation level for the three bolted assembly (green: full separation, black: separation with stick slip motion, blue: stick slip motion without separation and red: full stick motion)

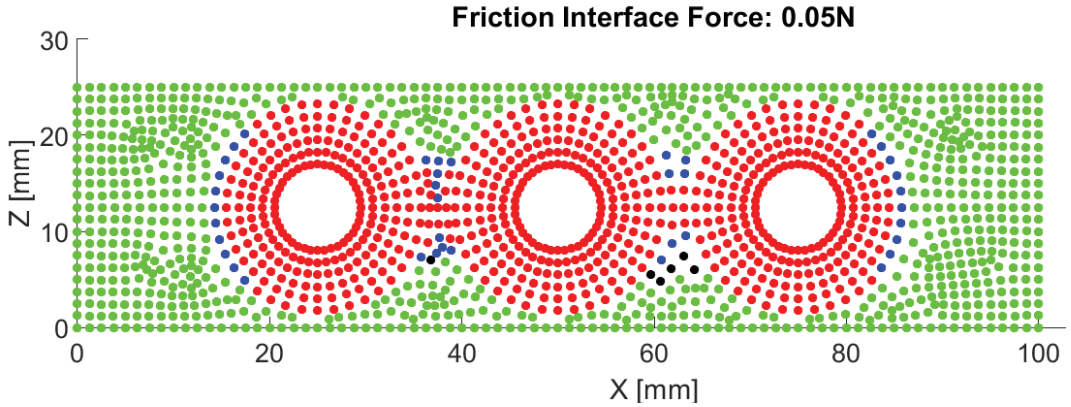

Figure 5.52. Contact states of peak point of FRF at 0.05 N excitation level for the three bolted assembly (green: full separation, black: separation with stick slip motion, blue: stick slip motion without separation and red: full stick motion)

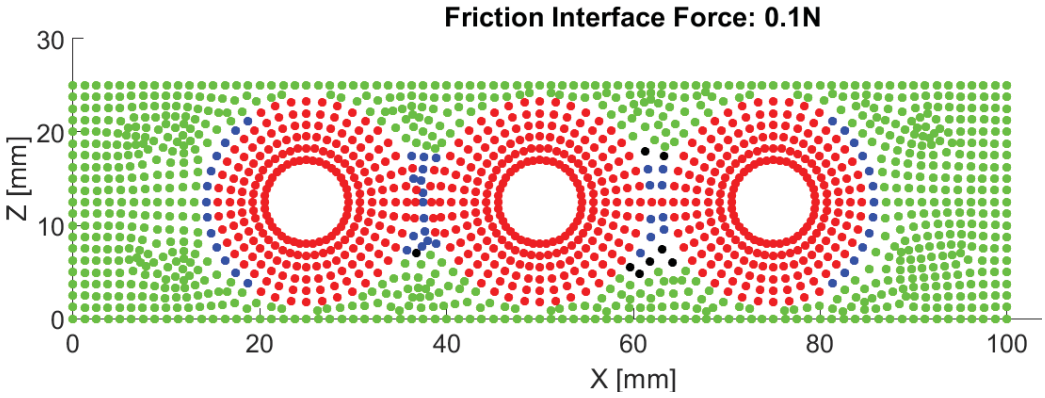

Figure 5.53. Contact states of peak point of FRF at 0.1 N excitation level for the three bolted assembly (green: full separation, black: separation with stick slip motion, blue: stick slip motion without separation and red: full stick motion)

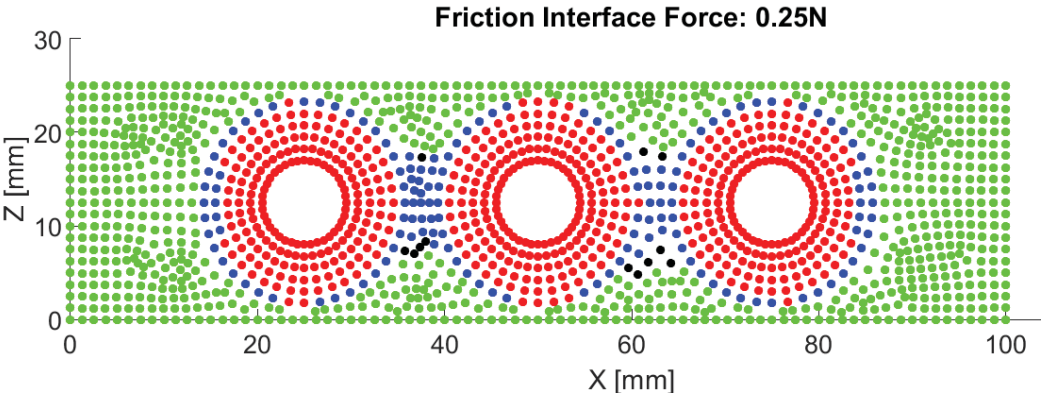

Figure 5.54. Contact states of peak point of FRF at 0.25 N excitation level for the three bolted assembly (green: full separation, black: separation with stick slip motion, blue: stick slip motion without separation and red: full stick motion)

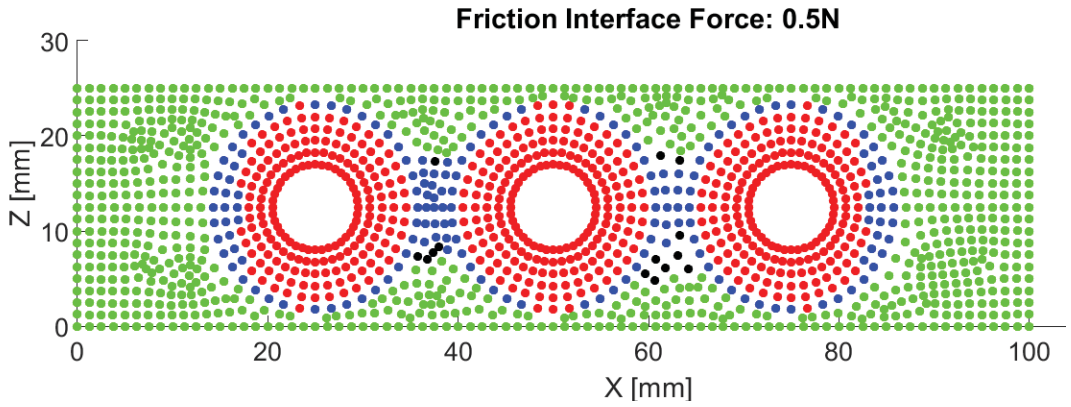

Figure 5.55. Contact states of peak point of FRF at 0.5 N excitation level for the three bolted assembly (green: full separation, black: separation with stick slip motion, blue: stick slip motion without separation and red: full stick motion)

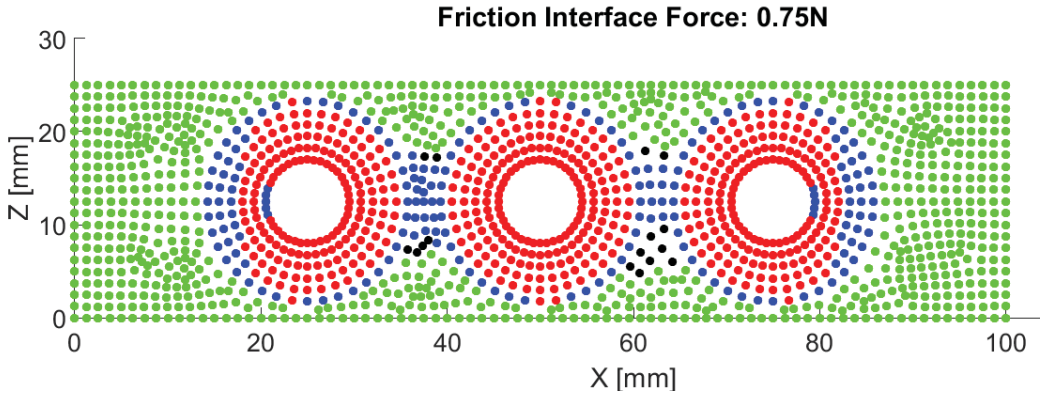

Figure 5.56. Contact states of peak point of FRF at 0.75 N excitation level for the three bolted assembly (green: full separation, black: separation with stick slip motion, blue: stick slip motion without separation and red: full stick motion)

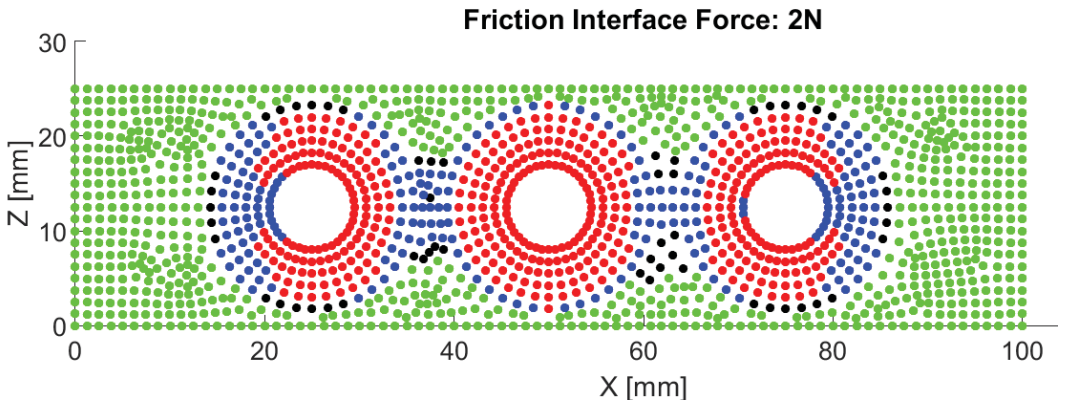

Figure 5.57. Contact states of peak point of FRF at 2 N excitation level for the three bolted assembly (green: full separation, black: separation with stick slip motion, blue: stick slip motion without separation and red: full stick motion)

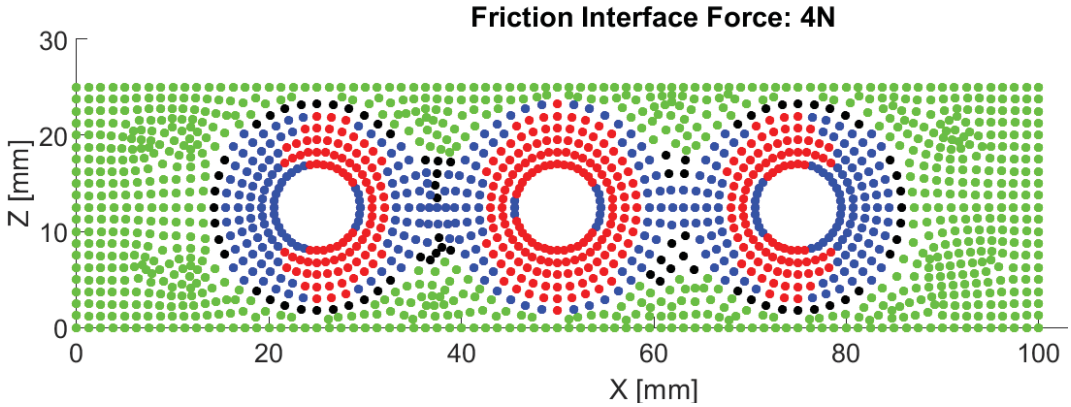

Figure 5.58. Contact states of peak point of FRF at 4 N excitation level for the three bolted assembly (green: full separation, black: separation with stick slip motion, blue: stick slip motion without separation and red: full stick motion)

5.3.2. Reduced Order Bolted Joint Model of Three-Bolted Assembly

By utilizing four joint model type, reduced order model of three-bolted assembly is constructed. In order to decide the joint regions, normal load distribution is plotted in as shown in Figure 5.60 from the mid-section of the contact region, which is given in

Figure 5.59. As can be seen from Figure 5.60, joint 1,4,5,8,9 and 12 approximate the low normal loads, and joint 2,3,6,7,10 and 11 approximate the high normal loads. The lumping locations of the reduced order model on 3D mesh can be seen in Figure 5.61. Comparison of Normalized FRFs of reduced order model with node-to-node contact model can be seen in Figure 5.62. As can be seen from the figure, four-joint type reduced order model approximated the node-to-node contact model with a good accuracy. In Figure 5.62, it can be seen that there is a small shift between the FRF plot of node-to-node contact model and reduced order model when the excitation is 0.001 N (full stick linear case). The accuracy of reduced order model can be increased by multiplying the stiffness values of microslip dry friction elements in reduced order model with a coefficient. The coefficient can be found with a trial and error such that resonance frequencies of full stick condition of node-to-node contact model and reduced order model is coincident. In this case, the stiffness values are multiplied with a coefficient of 1.015. The comparison of FRF plots of node-to-node contact model and new reduced order model is shown in Figure 5.63. From the Figure 5.63, it is clearly seen that the accuracy of the results especially at low excitation levels gets better.

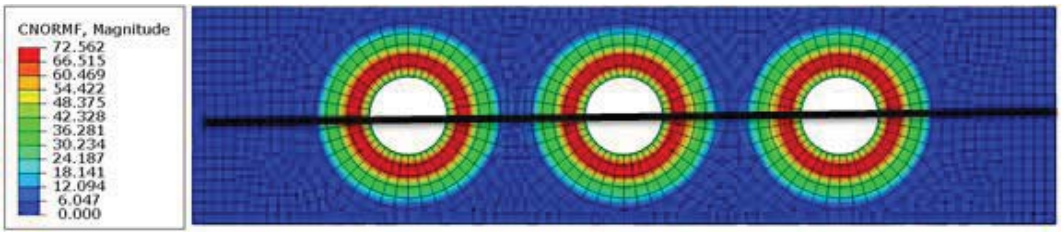

Figure 5.59. Mid-section path for the normal load distribution plot of three-bolted assembly

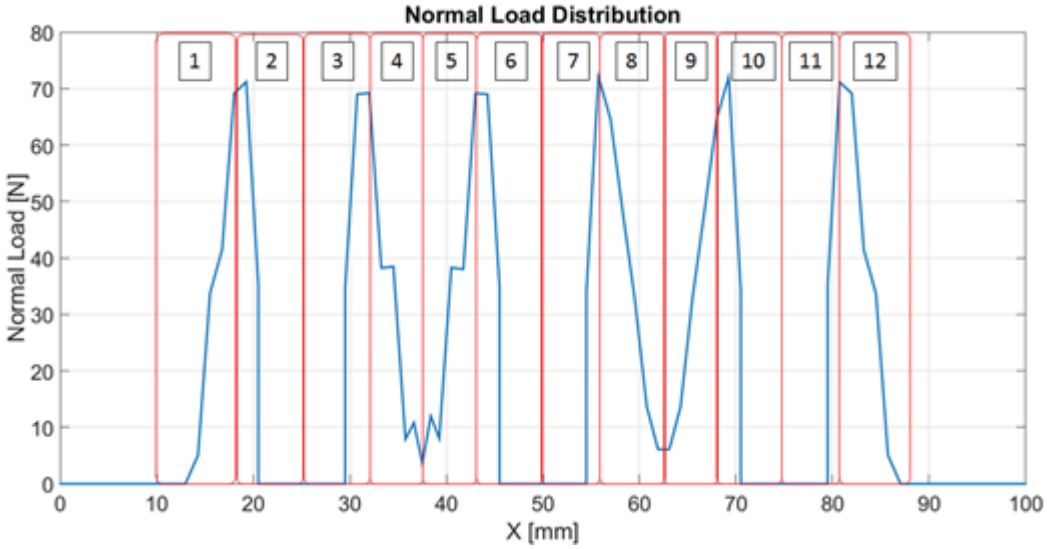

Figure 5.60. Normal load distribution plot from the mid-section of the beam for four-joint reduced order model of three-bolted assembly

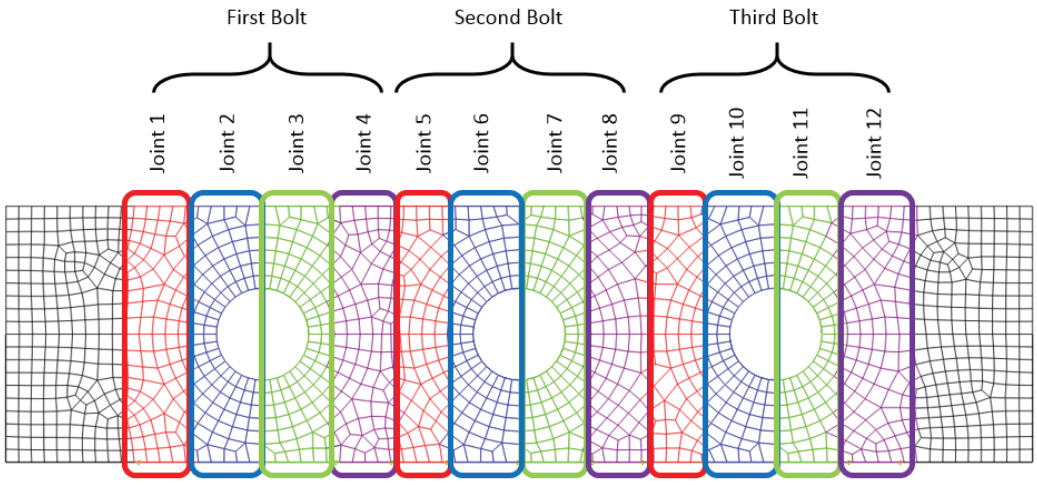

Figure 5.61. Location of joints in reduced order model of three-bolted assembly

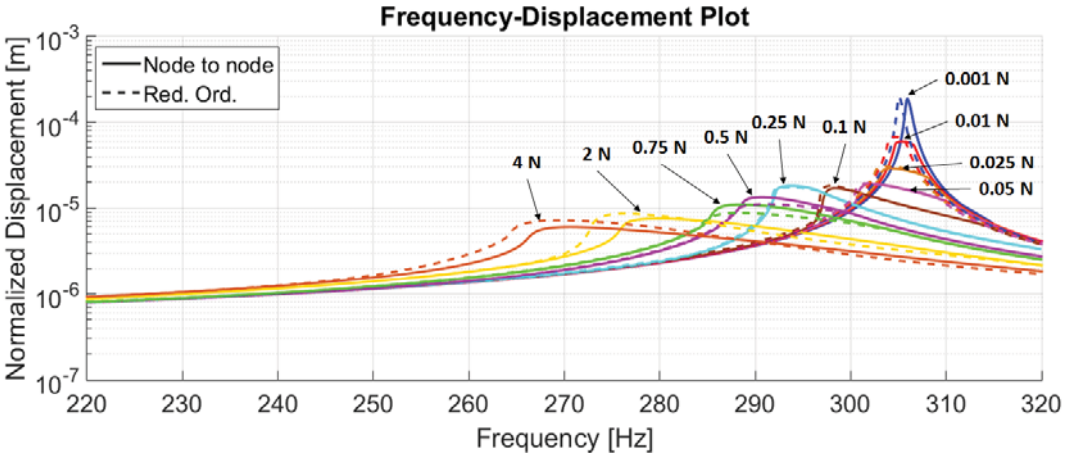

Figure 5.62. Comparison of FRF plots of node to node contact model of three bolted assembly with reduced order model

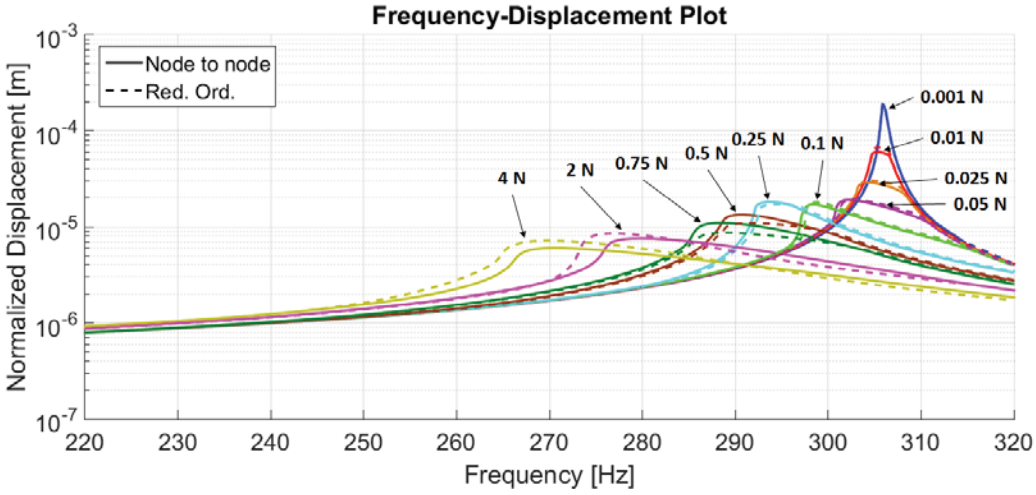

Figure 5.63. Comparison of FRF plots of node to node contact model of three bolted assembly with reduced order model multiplied with coefficient

Up to this point, all the FRF analysis are realized around the first mode of the assembled structure. In order to see the effect of reduction technique, FRF analysis

are repeated around the second mode utilized in modal superposition method for the three-bolted beam assembly. The obtained results for several excitation levels are given in Figure 5.64. As can be seen from the Figure 5.64, the reduction technique is accurate also for the higher frequencies.

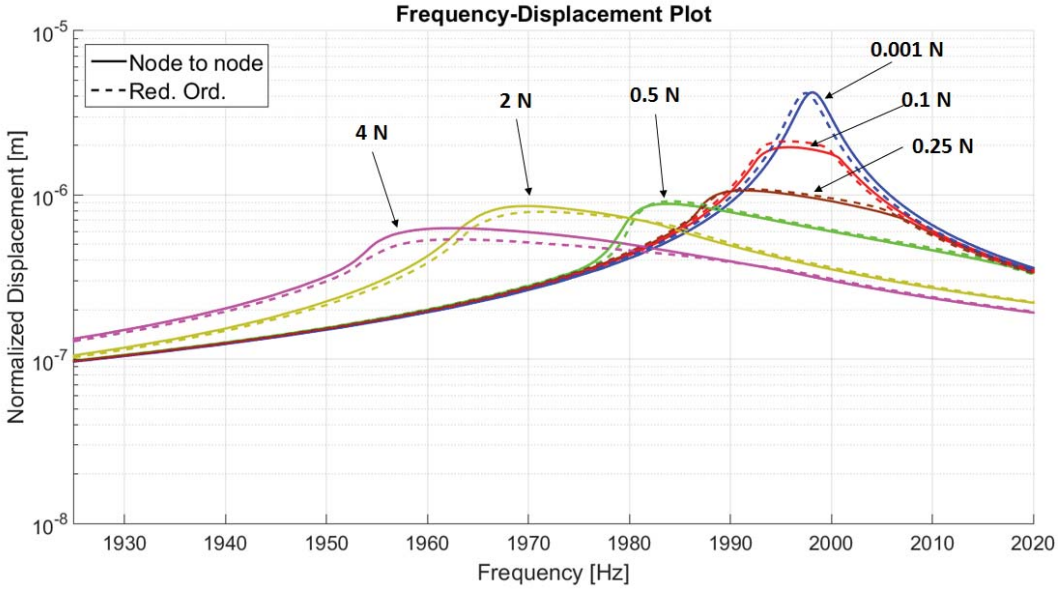

Figure 5.64. Comparison of FRF plots of node to node contact model of three bolted assembly with reduced order model around the second mode utilized in modal superposition method.

Secondary reduction is also realized for the three-bolted beam assembly in order to see the accuracy when the number of friction elements are decreased in each joint. Since the friction force in dry friction elements depends on not only tangential motion but also normal motion, there is not a single hysteresis loop. Therefore, an assumption is made such that the effect of normal motion is not considered when optimizing the hysteresis loops for the secondary reduction. However, the effect of normal load variation is included for the FRF analysis. The optimized normal stiffness values are taken as same with tangential stiffness.

The parameters are optimized with the same methodology introduced in chapter 4. Since the normal motion is not included in the optimization, only tangential stiffness

(k_u) and sliding force ($\mu \cdot N$) are optimized. In the optimization only 3 elements are utilized for each joint. Hysteresis loop of first joint before and after optimization are given in Figure 5.65. The parameters of stiffness and sliding force for each joint are given in Table 5.4. By utilizing the secondary reduced model, FRF plots for several excitation levels are obtain. The FRFs of node to node model, reduced order model with first reduction and with secondary reduction are given in Figure 5.66. FRFs of reduced order model with second reduction are given with first reduction and node to node model separately in Figure 5.67 and Figure 5.68.

The number of dry friction elements in each joint after the first reduction is given in *Table 5.5*. It can be seen that although the number of dry friction elements in each joint reduced drastically, The FRFs of second reduction are close to the FRFs of first reduction as can be seen from Figure 5.67. In Figure 5.68, it is seen that the reduced order model with secondary reduction estimated the node-to-node model with a good accuracy. There is a shift in low level of excitations. By multiplying the stiffness values of secondary reduced order model, the shift in low excitation levels can be decreased, where the similar procedure is applied for the reduced order model with first reduction in Figure 5.63.

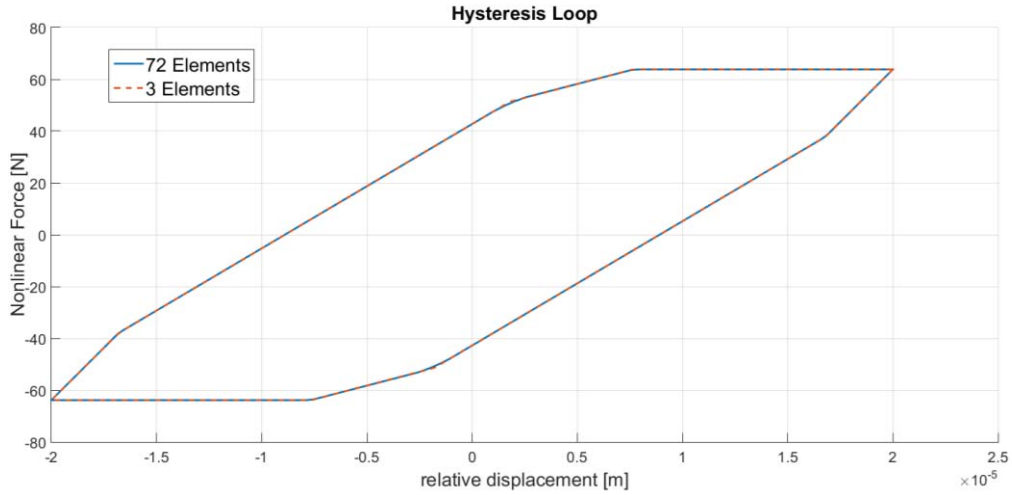

Figure 5.65. Hysteresis loop of joint 1 after first reduction and second reduction

Table 5.4. *Parameters of secondary reduced order model with three elements for joint 1 of three-bolted beam*

	k_1(N/mm)	k_2(N/mm)	k_3(N/mm)	μN_1(N)	μN_2(N)	μN_3(N)
Joint 1	3299838	2671463	2127897	5.296	29.127	29.419
Joint 2	2936533	11605360	11525163	5.560	136.266	269.947
Joint 3	12709442	13017306	3873830	295.183	150.346	7.746
Joint 4	2244148	2625059	5551187	25.450	34.552	11.117
Joint 5	2142656	4799273	4136295	1.812	59.229	10.609
Joint 6	3111407	11433879	11487377	6.231	131.923	266.669
Joint 7	12688720	3864847	13067952	294.544	7.461	149.926
Joint 8	4224125	2777666	2188435	8.863	41.617	21.735
Joint 9	2019707	2904733	4200253	31.770	31.861	9.036
Joint 10	3013438	11571886	11464599	5.698	133.445	265.772
Joint 11	12720160	13139832	3761997	297.880	153.809	7.308
Joint 12	3300006	2676251	2123001	5.301	29.133	29.276

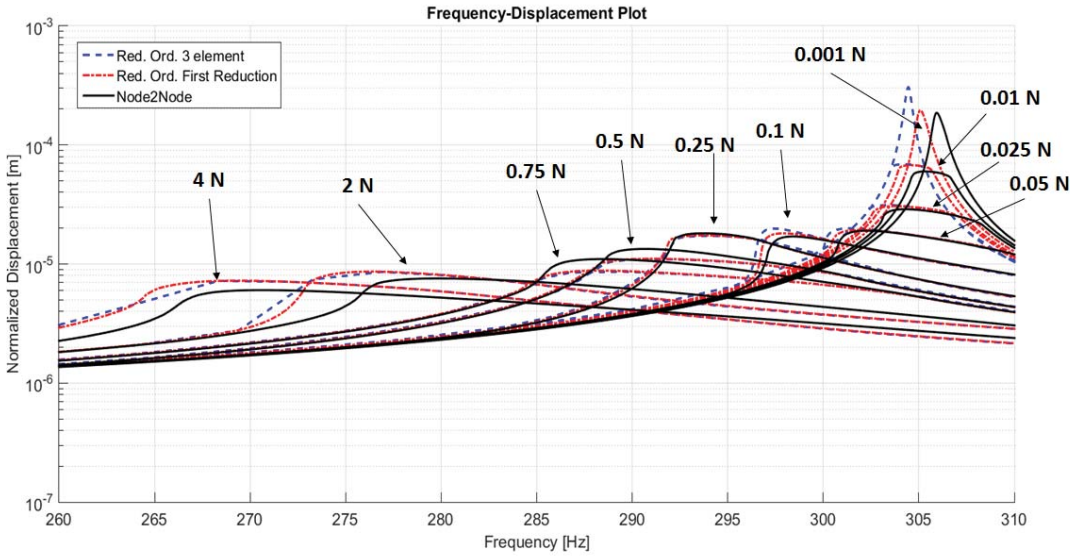

Figure 5.66. FRFs of node to node model, reduced order model with first reduction and reduced order model with secondary reduction (3 elements)

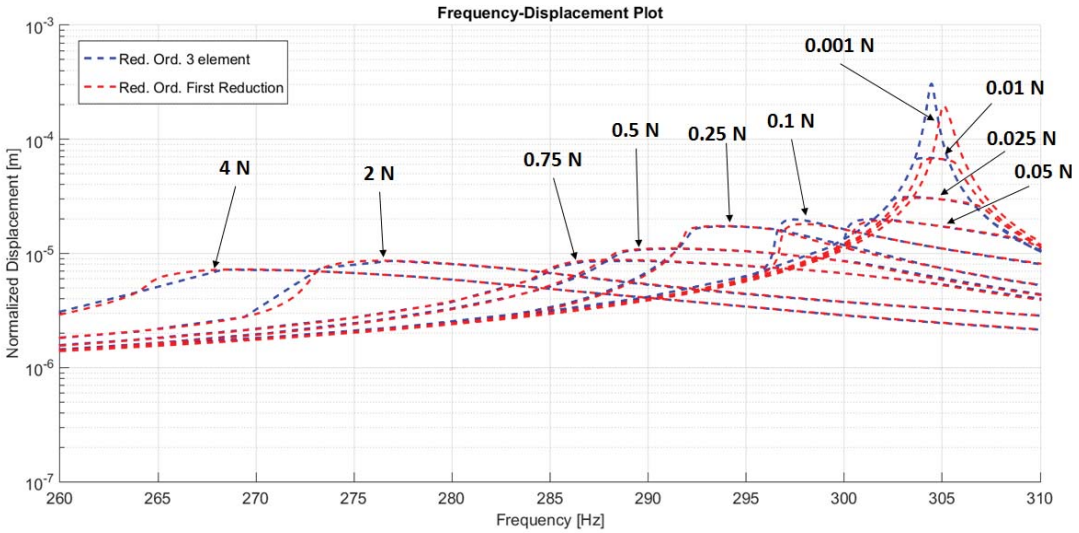

Figure 5.67. FRFs of reduced order model with first reduction and reduced order model with secondary reduction (3 elements)

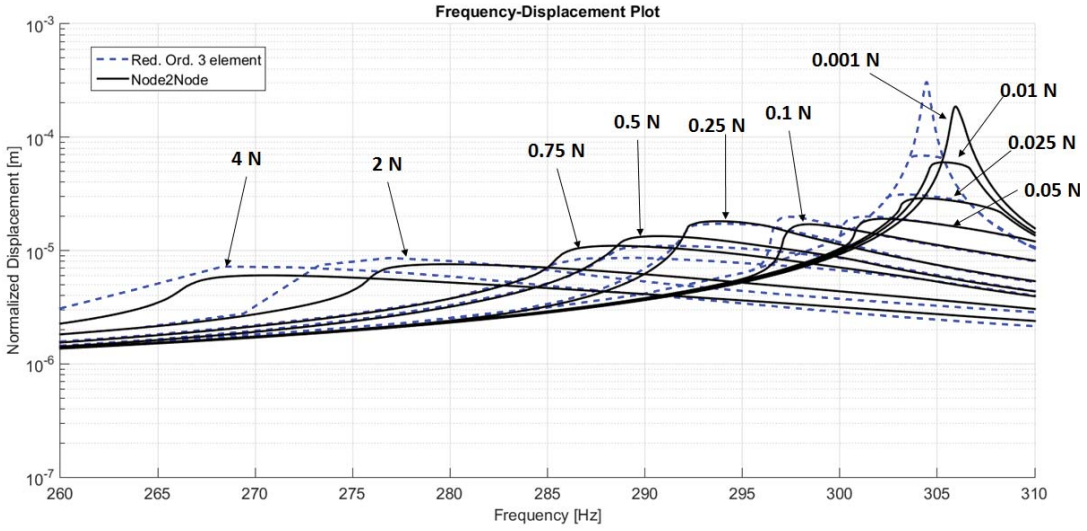

Figure 5.68. FRFs of node to node model and reduced order model with secondary reduction (3 elements)

Table 5.5. *Number of dry friction elements in each joint after the first reduction*

	Number of dry friction elements
Joint 1	72
Joint 2	107
Joint 3	123
Joint 4	83
Joint 5	81
Joint 6	108
Joint 7	123
Joint 8	76
Joint 9	78
Joint 10	107
Joint 11	121
Joint 12	72

To conclude, a new reduced order modeling methodology is developed in this chapter. Firstly, the reduced order model methodology, which is developed in the previous chapter, is reconstructed in a single bolted assembly by utilizing 1D dry friction elements with normal load variation. Besides, effect of contact stiffness values on the reduced order model accuracy is studied in the single bolted assembly. Afterwards, by utilizing the new reduced order model methodology, a three-bolted assembly is modeled. It is seen that the reduced order model gave good results in both the simple and the more complex models.

CHAPTER 6

CONCLUSION

In this thesis, a new nonlinear reduced order modeling methodology for bolted joints is proposed. In the presented method, distributed modeling of the contact interface is reduced to several microslip elements, which are combination of macroslip elements. Two types of friction models are studied for the reduction methodology and several case studies are conducted. Two-step reduction methodology is investigated in dry friction elements with constant normal load. Afterwards, first reduction methodology is studied in detail by utilizing the dry friction elements induced by normal load variation. The reduced order models are compared with the representative high fidelity models (node-to-node contact models). It was seen that reduced order models gave satisfactory results compared to the node-to-node contact models.

In the first reduction methodology, the main idea was that number of nonlinear forcing terms can be decreased by utilizing the same number of macroslip elements. This was realized by lumping the macroslip elements inside the certain area into microslip elements. It was shown in chapter 5 that the decision of which macroslip elements need to be lumped into the corresponding microslip element can be made by considering the normal load distribution of the contact interface. It should be noted that not only the normal load distribution but also the mode shape of interest affect the decision for the lumping of macroslip elements. However, in this thesis, only the effect of normal load distribution was considered for this decision. The second advantage of the first reduction technique is that it opened the doors of the second reduction method since the distributed contact model was represented by lumped microslip elements.

In the second reduction method, number of macroslip elements inside each microslip elements are decreased while maintaining the similar behavior of force-displacement curves. By doing so, accurate FRF plots are obtained by utilizing several number of macroslip elements compared to the node-to-node contact model. In *Table 6.1* and

Table 6.2, it can be seen that about 56% and 11% reduction is realized in reduced order models utilizing constant normal load and variable normal load respectively.

Table 6.1. *Normalized time of node to node model and reduced order model utilizing the dry friction elements with constant normal load*

	Normalized time
Node-to-node model	1
Reduced order model with secondary reduction	0.5558

Table 6.2. *Normalized time of node to node model and reduced order model utilizing the dry friction elements with variable normal load*

	Normalized time
Node-to-node model	1
Reduced order model with secondary reduction	0.1129

As a future work, the secondary reduction method might be extended in the dry friction elements with normal load variation. Hysteresis loops depend on the tangential motion and the normal motion. Therefore, effect of normal motion should be taken into consideration in the optimization problem of secondary reduction method. The developed methodology can also be extended to 2D or 3D friction elements. Thus, considerable amount of computational time can be saved while having sufficiently enough accuracy.

REFERENCES

[1] Tsai, J.-S., & Chou, Y.-F. (1988). The Identification of Dynamic Characteristics of a Single Bolt Joint. *Journal of Sound and Vibration*. https://doi.org/10.1016/0022-460X(88)90256-8

[2] Yang, T., Fan, S. H., & Lin, C. S. (2003). Joint Stiffness Identification Using FRF Measurements. *Computers and Structures*, *81*(28–29), 2549–2556. https://doi.org/10.1016/S0045-7949(03)00328-6

[3] Mehrpouya, M., Graham, E., & Park, S. S. (2013). FRF Based Joint Dynamics Modeling and Identification. *Mechanical Systems and Signal Processing*, *39*(1–2), 265–279. https://doi.org/10.1016/j.ymssp.2013.03.022

[4] Segalman, D. J. (2005). A Four-Parameter Iwan Model for Lap-Type Joints. *Journal of Applied Mechanics*, *72*(5), 752. https://doi.org/10.1115/1.1989354

[5] Bograd, S., Reuss, P., Schmidt, A., Gaul, L., & Mayer, M. (2011). Modeling the Dynamics of Mechanical Joints. *Mechanical Systems and Signal Processing*, *25*(8), 2801–2826. https://doi.org/10.1016/j.ymssp.2011.01.010

[6] Liao, X., Zhang, J., & Xu, X. (2016). Analytical Model of Bolted Joint Structure and Its Nonlinear Dynamic Characteristics in Transient Excitation, *2016*.

[7] Brake, Matthew R. W., Groß, J., Lacayo, R. M., Salles, L., Schwingshackl, C. W., Reuß, P., & Armand, J. (2018). Reduced Order Modeling of Nonlinear Structures with Frictional Interfaces. In *The Mechanics of Jointed Structures* (pp. 427–450). Cham: Springer International Publishing. https://doi.org/10.1007/978-3-319-56818-8_24

[8] Brake, M. R., Reuss, P., Segalman, D. J., & Gaul, L. (2014). Variability and Repeatability of Jointed Structures with Frictional Interfaces. *Conference Proceedings of the Society for Experimental Mechanics Series*, *1*, 252. https://doi.org/10.1007/978-3-319-04501-6_23

[9] Brake, M. R W. (2016). A Reduced Iwan Model That Includes Pinning for Bolted Joint Mechanics. *Nonlinear Dynamics*, *87*(2), 1–15. https://doi.org/10.1007/s11071-016-3117-2

[10] Petrov, E. P. (2017). Frequency-Domain Sensitivity Analysis of Stability of Nonlinear Vibrations for High-Fidelity Models of Jointed Structures. *ASME Journal of Turbomachinery*, *140*(JANUARY), 1–12. https://doi.org/10.1115/GT2017-64023

[11] Lacayo, R., Pesaresi, L., Groß, J., Fochler, D., Armand, J., Salles, L., … Brake, M. (2019). Nonlinear Modeling of Structures with Bolted Joints: A Comparison of Two Approaches Based on a Time-Domain and Frequency-Domain Solver. *Mechanical Systems and Signal Processing*, *114*, 413–438. https://doi.org/10.1016/j.ymssp.2018.05.033

[12] Menq, C. H., Bielak, J., & Griffin, J. H. (1986). The Influence of Microslip on Vibratory Response, Part I: A New Microslip Model. *Journal of Sound and Vibration*, *107*(2), 279–293. https://doi.org/10.1016/0022-460X(86)90238-5

[13] Menq, C.-H., Griffin, J. H., & Bielak, J. (1986). The Influence Vibratory of Microslip Response , with on Results Part II : a Comparison. *Journal of Sound and Vibration*, *107*(2), 295–307. https://doi.org/10.1016/0022-460X(86)90239-7

[14] Yang, B. D., Chu, M. L., & Menq, C. H. (1998). Stick – Slip – Separation Analysis and Non-Linear Stiffness and Damping Characterization of Friction Contacts Having Variable Normal Load. *Journal of Sound and Vibration*, *210*, 461–481.

[15] Cigeroglu, E., Lu, W., & Menq, C. H. (2006). One-Dimensional Dynamic Microslip Friction Model. *Journal of Sound and Vibration*, *292*(3–5), 881–898. https://doi.org/10.1016/j.jsv.2005.09.019

[16] Ciğeroğlu, E., & Özgüven, H. N. (2006). Nonlinear Vibration Analysis of Bladed Disks with Dry Friction Dampers. *Journal of Sound and Vibration*, *295*(3–5), 1028–1043. https://doi.org/10.1016/j.jsv.2006.02.009

[17] Cigeroglu, E., An, N., & Menq, C. H. (2007). A Microslip Friction Model with Normal Load Variation Induced by Normal Motion. *Nonlinear Dynamics*, *50*(3), 609–626. https://doi.org/10.1007/s11071-006-9171-4

[18] Cigeroglu, E., An, N., & Menq, C.-H. (2009). Forced Response Prediction of Constrained and Unconstrained Structures Coupled Through Frictional Contacts. *Journal of Engineering for Gas Turbines and Power*, *131*(2), 022505. https://doi.org/10.1115/1.2940356

[19] Ferhatoglu, E., Cigeroglu, E., & Özgüven, H. N. (2018). A New Modal Superposition Method for Nonlinear Vibration Analysis of Structures Using Hybrid Mode Shapes. *Mechanical Systems and Signal Processing*, *107*, 317–342. https://doi.org/10.1016/j.ymssp.2018.01.036

APPENDICES

A. IMAC-XXXVII Conference and Exposition on Structural Dynamics

Reduced Order Modeling of Bolted Joints in Frequency Domain

Gökhan Karapıstık [1,2], Ender Cigeroglu[1]

[1] Middle East Technical University Department of Mechanical Engineering, 06800 Ankara, Turkey

[2] ROKETSAN A.Ş., Kemalpaşa Mah. Şehit Yüzbaşı Adem Kutlu Sok. No:21 06780 Ankara, Turkey

ABSTRACT

Most of the structural systems assembled by using bolted joints. Therefore, bolted joint models have a critical importance to estimate the behavior of the overall assembled system. There are several linear bolted joint models which consist of spring and dashpot elements in literature. While they can estimate the resonant frequency of the overall system with a sufficient accuracy, linear bolted joint models are inadequate for approximating the damping which arises from the friction in the contact interface of assembled system. On the other hand, there are examples of nonlinear bolted joint models which utilize 3D contact models to account for the frictional damping behavior in the literature. However, modeling the structures with many bolted joints by using high fidelity 3D contact models is very time consuming. Therefore, reduced order bolted joint models with sufficient accuracy are in need. In this paper, a method for modeling bolted joints in frequency domain is introduced. The joint model consists of microslip friction elements each one of which is constructed by several Coulomb friction elements in parallel and located at both sides of bolt holes.

INTRODUCTION

Bolts are utilized to establish connection in many structural components. Fastening a structural component with bolts introduce complexity to the structural integrity in terms of both stiffness and damping characteristics. There are several studies to estimate the behavior of the bolted joints with linear springs and dashpots [1, 2]. However, inadequacy in capturing the energy loss of the structural system, especially with changing excitation levels, is a shortcoming of the linear joint models. To deal with the shortage of damping estimation, high fidelity models have been studied in the past few decades [3-5]. Nonetheless, computational cost of high fidelity models is considerable if a structural system with a lot of bolts is to be modeled. Main reason in this insufficiency of damping behavior in reduced order linear models is the absence of microslip friction model in the contact area. Structures with bolted joint have a complicated contact area exhibiting a variable contact force distribution. The contact forces near the bolt hole are sufficiently high; whereas, they become very low at some distant. Due to variability in contact forces, microslip like behavior arises. Hence, it is crucial to model the microslip friction present in the contact area. In order to model the microslip behavior, either specific microslip models [6-10] or distributed macroslip models are utilized [11,12]. In macroslip models, entire surface associated with the friction model is either in slip state or in stick state. However, in microslip models, unlike macroslip models, partial slips in localized areas are allowed in the contact interface; hence, energy can be dissipated without the necessity of gross slip. In this study, the microslip friction element developed by Cigeroglu et al. [6] is used in modeling of bolted connections. However, since the variations of normal force in the bolted joints are relatively small, in this study, normal load variation is neglected. A reduced order joint model is introduced and it is compared with a representative high fidelity model obtained by utilizing multiple macroslip elements which is common in the modelling of friction contacts in bladed disks [11,12,13]. The Brake-Reuß beam [14] is considered for the comparison of the two different friction models. A nonlinear static analysis is performed in order to obtain the contact force distribution in the joint area which is used as the normal forces acting on the macroslip elements used in the high fidelity model similar to [13]. For the reduced order joint modeling, microslip friction elements are attached at both sides of bolt holes. Both systems are analyzed and the results obtained are compared with each other.

THEORY

Nonlinear static analysis of Brake-Reuß beam

Abaqus FEA software is used for the nonlinear static analysis of the Break-Reuß beam. In this model; bolts, washers and nuts are connected to each other so that they behave as a single part (tie constraint). Surface to surface contact algorithm with the penalty method is imposed between the contacting surfaces of beam structures in order to obtain the contact pressure distribution. 11500 N preload is applied from the center of the bolt shank to each bolt in the model. Finite element model (FEM) of Break-Reuß beam and the normal contact force distribution obtained through stacte analysis are shown in Fig. 1.

(a)

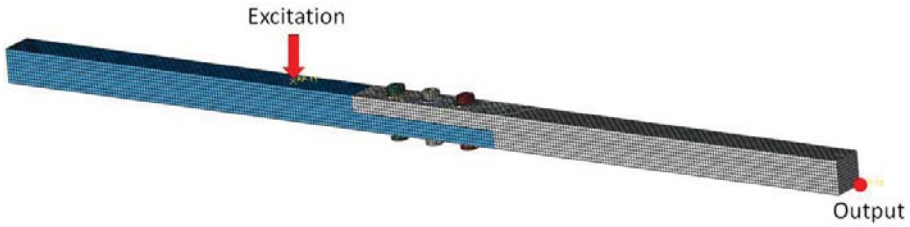

(b)

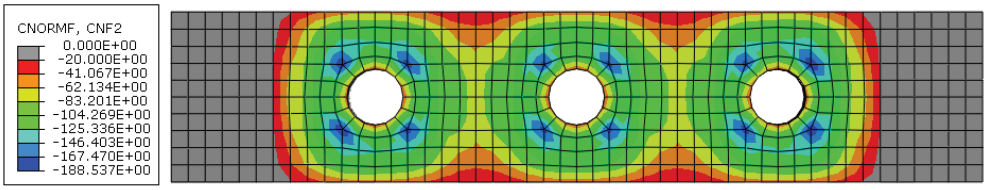

Fig. 1 (a) FEM of Break-Reuß beam and (b) normal contact force distribution [N]

Representative high fidelity model

In this model all the nodes coincident to each other in the contact area are connected with one dimensional macroslip friction elements with constant normal loads. 1D macroslip friction elements consist of three parameters: tangential stiffness, normal load and coefficient of friction. In this model, tangential stiffness and coefficient of friction for all the friction elements are assumed to be 1000 N/mm and 0.12, respectively. Normal contact forces obtained from nonlinear static analysis are used as the normal loads acting on the friction elements. Locations of the contact nodes used in the high fidelity model are shown in Fig. 2 which are selected based on the normal contact force distribution given in Fig. 1b.

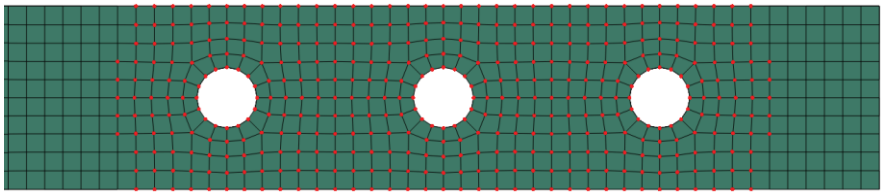

Fig. 2 Contact nodes used in the high fidelity model

obtained by optimizing the summation of hysteresis loops of representative high fidelity model in the corresponding region of virtual nodes.

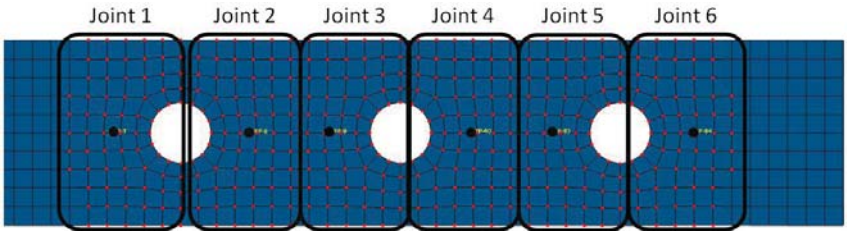

Fig. 3 Locations of the virtual nodes used for reduced joint model

RESULTS AND DISCUSSION

For high fidelity model and reduced order joint model, harmonic balance method with a single harmonic content is used for the frequency domain solution. Modal superposition method [15] is employed in order to reduce the number of nonlinear equations resulting from the use of FEM. Rigid body modes and first three bending modes of the system are included in the modal superposition. Excitation and output locations are shown in Fig. 1a. Both models are solved with free-free boundary conditions and 0.2% structural damping is imposed.

Normalized displacement for both high fidelity model and reduced order model are obtained for several excitation levels which are shown in Fig. 4. In the high fidelity model, 400 1D macroslip friction elements are used in total. However, in the reduced order joint model, 18 friction elements (6 reduced order joints and 3 1D macroslip friction elements for each joint) are used in total. Although there is a great difference in the number of friction elements utilized, results show that dynamic behavior of the jointed structure with the reduced order joint model can be estimated with similar accuracy as the one estimated from the high fidelity contact model.

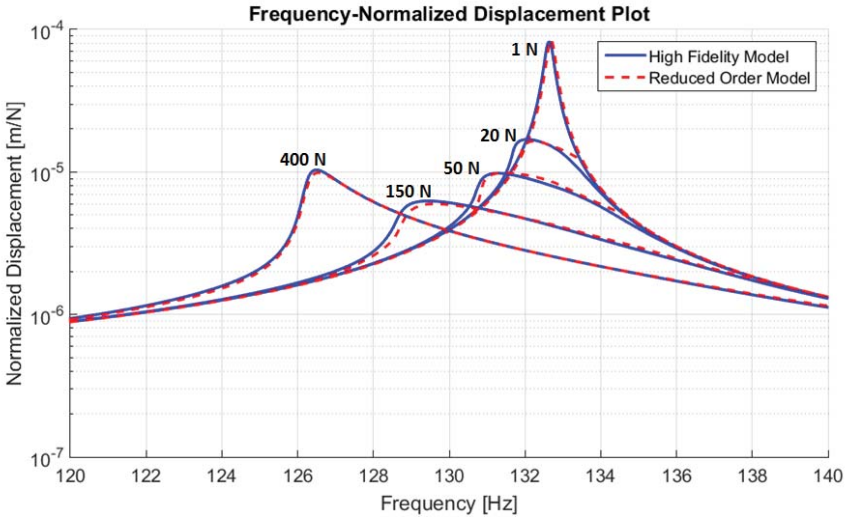

Fig. 4 Comparison of normalized displacement of high fidelity and reduced order joint models

REFERENCES

[1] Tsai, J.-S., and Chou, Y.-F., "The Identification of Dynamic Characteristics of a Single Bolt Joint," J. Sound Vib., vol. 125, no. 3, pp. 487–502, 1988.

[2] Mehrpouya, M., Graham, E., and Park, S. S., "FRF Based Joint Dynamics Modeling and Identification," Mech. Syst. Signal Process., vol. 39, no. 1–2, pp. 265–279, 2013.

[3] Bograd, S., Reuss, P., Schmidt, A., Gaul, L., and Mayer, M., "Modeling the Dynamics of Mechanical Joints," Mech. Syst. Signal Process., vol. 25, no. 8, pp. 2801–2826, 2011.

[4] Petrov, E. P., "Frequency-Domain Sensitivity Analysis of Stability of Nonlinear Vibrations for High-Fidelity Models of Jointed Structures," ASME J. Turbomach., vol. 140, pp. 1–12, 2017.

[5] Lacayo, R., Pesaresi, L., Groß, J., Fochler, D., Armand, J., Salles, L., Schwingshackl, C., Allen, M., and Brake, M, "Nonlinear Modeling of Structures with Bolted Joints: A Comparison of Two Approaches Based on a Time-Domain and Frequency-Domain Solver," Mech. Syst. Signal Process., vol. 114, pp. 413–438., 2019.

[6] Cigeroglu, E., An, N., and Menq, C. H., "A Microslip Friction Model with Normal Load Variation Induced by Normal Motion," Nonlinear Dyn., vol. 50, no. 3, pp. 609–626, 2007.

[7] Tworzydlo, W. W., Cecot, W., Oden, J. T., and Yew, C. H., ''Computational Micro- and Macroscopic Models of Contact and Friction: Formulation, Approach and Applications,'' Wear, 220, pp. 113–140, 1998.

[8] Menq, C.H., Bielak, J., Griffin, J.H.: The influence of mi- croslip on vibratory response, Part I A new microslip model. J. Sound Vib. vol. 107, no. 2, pp. 279–293, 1986.[9] Menq, C.H., Bielak, J., Griffin, J.H.: The influence of microslip on vibratory response, Part II A comparison with experimental results. J. Sound Vib. vol. 107, no. 2, pp. 295–307, 1986.

[10] Cigeroglu, E., Lu, W., and Menq, C. H., "One-Dimensional Dynamic Microslip Friction Model," J. Sound Vib., vol. 292, no. (3–5), pp. 881–898, 2006.

[11] Cigeroglu E, Menq CH, "A Microslip Friction Model for the Analysis of Frictionally Damped Turbine Blades",IMECHE Ninth International Conference on Vibrations in Rotating Machinery, vol. 1, pp. 185-196, 2008.

[12] Petrov, E. P., and Ewins, D. J., "Analytical Formulation of Friction Interface Elements for Analysis of Nonlinear Multi-Harmonic Vibrations of Bladed Disks," J. Turbomach., vol. 125, no. 2, p. 364, 2003.

[13] Cigeroglu, E., An, N., and Menq, C.-H., "Forced Response Prediction of Constrained and Unconstrained Structures Coupled Through Frictional Contacts," J. Eng. Gas Turbines Power, vol. 131, no. 2, p. 022505, 2009.

[14] Brake, M. R., Reuss, P., Segalman, D. J., and Gaul, L., "Variability and Repeatability of Jointed Structures with Frictional Interfaces," Conf. Proc. Soc. Exp. Mech. Ser., vol. 1, p. 252, 2014.

[15] Ferhatoglu, E., Cigeroglu, E., and Özgüven, H. N., "A New Modal Superposition Method for Nonlinear Vibration Analysis of Structures Using Hybrid Mode Shapes," Mech. Syst. Signal Process., vol. 107, pp. 317–342, 2018.